CHAPTER 5
HYDROTHERMAL PHASE PARAGENESES AND GEOCHEMISTRY

5.1 INTRODUCTION

Although they are the result of the same evolving system, silicates, carbonates, oxides and sulphides produced by hydrothermal fluid-rock reactions are divided for clarity of presentation into "alteration" and "mineralization" parageneses. Alteration phases are those silicates, carbonates and oxides of no economic interest in this prospect. Mineralization phases are those containing base and precious metals being sought in marketable concentrations. At time of writing, mineralization at Mount Dore is sub-economic.

Alteration and mineralization at Mount Dore are intimately associated with each other, and with brecciation. Parageneses are complex, and vary depending on the lithology in which they have developed. The effects of early regional and contact metamorphism in modifying the mineralogy must be considered in addition to metasomatic events. This chapter documents alteration and mineralization parageneses and geochemistry, and discusses this preliminary constraints imposed on the composition and evolution of the hydrothermal fluid by this information. Parageneses are interpreted from overprinting relationships between veins, from apparent filling sequences in vughs, and from replacement textures. Phase geochemistry was measured via electron microprobe to determine whether there is a variation depending on the lithology in which they have developed, and to provide a database for future geochemical studies. Analytical techniques and full chemical data are recorded in Appendices C and D, respectively. More detailed fluid geochemical studies are

recorded in the following chapter. The works of Ophel (1980) and Scott (1988) provide valuable additional paragenetic and geochemical data for minor phases, and where used are duly acknowledged.

5.2 DISTRIBUTION AND PARAGENESES

5.2.1 Identity and distribution of phases

Alteration and mineralization are concentrated at the southwestern corner of the Mount Dore Granite pluton, in a zone affected by three regional ductile deformation events (D_1, D_2, D_3) and a major late faulting event (Chapter 3). Alteration extends east and west beyond the faulted metasediment-granite and metasediment-quartzite contacts, and is larger than the zone of mineralization, which is contained between these contacts, within the narrow band of more heavily brecciated metasediments.

The three most abundant and pervasive alteration phases are microcline, quartz, dolomite and calcite. The distributions of these phases are depicted as thick tabular or flattened pipe-like bodies dipping to the east and centred on the Mount Dore Fault Zone (Figure 5.1). The full extent of alteration was not intersected during drilling, however, and they are actually unbounded to the north and south, and at depth. Quartz and microcline are broadly coincident in space, although silicification and quartz veining appear to be slightly more extensive (Figure 5.1a,b). Some of this may, however, be the result of the regional metasomatism which produced the quartzite unit; the effects of the two events are difficult to separate. Carbonate distribution is more restricted. Dolomite occurs in an irregular pipe in the deep north, unbounded at depth but closing upwards to the south (Figure 5.1c). Absence at higher levels may be through removal by weathering, or it may never have been present. Calcite is more common in the southern part of the prospect, in Staveley Formation calcilutites. Much is clearly metasomatic, but some may be primary.

FIGURE 5.1: Isometric block diagrams showing the distribution of main alteration phases and copper mineralization at Mount Dore, based on drill core logging: (a) microcline; (b) quartz (includes both veins and replacement style, and may also include early regional scale silicification) and tourmaline; (c) carbonate (dolomite and calcite); and (d) copper for grades exceeding approximately 0.1% Cu (based on Cyprus Minerals Australia Company drillcore assays). Note that drill holes generally do not pass through the complete width of the alteration zone, and also that both alteration and base metal mineralization continue for an unknown distance down the dip of the fault zone.

FIGURE 5.1a: K-feldspar distribution

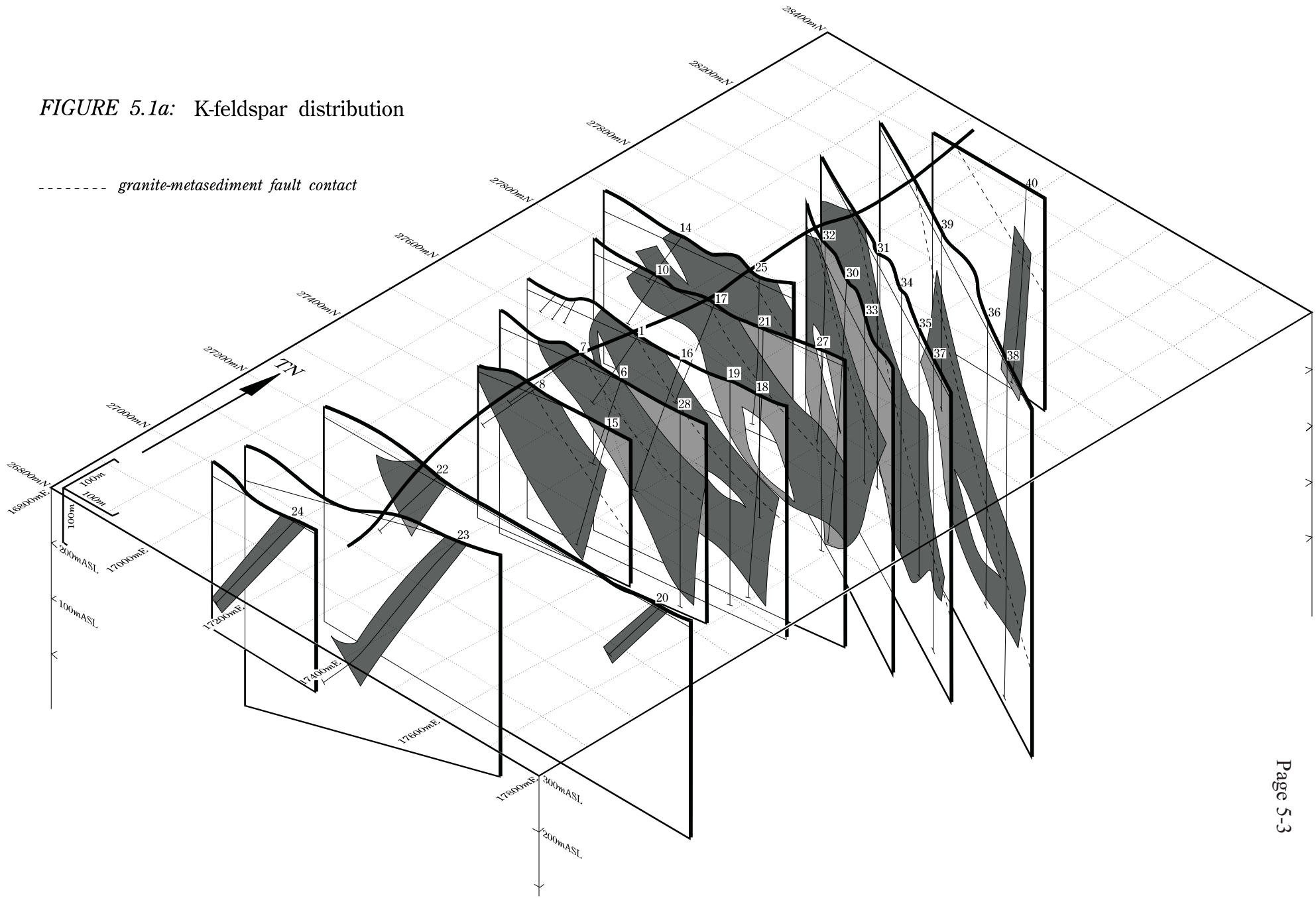

FIGURE 5.1b: Quartz and tourmaline distribution

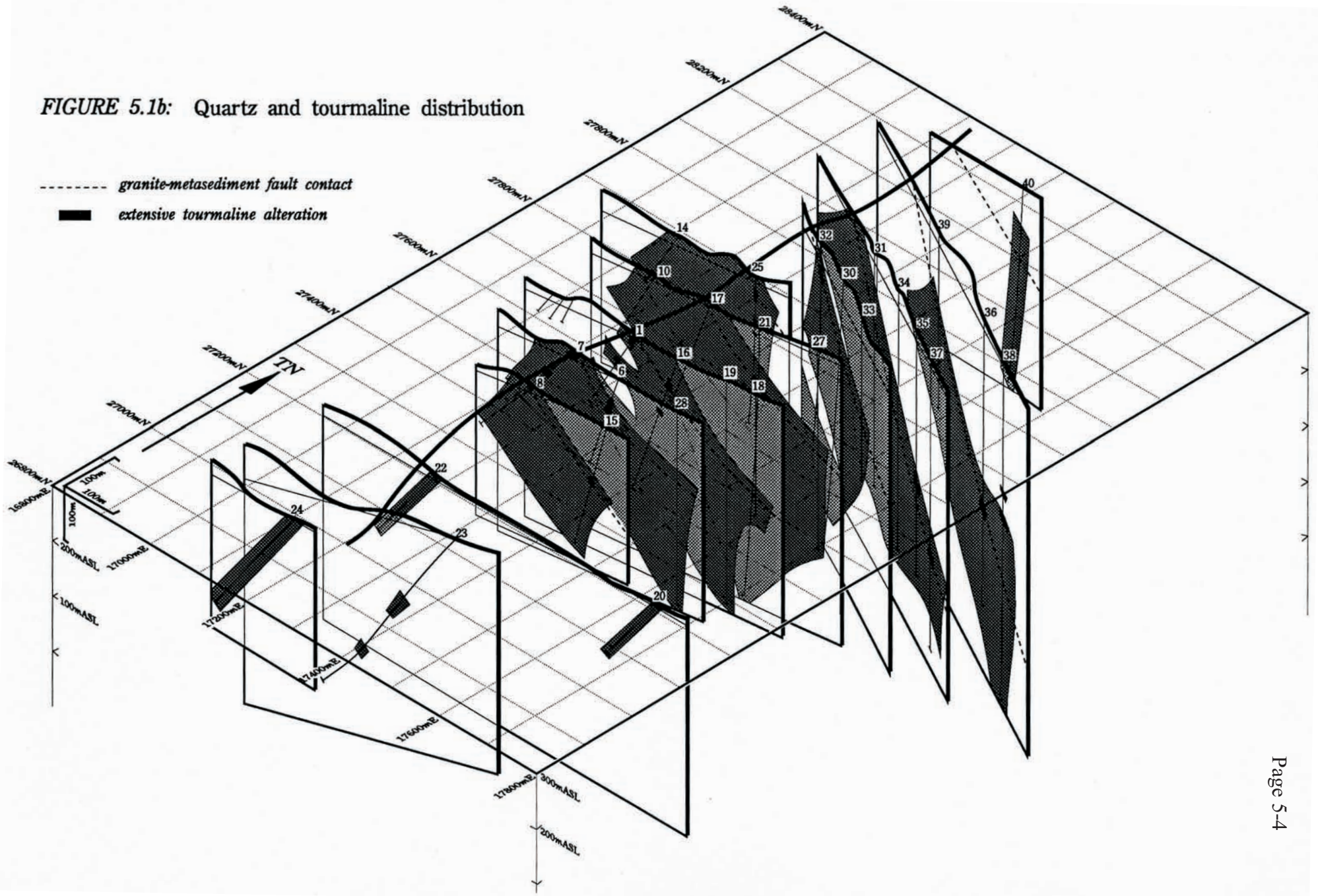

FIGURE 5.1c: Carbonate distribution

FIGURE 5.1d: Cu >0.1% distribution

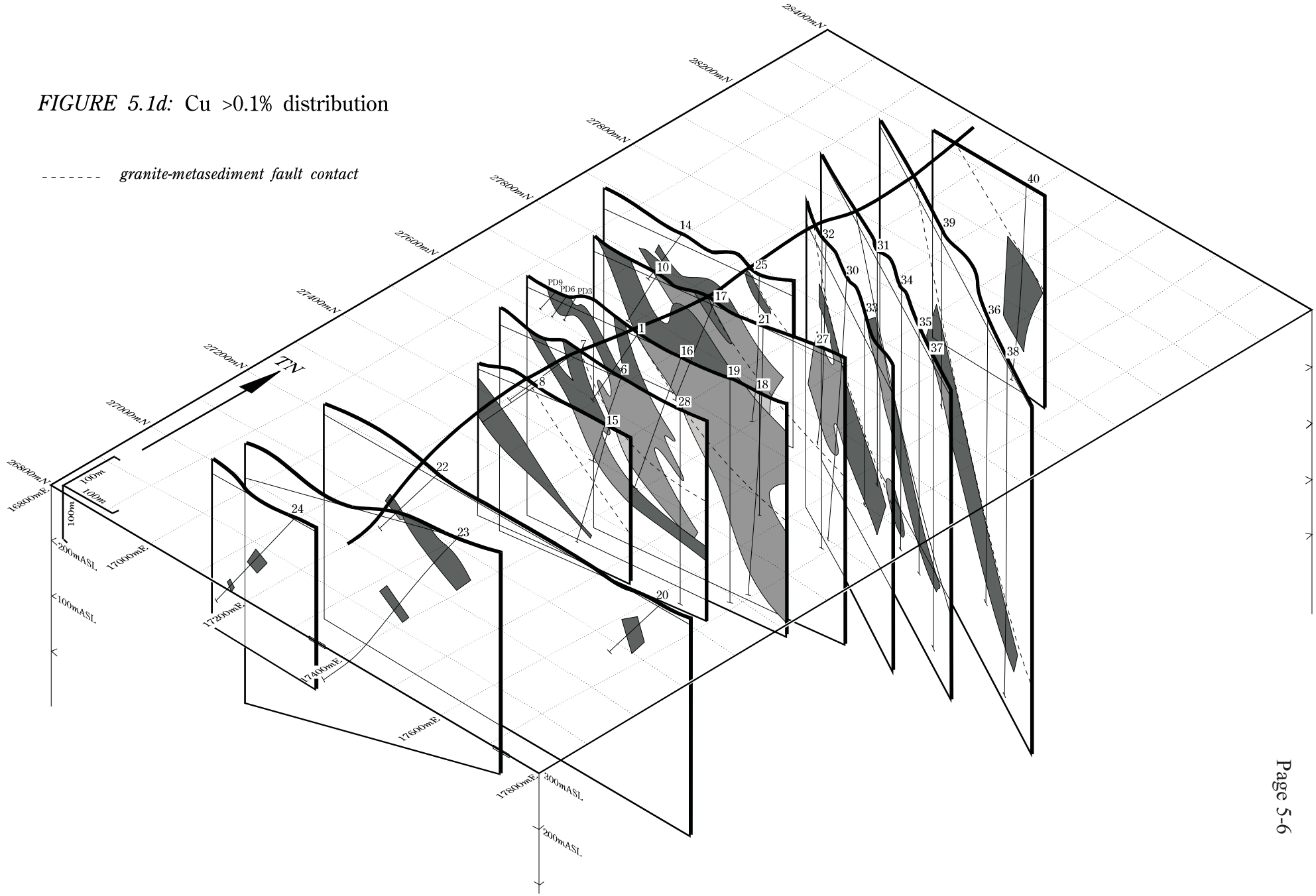

Other alteration phases present in varying amounts are muscovite, biotite, tourmaline, haematite, magnetite, apatite, chlorite and fluorite. Muscovite is most common in the granite and calcilutites. Tourmaline generally occurs within (and usually much less than) 100 metres of the fault contact with the Mount Dore Granite (Figure 5.1b). Haematite occurs as a fine dusting in microcline, but is also present as a discrete phase in altered granite and calcilutites. Magnetite has only been observed in the latter, and hydrothermal biotite is also only extensive here. Apatite and fluorite are usually only accessory phases associated with silicification, but in places apatite is a major constituent. Chlorite is more patchy, but commonly associated with carbonate.

All alteration phases occur as vein or vugh infill, but replacement-style is dominant, and is more pervasive in (originally) highly permeable or more reactive lithologies. Breccias in all metasedimentary hosts are commonly almost completely replaced. Unbroken calcareous Staveley Formation rocks are also in many instances so pervasively altered as to be almost unrecognisable, whereas unbroken carbonaceous slates and quartz-muscovite schists may be altered to only a few centimetres from veins.

The dominant sulphide phases are pyrite, chalcopyrite and chalcocite. The latter is probably the product of supergene enrichment, being usually found only in the upper levels in the southern and central parts of the prospect. Along or close to the highly permeable contact with granite it can occur to depths greater than 250 metres. Less abundant primary sulphide phases are sphalerite and galena, which are most abundant at depths greater than 350 metres in the northern part of the deposit, spatially associated with dolomite alteration, and also with carbonaceous slates and quartz-muscovite schists (*e.g.* JCU-27223, 27224), and rare cobaltite and arsenopyrite. Probable supergene base metal sulphide, oxide, silicate, carbonate and native phases include bornite, digenite, covellite, cuprite, copper, chrysocolla, malachite and azurite. Minor phases not seen in this study, but identified by Scott (1988) are carollite, djurleite and native silver (Table 5.1). Most mineralization appears to be replacive, reusing alteration veinlets or disseminated in vein alteration haloes and finely milled breccia matrices (*e.g.* JCU-27197, JCU-27213).

TABLE 5.1: Identity and chemical formulae of base metal phases identified at Mount Dore; asterisk (*) denotes phases observed by Ophel (1980) or Scott (1988), but not seen in this study.

PHASE	**FORMULA**
arsenopyrite	FeAsS
azurite	$Cu_3(CO_3)_2(OH)_2$
bornite	Cu_5FeS_4
carollite*	$Cu(Co,Ni)_2S_4$
chalcocite	Cu_2S
chalcopyrite	$CuFeS_2$
chrysocolla	$CuSiO_3.2H_2O$
cobaltite	CoAsS
covellite	CuS_2
cuprite	Cu_2O
digenite	Cu_9S_5 (approx.)
djurleite*	$Cu_{31}S_{16}$
galena	PbS
malachite	$Cu_2CO_3(OH)_2$
native silver	Ag
pyrite	FeS_2
sphalerite	ZnS

Chips and drill core from 24 percussion and 40 diamond drill holes spaced at approximately 100 to 200 metre intervals (Figure 4.1) were assayed by Amoco Minerals for Cu, Pb, Zn, Ag, Co, Au, and U. The prospect is currently viewed as a copper and silver resource, with potential extra lead, zinc and cobalt credits. As such, modelling of assay data by the company outlined an optimum resource of 40 million tonnes grading 1.08% copper and 6.5 g/t Ag to a depth of 300 metres, using a 0.3% copper cut-off grade. The shape of the mineralized "pipe" is broadly tabular, dipping about 45^{o} to the east beneath the granite contact (Figure 5.1d). Grades of up to 3.9% Cu over 9 metres and 34 g/t Ag were recorded (*e.g.* in SHQ-76-7 and SHQ-78-35, respectively). Zinc approaches or exceeds copper grades in places, though more often is considerably less abundant. Other metals are also much less abundant, but there is a generally sympathetic trend of increasing Zn, Pb, Ag and Co concentrations with increasing Cu (Figure 5.2). Gold, however, is present in trace amounts only (generally less than 0.3 ppm), and U values are variable.

The greatest concentrations of base and precious metals occur in the zones of milled breccias (*e.g.* DDH SHQ-78-35; Figure 5.2). Elevated values also continue beyond the limits of diamond and percussion drilling to the north and to depth. Mineralization is only weakly developed in the southern part of the prospect, rarely exceeding a few hundred ppm total metals. Later supergene processes have been important for upgrading base metal concentrations, and metals have been incorporated into the structures of weathering-related clays (Scott, 1988). Weathering is unrelated to the primary alteration and mineralization processes, however, and is only briefly considered herein.

FIGURE 5.2: Pictorial drill log, showing the relationship between lithology, alteration, brecciation, and metal grades, for a typical drill hole through the primary sulphide zone (SHQ-78-35). Metal values are from data collected by Cyprus Minerals Ausrtralia Company, an recorded in their drill logs. Note the change of scales between right- and left-hand sides of the diagram.

5.2.2 Alteration parageneses

All five lithologies in the Mount Dore region are altered to some degree. To unravel the mineralogical changes ensuing from alteration, sequences of observations have been made passing from unaltered protoliths into progressively more altered rock. Each lithology has developed its own distinct paragenesis, described below and summarized in Figure 5.3.

Granite

The effects of alteration in the granite are visible up to several hundred metres from the fault contact with metasediments, occurring in both brecciated and unbrecciated material. The alteration paragenesis is most clearly determined from the latter, but appears to be the same in the former, although here relative timing between some phases is equivocal (Figure 5.3a).

Furthest from the contact, in unbroken granite, the earliest alteration occurs as progressive replacement of plagioclase by muscovite, from the central parts of grains outwards. Complete pseudomorphism of plagioclase yields the pale-green colour reported in company drill logs as chloritization. Haematite dusting of the micas is common. Quartz veins clearly cut muscovite alteration, but replacement of plagioclase by the latter is most intense adjacent to the veins. Vein quartz is strained, but less so than magmatic quartz. Accessory phases in the veins include haematite, which appears from textures to have formed contemporaneously with quartz, and later tourmaline, carbonate and fluorite (*e.g.* JCU-27225). The dark blue to green-brown tourmaline formed earlier than carbonate. The three later phases become more abundant as both vein and host infill and replacement phases as the faulted granite-metasediment contact is approached, in places almost completely replacing earlier quartz. All formed later than muscovite. Veins appear to have provided long-lived channelways for fluid ingress. Magmatic biotite is generally completely replaced by chlorite. Rutile occurs sporadically as unaligned needles in chlorite, suggesting immobility of TiO_2 released

FIGURE 5.3: Alteration and mineralization parageneses for major lithologies at Mount Dore: (a) granite; (b) quartz-muscvovite schist; (c) carbonaceous slate; (d) meta-calcilutites.

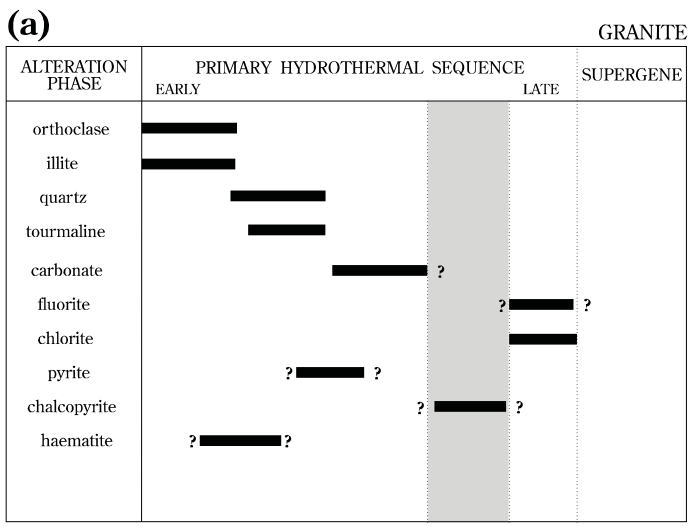
(a)
GRANITE
ALTERATION PHASE
PRIMARY HYDROTHERMAL SEQUENCE
EARLY
LATE
SUPERGENE
orthoclase
illite
quartz
tourmaline
carbonate
fluorite
chlorite
pyrite
chalcopyrite
haematite

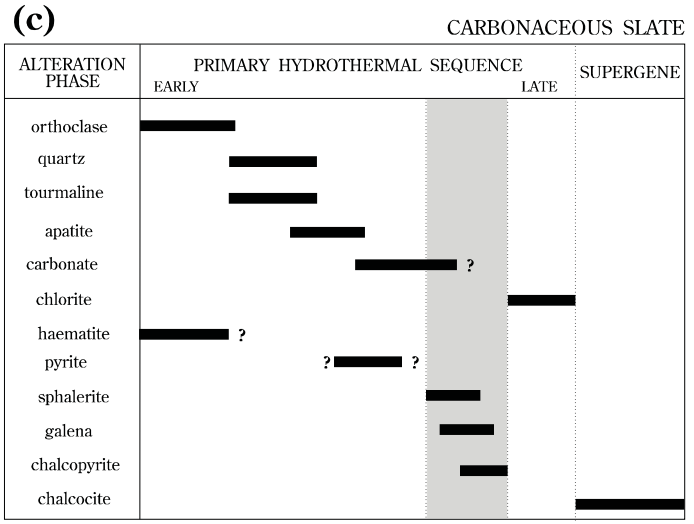
(c)
CARBONACEOUS SLATE
ALTERATION PHASE
PRIMARY HYDROTHERMAL SEQUENCE
EARLY
LATE
SUPERGENE
orthoclase
quartz
tourmaline
apatite
carbonate
chlorite
haematite
pyrite
sphalerite
galena
chalcopyrite
chalcocite

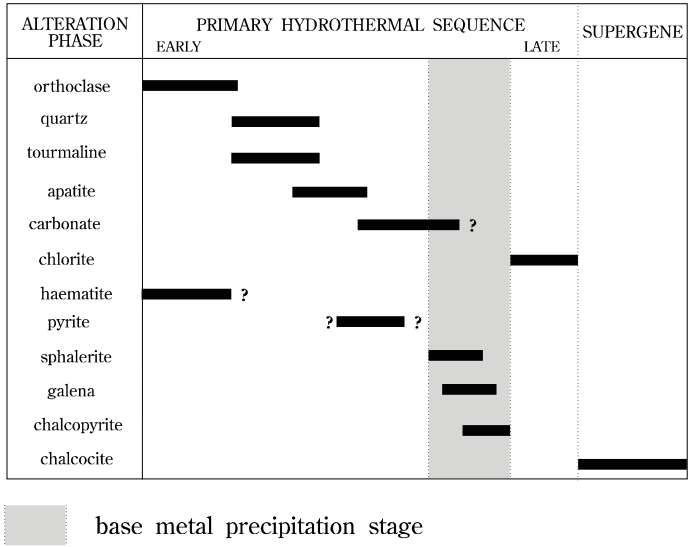
(b)
QUARTZ-MUSCOVITE SCHIST
ALTERATION PHASE
PRIMARY HYDROTHERMAL SEQUENCE
EARLY
LATE
SUPERGENE
orthoclase
quartz
tourmaline
apatite
carbonate
chlorite
haematite
pyrite
sphalerite
galena
chalcopyrite
chalcocite
base metal precipitation stage

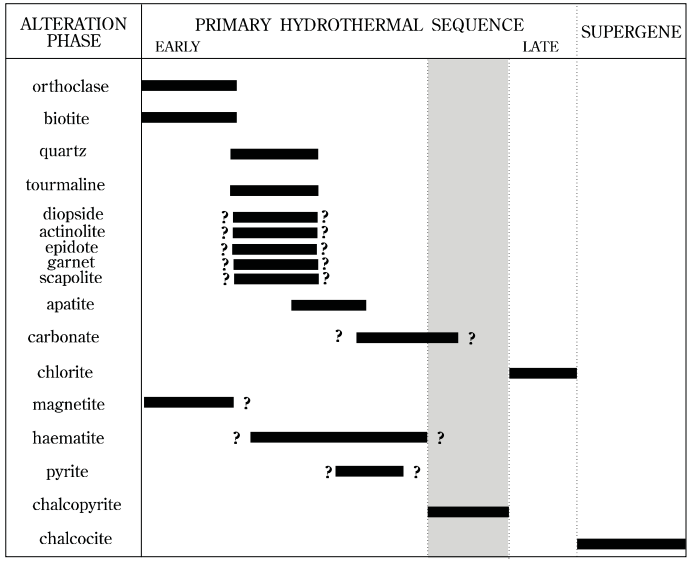
(d)
CALCILUTITE
ALTERATION PHASE
PRIMARY HYDROTHERMAL SEQUENCE
EARLY
LATE
SUPERGENE
orthoclase
biotite
quartz
tourmaline
diopside
actinolite
epidote
garnet
scapolite
apatite
carbonate
chlorite
magnetite
haematite
pyrite
chalcopyrite
chalcocite

from the biotite. Chlorite also appears in narrow, irregular veinlets along feldspar-feldspar and feldspar-quartz boundaries, and penetrates into muscovitized plagioclase. Muscovite and tourmaline are replaced or cross-cut in some places by narrow, irregular veinlets of chlorite. Chlorite probably formed later than carbonate, though textures are commonly ambiguous. Both replace magmatic sphene.

The alteration paragenesis in extensively brecciated granite is similar, except that the earliest alteration phase is microcline, occurring as infill between disrupted grains of microcline and quartz. It completely replaces plagioclase, and can be differentiated from the original microcline by being in crystallographic discontinuity, or having a different degree of haematite dusting (either cleaner or dirtier). It is impossible to tell whether the magmatic microcline has been replaced to any extent. Muscovite commonly replaces fine matrix fragments or occurs in fractures in grains, and is coarser where fragment size and abundance increases. It is later than the metasomatic microcline. Tourmaline is locally abundant as replacement of the matrix, occurring as fine (less than 0.1 mm), irregular to subhedral disseminated grains sometimes gathered into diffuse aggregates up to 6 mm (but usually less) in diameter. Apatite is spatially associated with tourmaline in the breccia matrix. It displays a similar grainsize, and perhaps a similar timing, though this is equivocal. Carbonate occurs as late matrix replacement and infill. Rare veins cross-cut the breccias, and carbonate replacement decreases in intensity away from these veins (*e.g.* JCU-27242). It is inferred from less disrupted granite to be later than tourmaline, although in the breccias this is difficult to demonstrate. Chlorite occurs as a late, matrix-replacement or vein infill phase. It is later than tourmaline. Again, its timing with respect to carbonate is equivocal. Platy haematite is scattered throughout the sample, in irregular trains or single crystals. Its position in the paragenesis is uncertain, though possibly after muscovite and before chlorite.

Quartz-muscovite schist

The comparatively simple mineral assemblage of the unaltered quartz-muscovite schist allows the alteration paragenesis to be readily discerned (Figure 5.3b). The unit is therefore an important standard with which alteration in the other units can be compared. The earliest alteration phase is microcline, containing abundant haematite dusting, and thereby giving the rock an overall orange-pink colour. In unbroken rock, it has been introduced along narrow fractures up to a few millimetres wide, and has permeated into the host along cleavage planes. It grows over S_3 crenulations, relics of which may be preserved just inside the alteration front by haematite and biotite inclusions in the microcline (*e.g.* JCU-27065). Ahead of the microcline alteration front, fine sericite, biotite or tourmaline may replace primary muscovite, commonly in the hinge zones of S_3 crenulations. In milled breccias, microcline attacks fragment margins, and remnants of the original lithology are generally only preserved in fragments larger than a few centimetres in diameter; smaller fragments are completely replaced.

Tourmaline formed later than microcline, and is generally replacive, after primary muscovite or later microcline (*e.g.* JCU-27064). In milled breccias, it penetrates along the foliation in fragments, as trains of irregular to subhedral grains up to 0.1 mm long. It also occurs as both an interstitial cement and a fragmental phase in milled breccia matrices. Some of the coarser, euhedral tourmaline is zoned, and partly fills vughs, the remainder of which are filled with later quartz. Alteration-related quartz is a relatively minor phase, occurring in rare veins or in minor vughs.

Sub- to euhedral crystals to 0.2mm of apatite are spatially associated with and appears to have formed after tourmaline and quartz, although relative timing is equivocal. Apatite grains are cross-cut by veinlets of carbonate and chlorite (*e.g.* JCU-27086). Carbonate is largely dolomite, as massive, pervasive replacement after comminuted breccias, and as vein and vugh infill away from these bodies. Chlorite formed last, as a predominantly replacive phase. There is a spatial association with carbonate, where this phase is present. In the shallow, southern parts of the deposit, it

occurs without carbonate, and imparts a very dark green colour to breccia matrices (*e.g.* JCU-27087). It has attacked all other alteration and mineralization phases, along grain boundaries and as subradiating clusters penetrating or completely replacing them. There is a preference for replacement of K-feldspar, biotite and carbonate.

Carbonaceous slate

The alteration paragenesis in carbonaceous slate is similar to that in the quartz-muscovite schist (Figure 5.3c). Highly brecciated slate is the most intensely altered, and in places the original rock type is totally obscured. The parent can only be deduced by assuming the breccia comprises fragments of the same material as occurs around it (up and down hole).

Early microcline is most obvious as pink-orange infill in veins, but also occurs in alteration haloes in host rock immediately adjacent to these veins. Haloes can extend up several times vein widths into the host. The zone closest to the vein generally comprises microcline and fine (<0.1 mm) tourmaline. Late chlorite occurs in the outer parts of the haloes, and may partly replace the inner zone, or cross-cut it in veinlets. Contact metamorphic chiastolite porphyroblasts close to veins are invariably altered to microcline, which may then be partly replaced by later alteration phases (*e.g.* JCU-27259).

Fine, massive replacement of host and replacive microcline by quartz is much more prevalent than in other lithologies. Alteration fronts extending relatively large distances from the source veins (tens of widths) are common, and such areas are generally bleached through removal of carbon (*e.g.* JCU-27219). Apatite is particularly common in zones of pervasive silicification, suggesting contemporaneity. Tourmaline is usually present in extensively silicified zones as pale-pink to dark (olive?) green, triangular prismatic crystals up to 1 mm in length (*e.g.* JCU-27092). Textural relationships indicate that tourmaline and quartz are also close to contemporaneous, but that the former is slightly earlier (*e.g.* JCU-27218).

Carbonate formed after quartz (and apatite?), as massive replacement of matrix and fragments in milled breccias (*e.g.* JCU-27217), along veins of earlier phases (particularly quartz), or in new veins. Chlorite is again last in the paragenesis, replacing all other phases to varying degrees.

Calcilutites

The best intersections of Staveley Formation lithologies were observed in the southern part of the prospect (*e.g.* DDH SHQ-78-23). These rocks were much more reactive throughout the metamorphic and metasomatic history, and consequently have complex parageneses, which have only been partially unravelled (Figure 5.3d). There is much ambiguity, and in some cases parageneses are inferred by analogy with sequences observed in other lithologies, but a general pattern is apparent.

Three rock types showing banding or well-developed foliation were considered as possible protolith candidates. The dominant banded lithology is a brick-red-brown to pink-orange, fine-grained (0.01-0.02 mm) quartz-feldspar rock, sometimes also containing fine biotite (e.g. JCU-27144, 27156). It is commonly extensively veined and partially replaced by hydrothermal microcline, quartz or carbonate. Epidote, actinolite and less commonly scapolite are also observed as euhedral to irregular crystals up to 0.5 mm long in or adjacent to quartz or carbonate veins (*e.g.* 27129, 27130, 27132). A single example of garnet associated with epidote and actinolite was observed in extensively altered host (JCU-27133). In most cases carbonate is clearly replacing quartz and calc-silicates, simply reusing and permeating out from existing vein structures. Most calc-silicate phases therefore appear to be at latest temporally associated with the introduction of quartz.

Another lithology clearly preceding hydrothermal alteration is fine-grained (<0.05 mm), green-brown, well-foliated quartz-biotite phyllite (*e.g.* JCU-27144, 27170). The earliest alteration in this lithology is microcline, as relatively coarse vein infill and as replacement at similar grain size as the host adjacent to veins. The veins

are commonly subsequently reused by later quartz, carbonate and coarse muscovite (*e.g.* JCU-27150). Quartz occurs mainly as infill, and the carbonate is clearly later, replacing both quartz and microcline, and commonly extends into the host as rhomboidal porphyroblasts (*e.g.* JCU-27170). The position of muscovite in the paragenesis is uncertain.

A third possible protolith has pale green bands one to two centimetres thick comprising interlocking arrays of coarse (up to 2 mm) diopside, actinolite, scapolite and minor carbonate interlayered with pale grey bands up to 10 centimetres thick consisting predominantly of carbonate, but also containing partially replaced small (0.2-0.3 mm) sub-euhedral cleavage fragments of actinolite and lesser diopside, quartz and microcline (*e.g.* JCU-27122). Such a rock could be explained in terms of (possibly contact) metamorphism of a layered sequence of variably siliceous and dolomitic sediments. The carbonate in the pale green layers occurs as replacement and vein infill after the other phases, and in the pale grey layers appears to be at least partly replacive, although veins do not cut these layers. It has therefore been at least remobilized. The other phases may be contemporaneous with each other, but this cannot be conclusively demonstrated.

The association of many calc-silicate phases with quartz or carbonate alteration, in zones of extensive veining or suspected intense brecciation, suggests that they could alternatively be the products of metasomatic reactions, rather than or in addition to contact metamorphism. They are certainly early in the paragenesis. Partial to complete pseudomorphic replacement of these phases is common, particularly of actinolite, usually by fine sericite (*e.g.* JCU-27099, 27107, 27130), and subsequently by carbonate or chlorite or both (*e.g.* JCU-27099). Fine Fe-oxide (haematite?) was released during sericitization. Fine sericite also replaces quartz in some instances (*e.g.* JCU-27143).

Hydrothermal biotite is also an early alteration phase. It is occasionally observed as scattered flakes in diopside, and in associated, partly to completely sericitized actinolite (*e.g.* JCU-27123). This texture is ambiguous; biotite may have been trapped as inclusions, and therefore be earlier, or have formed as later patchy

replacement. All these phases formed earlier than the carbonate and chlorite alteration, however. More commonly, however, biotite is developed as relatively coarse-grained (up to 0.2 mm) masses, usually in association with, but preceding, extensive carbonate replacement (*e.g.* JCU-27140). Minor late quartz and fluorite infill precipitated after carbonate (*e.g.* JCU-27142). The biotite-carbonate zones are commonly interlayered with the fine quartz-feldspar rock (*e.g.* SHQ-78-23: 138-143 m), and may be extensively altered breccia zones. Actinolite and magnetite are occasionally also present, and partly replaced by carbonate (*e.g.* JCU-27141). In some samples the hydrothermal biotite has burst apart along cleavage planes, and the spaces have filled with fibrous haematite-dusted microcline or quartz. Biotite cleavage planes are commonly kinked (*e.g.* JCU-27128).

Magnetite is the main coarse-grained Fe-oxide phase, and was produced in at least two stages by release and reduction of haematite from microcline-rich host during alteration. The earliest is associated with quartz veins and adjacent silicification, and commonly has fractures filled with carbonate (*e.g.* JCU-27132, 27134). The second is associated with extensive chloritization. Magnetite is usually replaced along grain rims by haematite, but the timing of haematite with respect to other phases is uncertain (*e.g.* JCU-27134).

Tourmaline is rare in altered calcilutites, although in quartz-microcline rocks close to the southward extension of the fault contact with the granite there is a zone of quartz veins with haloes of silicification also containing abundant tourmaline as euhedral grains up to 1.5 mm long. Textures suggest tourmaline formed just prior to introduction of quartz, and is certainly cut by carbonate veins (*e.g.* JCU-27147).

Chlorite is the latest alteration phase. It occurs both as radiating clusters or irregular veinlets partially to completely replacing selected earlier phases (particularly biotite), and also as massive replacement of the entire rock. In the latter situation, alteration fronts well-defined, and chlorite-filled veins apparently cut chloritized rock, although close inspection shows the vein material to in fact be replacive after earlier infill phases (quartz and carbonate; *e.g.* JCU-27134).

In summary, Staveley Formation lithologies have experienced a complex history of fluid-rock interaction, producing a variety of calc-silicate, K-silicate, carbonate and oxide phases. Apart from the calc-silicate phases, however, the same succession of potassic, through silicic, carbonatic and finally chloritic alteration as recognized from other lithologies appears to have prevailed. Calc-silicate minerals may be contact metamorphic in origin, or have formed by early interaction of the hydrothermal fluid with reactive calcareous rocks.

Quartzite

Brecciation and alteration observed only rarely in this lithology. In such examples (*e.g.* JCU-27106) interfragment material is microcline and later muscovite, as irregular "veinlets". Chlorite may partly replace the former. Minor tourmaline occurs as small replacive aggregates of euhedral crystals. Late quartz alteration may be present, but is indistinguishable from the host. All metasomatic phases are fine-grained.

5.2.3 Mineralization parageneses

All sulphide phases occur at consistent places in the paragenesis, regardless of the lithology in which they are developed. Some selected textural relationships are illustrated in Figure 5.4. Pyrite is the earliest sulphide, occurring as replacive vein-like stringers along veins of earlier alteration phases, and as replacive, small to large (up to 5 mm), sub- to euhedral grains to irregular blebs and masses in altered host, commonly with inclusions of microcline, tourmaline and quartz (*e.g.* JCU-27080, 27108). It shows a strong spatial association with quartz veining or silicification, and carbonate precipitated afterwards. Where relatively coarse-grained Fe-oxides occur with pyrite, the latter crystallized later, by nucleating on and in brecciated examples of the former (*e.g.* JCU-27134). Cobaltite is uncommon, but occurs as euhedral grains in galena and sphalerite, or closely associated with pyrite. It sometimes contains minor arsenopyrite

FIGURE 5.4: Reflected light photomicrographs of representative sulphide and oxide textures: (a) cobaltite and arsenopyrite spatially (and temporally?) associated with pyrite (JCU-27263); (b) cobaltite as inclusions in sphalerite and galena (JCU-27223); (c) sulphide replacement after microcline and quartz in a vein; early pyrite is fractured and replaced by sphalerite, galena and chalcopyrite (JCU-27275); (d) irregular chalcopyrite veining and partial replacement after pyrite; secondary digenite forms a rim on chalcopyrite (JCU-27271); (e) chalcopyrite infill and replacement in fractured and fragmented sphalerite (JCU-27216); (f) galena and chalcopyrite filling in fracture in sphalerite; chalcopyrite also occurs as a spotty "disease" in sphalerite (JCU-27275); (g) chalcopyrite replacement after galena (JCU-27213); (h) bornite as a late replacive rim around chalcopyrite in a carbonate (after quartz) vein; haematite formed earlier than both sulphides (JCU-27096); (i) bornite and digenite replacing chalcopyrite (JCU-27263); (j) chalcocite filling interstices between and replacing rims of fractured pyrite (JCU-27078). All photomicrographs were taken under plane polarized light.

ABBREVIATIONS: **asp** - arsenopyrite; **bor** - bornite; **chc** - chalcocite; **co** - cobaltite; **cpy** - chalcopyrite; **dig** - digenite; **gal** - galena; **hm** - haematite; **py** - pyrite; **sph** - sphalerite

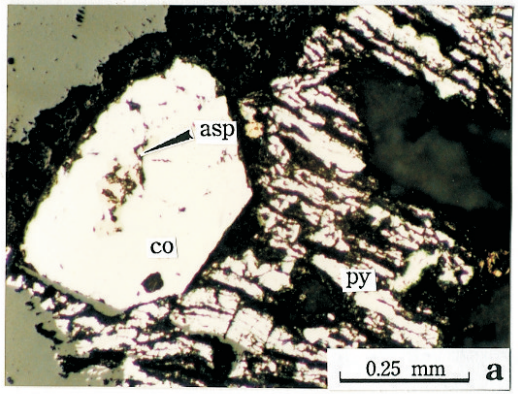
asp
co
py
0.25 mm
a

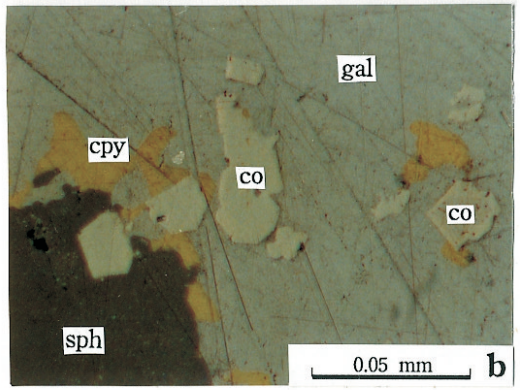
gal
cpy
co
co
sph
0.05 mm
b

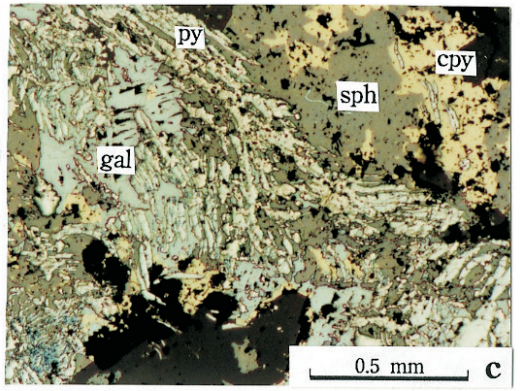
py
cpy
sph
gal
0.5 mm
c

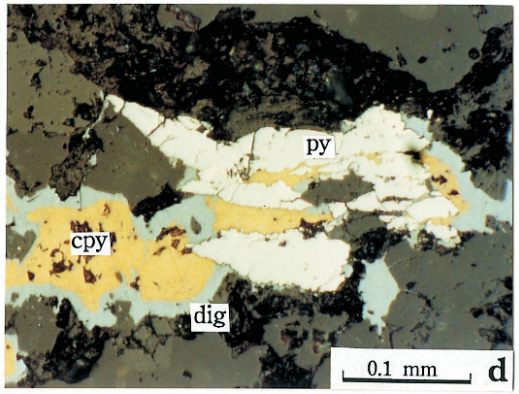
py
cpy
dig
0.1 mm
d

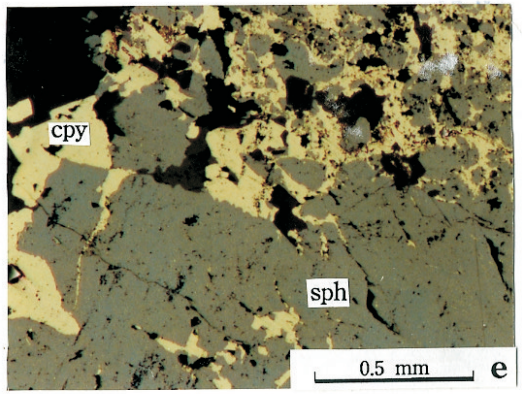
cpy
sph
0.5 mm
e

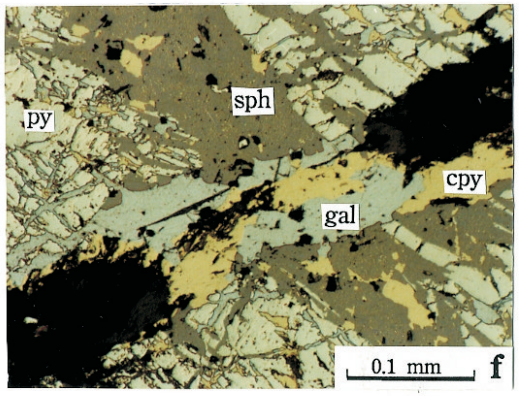
py
sph
cpy
gal
0.1 mm
f

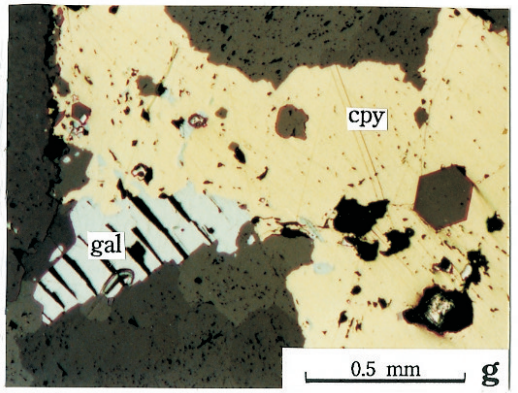
cpy
gal
0.5 mm
g

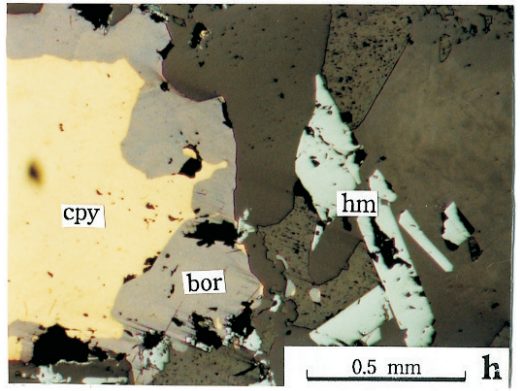
cpy
hm
bor
0.5 mm
h

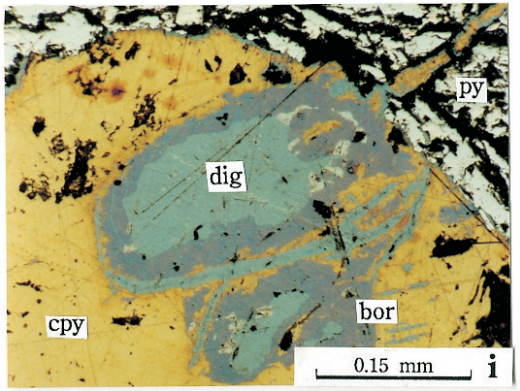
py
dig
cpy
bor
0.15 mm
i

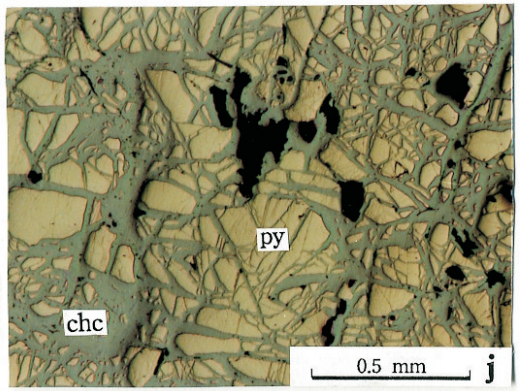
py
chc
0.5 mm
j

(*e.g.* JCU-27223, 27263; Figure 5.4a,b). Timing is somewhat equivocal, but arsenosulphides may have precipitated coevally with pyrite.

Pyrite is the only sulphide found in the quartzite, as small, rare grains. It is also the dominant phase in the granite, though still comparatively rare, and becoming conspicuous only in the fine breccias as sub- to euhedral crystals and fragments to 0.5 mm, close to the contact with the metasediments. Chalcopyrite is very rare in the granite, precipitating on or replacing some of the pyrite. Metasediments within the Mount Dore Fault Zone have much more abundant copper, lead and zinc sulphides. All these sulphides are later than, but show a strong spatial association with pyrite. In these situations, pyrite is invariably extensively fractured or fragmented, and other sulphides surround and fill in fractures in grains (JCU-27216; Figure 5.4c,d). They also precipitated after dolomitic alteration, partly replacing breccia matrices in their most spectacular form (*e.g.* JCU-27217). Sphalerite is zoned, suggesting fluctuating Fe content or incremental growth. It also commonly contains fine inclusions of chalcopyrite. These may form by exsolution, copreciptation, or replacement (Bortnikov *et al.*, 1991). The first two processes seem unlikely, however, because elsewhere sphalerite is brecciated and the fractures filled with later chalcopyrite, suggesting that the spotty inclusions are replacement features (Figure 5.4e). Galena shows a similar relationship to sphalerite (Figure 5.4f), indicating later growth, and is itself replaced by chalcopyrite (Figure 5.4g).

Minor, probably secondary (*i.e.* related to late weathering) sulphides are bornite, covellite and digenite. Covellite occurs along chalcopyrite-pyrite boundaries. Bornite and digenite generally form narrow rims around chalcopyrite, although the latter may occur in narrow fractures cutting altered host (Figure 5.4h,i). Scott (1988) observed carollite associated with sphalerite (CSIRO-101463) and pyrite (CSIRO-101295), and native silver replacing pyrite (CSIRO-101383 and 101463) and secondary djurleite (CSIRO-101340).

Chalcocite is a significant sulphide phase, particularly at shallower levels. It occurs as irregular blebs and veins up to several centimetres in diameter or width

replacing milled breccia matrices. It is probably also of supergene origin, but has also formed by replacement of fractured and fragmented pyrite (*e.g.* Figure 5.4j; JCU-27085). It contains inclusions of earlier alteration phases (*e.g.* JCU-27077), but these are likely to have been inclusions originally present in the pyrite. Carbonate is generally absent where chalcocite occurs, but may have been leached away. Minor covellite replaces chalcocite in patches (JCU-27093). Chrysocolla is also present in samples from close to the surface (*e.g.* JCU-27085), in veins and replacement rims in and around chalcocite. Ophel (1980) noted trace cuprite and chalcotrichite (DDH-SHQ-76-12: 187.5 m) and native copper (same DDH: 175.7 m) along late fractures.

5.3 MINERAL GEOCHEMISTRY

5.3.1 Diopside

Pyroxene was identified in two samples of banded calc-silicate rocks (JCU-27122, JCU-27123), both interpreted to be contact metamorphosed Staveley Formation. Optical properties are consistent with diopside, and two microprobe analyses of this phase obtained by Ophel (1980) show it to be almost the pure end-member, with very little substitution of Mg^{2+} by Fe^{2+} (Table 5.2; Figure 5.5).

5.3.2 Amphibole

All amphiboles observed at Mount Dore come from variably altered Staveley Formation lithologies. 36 analyses from eight minerals in six samples were obtained in this study. Twenty-six analyses from five samples are also available from Ophel (1980). Structural formulae were calculated on the basis of 24(O+OH+Cl) per formula unit, and Fe^{3+} content estimated by charge balance (Table 5.3). Compositions are plotted on Figure 5.6 using the programme **AMPHIBOL** (Richard and Clarke, 1990). The specimens are named according to the recommendations of Leake (1978).

TABLE 5.2: Diopside compositional information obtained by Ophel (1980). Structural formulae calculated on the basis of six oxygens per formula unit, using the PYROXENE.EXE subroutine in MINFILE program (Afifi and Essene, 1988). Fe_2O_3 is calculated using charge balance and assuming four cations. Sample locality and brief description is provided in Table D2 (Appendices).

	59295/14	**59295/15**
SiO_2	53.68	52.95
TiO_2	0.06	0.06
Al_2O_3	0.3	0.26
Cr_2O_3	0.03	0.03
Fe_2O_3	2.24	3.3
FeO	1.87	1.27
MnO	0.21	0.18
MgO	15.78	15.87
CaO	25.45	25.27
Na_2O	0.3	0.27
K_2O	0.01	-
TOTAL	**99.93**	**99.46**
#Si IV	1.971	1.956
#Al IV	0.013	0.011
T site	**1.984**	**1.967**
#Al VI	-	-
#Ti	0.002	0.002
#Cr	0.001	0.001
#Fe3+	0.062	0.092
#Fe2+	0.058	0.039
#Mn2+	0.007	0.006
#Mg	0.864	0.874
#Ca	1.001	1.0
#Na	0.021	0.019
#K	-	-
M1,M2	**2.016**	**2.033**
#O	6.000	6.000

FIGURE 5.5: Pyroxene quadrilateral (after Morimoto, 1988), showing the composition of pyroxenes from Mount Dore as determined by Dimo (1980). Although they actually fall outside the diagram (probably due to analytical error), they are clearly diopsidic.

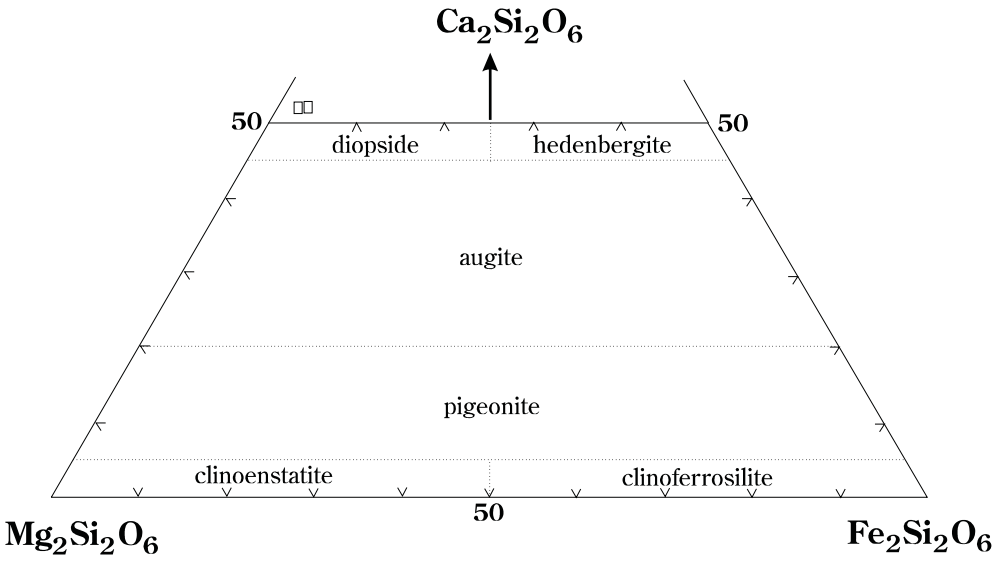

TABLE 5.3: Summary compositional information for amphiboles at Mount Dore. Numbers in parentheses indicate number of analyses from each grain. Structural formulae have been calculated on the basis of 24(O+OH+F+Cl). Samples with the prefix 59- are from the data set of Ophel (1980). Sample localities and brief descriptions are given in Tables D1 and D2, and complete compositional data in Table D4 (all in Appendices).

	27099/1 (5)	**27121/1 (9)**	**27121/3 (4)**	**27130/1 (4)**	**27130/4 (3)**	**27133/3 (4)**	**27141/2 (4)**	**27145/1 (3)**	**59284 (5)**	**59295 (10)**	**59308 (5)**	**59313 (3)**	**59314 (3)**
SiO_2	54.17	54.379	55.365	52.505	54.77	53.772	58.875	56.263	52.594	53.833	53.906	53.587	49.9
TiO_2	0.084	0.036	0.07	-	-	0.018	-	0.1	0.088	0.035	0.08	0.027	0.003
Al_2O_3	2.32	1.662	1.482	2.787	0.837	1.952	0.112	1.553	2.93	1.009	1.64	2.547	3.303
Cr_2O_3	0.024	0.049	0.013	0.02	-	0.013	0.063	0.023	0.026	0.004	-	-	-
Fe_2O_3	0.001	0.002	-	0.001	0.003	-	-	-	0.002	-	0.003	0.001	-
FeO	9.428	9.524	10.328	13.719	14.434	11.913	2.142	5.667	9.224	10.813	11.321	11.356	12.553
MnO	0.195	0.772	0.635	0.157	1.08	0.87	0.06	0.19	0.516	0.13	0.102	0.33	0.133
MgO	17.5	17.18	17.215	14.813	13.963	17.0	23.433	20.537	18.75	17.574	17.456	18.043	16.027
CaO	12.588	12.787	12.693	12.078	12.507	11.257	13.515	12.927	12.094	13.195	12.722	12.97	12.07
Na_2O	0.586	0.318	0.347	0.822	0.263	0.213	0.108	0.423	0.266	0.223	0.182	0.323	0.883
K_2O	0.254	0.211	0.138	0.507	0.063	0.063	0.018	0.137	0.362	0.085	0.136	0.257	0.07
H_2O	2.079	2.078	2.112	2.023	2.061	2.075	2.204	2.155	2.082	2.068	2.081	2.122	2.007
Cl	0.074	0.041	0.015	0.13	0.023	0.013	0.015	-	0.02	0.032	0.036	-	-
O=Cl	-0.017	-0.009	-0.003	-0.029	-0.005	-0.003	-0.003	-	-0.005	-0.007	-0.008	-	-
TOTAL	**99.286**	**99.03**	**100.41**	**99.533**	**99.999**	**99.156**	**100.542**	**99.975**	**98.95**	**98.994**	**99.657**	**101.563**	**96.949**
#Si IV	7.741	7.808	7.844	7.657	7.947	7.759	7.994	7.828	7.556	7.774	7.734	7.572	7.454
#Al IV	0.259	0.192	0.156	0.343	0.053	0.241	0.006	0.172	0.444	0.172	0.266	0.424	0.546
#Fe +3	-	-	-	-	-	-	-	-	-	-	-	-	-
#Ti IV	-	-	-	-	-	-	-	-	-	0.004	-	0.003	-
T site	**8.000**	**8.000**	**8.000**	**8.000**	**8.000**	**8.000**	**8.000**	**8.000**	**8.000**	**7.95**	**8.000**	**7.999**	**8.000**
#Al VI	0.132	0.089	0.092	0.136	0.09	0.091	0.012	0.083	0.053	-	0.012	-	0.035
#Fe +3	-	-	-	-	-	-	-	-	-	-	-	-	-
#Ti	0.009	0.004	0.007	-	-	0.002	-	0.01	0.01	-	0.009	-	-
#Cr	0.003	0.006	0.001	0.002	-	0.001	0.007	0.003	0.003	-	-	-	-
#Mg	3.728	3.677	3.636	3.22	3.02	3.657	4.743	4.26	4.016	3.783	3.734	3.801	3.569
#Fe +2	1.127	1.144	1.224	1.641	1.751	1.248	0.238	0.645	0.919	1.216	1.246	1.199	1.396
#Mn	0.002	0.08	0.039	-	0.133	-	-	-	-	-	-	-	-
#Ca	-	-	-	-	0.006	-	-	-	-	-	-	-	-
M1,2,3	**5.000**	**5.000**	**5.000**	**5.000**	**5.000**	**5.000**	**5.000**	**5.000**	**5.000**	**5.000**	**5.000**	**5.000**	**5.000**
#Mg	-	-	-	-	-	-	-	-	-	-	-	-	-
#Fe +2	-	-	-	0.032	-	0.19	0.005	0.014	0.19	0.09	0.113	0.143	0.172
#Mn	0.022	0.014	0.037	0.019	-	0.106	0.007	0.022	0.063	0.016	0.012	0.039	0.017
#Ca	1.927	1.967	1.927	1.887	1.939	1.704	1.966	1.927	1.748	1.894	1.875	1.818	1.811
#Na	0.051	0.019	0.036	0.061	0.061	-	0.022	0.036	-	-	-	-	-
M4 site	**2.000**	**2.000**	**2.000**	**2.000**	**2.000**	**2.000**	**2.000**	**2.000**	**2.000**	**2.000**	**2.000**	**2.000**	**2.000**
#Ca	-	-	-	-	-	0.036	-	-	0.114	0.147	0.081	0.146	0.121
#Na	0.111	0.07	0.059	0.171	0.013	0.06	0.006	0.078	0.074	0.062	0.051	0.088	0.256
#K	0.046	0.039	0.025	0.094	0.012	0.012	0.003	0.024	0.066	0.016	0.025	0.046	0.013
A site	**0.158**	**0.108**	**0.084**	**0.266**	**0.024**	**0.107**	**0.01**	**0.102**	**0.255**	**0.225**	**0.156**	**0.281**	**0.39**
#O	22.000	22.000	22.000	22.000	22.000	22.000	22.000	22.000	22.000	22.000	22.000	22.000	22.000
#OH	1.982	1.99	1.996	1.968	1.995	1.997	1.996	2.00	1.995	1.992	1.992	2.000	2.000
#Cl	0.018	0.01	0.004	0.032	0.006	0.003	0.003	-	0.005	0.008	0.009	-	-
Charge	**0.000**	**0.000**	**0.000**	**0.000**	**0.000**	**0.000**	**0.000**	**0.000**	**0.000**	**0.000**	**0.000**	**0.000**	**0.000**
Cations	**16.000**	**16.000**	**16.000**	**16.000**	**16.000**	**16.000**	**16.000**	**16.000**	**16.000**	**16.000**	**16.000**	**16.000**	**16.000**
Species	**act**	**act**	**act**	**act**	**act**	**act**	**trem**	**act**	**act**	**act**	**act**	**act**	**act[c] hb**

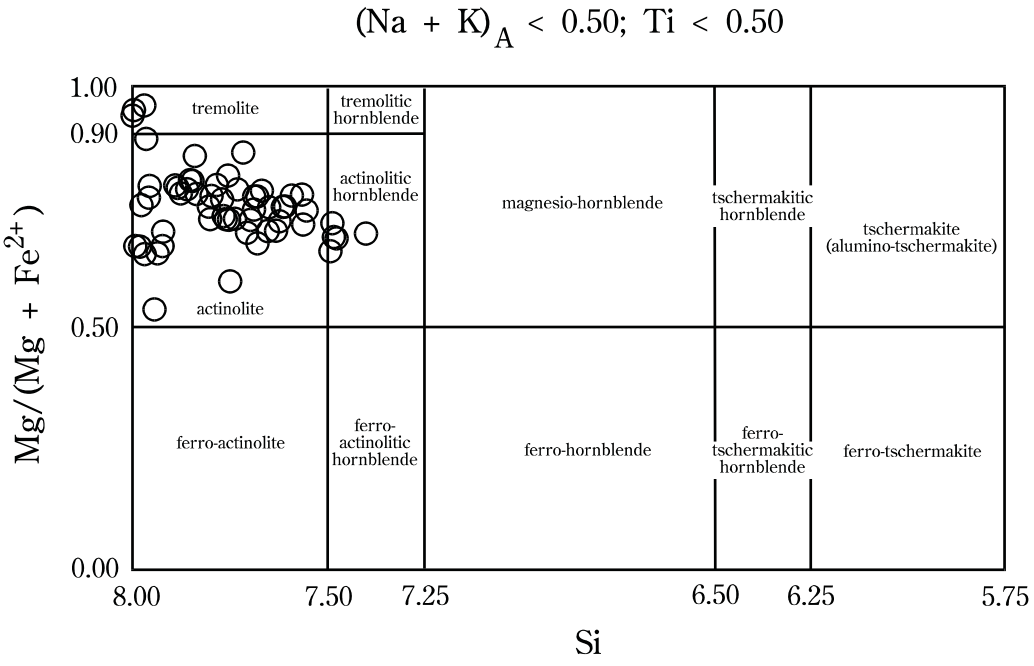

FIGURE 5.6: Plot of all compositional data for amphiboles, on the appropriate diagram as recommended by Leake (1978). Most analyses fall within the actinolite field.

Eleven of the thirteen samples are actinolite, one is tremolite, and one actinolitic hornblende. The Cl content of the amphiboles is uniformly very low. This is expected, given the relatively Mg-rich character of the amphiboles, and the demonstrated Mg-Cl avoidance shown by silicates (*e.g.* Munoz, 1984). Unfortunately, the low Cl-content leads to an interpreted OH-content very close to the maximum of two per formula unit. This is unlikely to be the case, because there is also a known preference for F over OH in silicates with high Mg/Fe ratios (Ekström, 1972). No amphiboles from Mount Dore have been analysed for F, but a high content is probable. These calcic, Al-poor compositions are consistent with an origin by either metamorphism or hydrothermal alteration of calcareous sediments.

5.3.3 Scapolite

Scapolite occurs in several specimens (*e.g.* JCU-27122, 27132), as part of the early paragenesis in calcareous Staveley Formation rocks. Structural formulae have been calculated on the basis of 12(Si+Al) for the two available scapolite analyses from Ophel (1980)(Table 5.4). Both lie close to the line joining marialite ($Na_4[Al_3Si_9O_{24}]Cl$) and mizzonite ($NaCa_3[Al_5Si_7O_{24}]CO_3$)(Figure 5.7).

5.3.4 Epidote

Epidote is also only observed in Staveley Formation lithologies. Twenty-two analyses of epidote were obtained from two of my specimens (JCU-27130 and 27133), and a further eight analyses from two additional samples (USyd-59255 and 59314) from Ophel (1980)(Table 5.5). All iron Fe was assumed to be ferric, and structural formulae were calculated on the basis of 12 oxygens per formula unit. A plot of Fe3+ versus Al_{tet} (Figure 5.8) shows a "normal" epidote composition, with substitution of about one atom of Fe3+ for tetrahedral Al per formula unit. The plot does show an approximately linear trend of decreasing Fe^{3+} with increasing Al(IV), and one sample (JCU-27133) was mapped to test for regular compositional variation from crystal core to rim. The data are extremely sketchy, however, and no conclusions can be drawn.

TABLE 5.4: Scapolite compositional information obtained by Ophel (1980). Structural formulae are calculated on the basis of 12(Si+Al). #CO_3 is estimated as (1-#Cl). Sample locality and brief description is provided in Table D2 (Appendices).

	59295/1	**59295/2**
SiO_2	52.61	50.65
TiO_2	-	0.01
Al_2O_3	24.76	24.52
Cr_2O_3	0.02	0.03
Fe_2O_3	0.08	0.09
CaO	12.47	12.09
Na_2O	6.12	6.69
K_2O	1.1	0.66
Cl	1.63	1.72
O=Cl	-0.37	-0.39
TOTAL	**98.42**	**96.07**
#Si+4	7.719	7.641
#Ti+4	-	0.001
#Al+3	4.281	4.359
#Cr+3	0.002	0.004
#Fe+3	0.009	0.010
#Ca+2	1.960	1.954
#Na+1	1.741	1.957
#K+1	0.206	0.127
# cations	**15.918**	**16.053**
#Cl	0.405	0.44
CO_3	0.595	0.560
charge	**49.214**	**49.239**

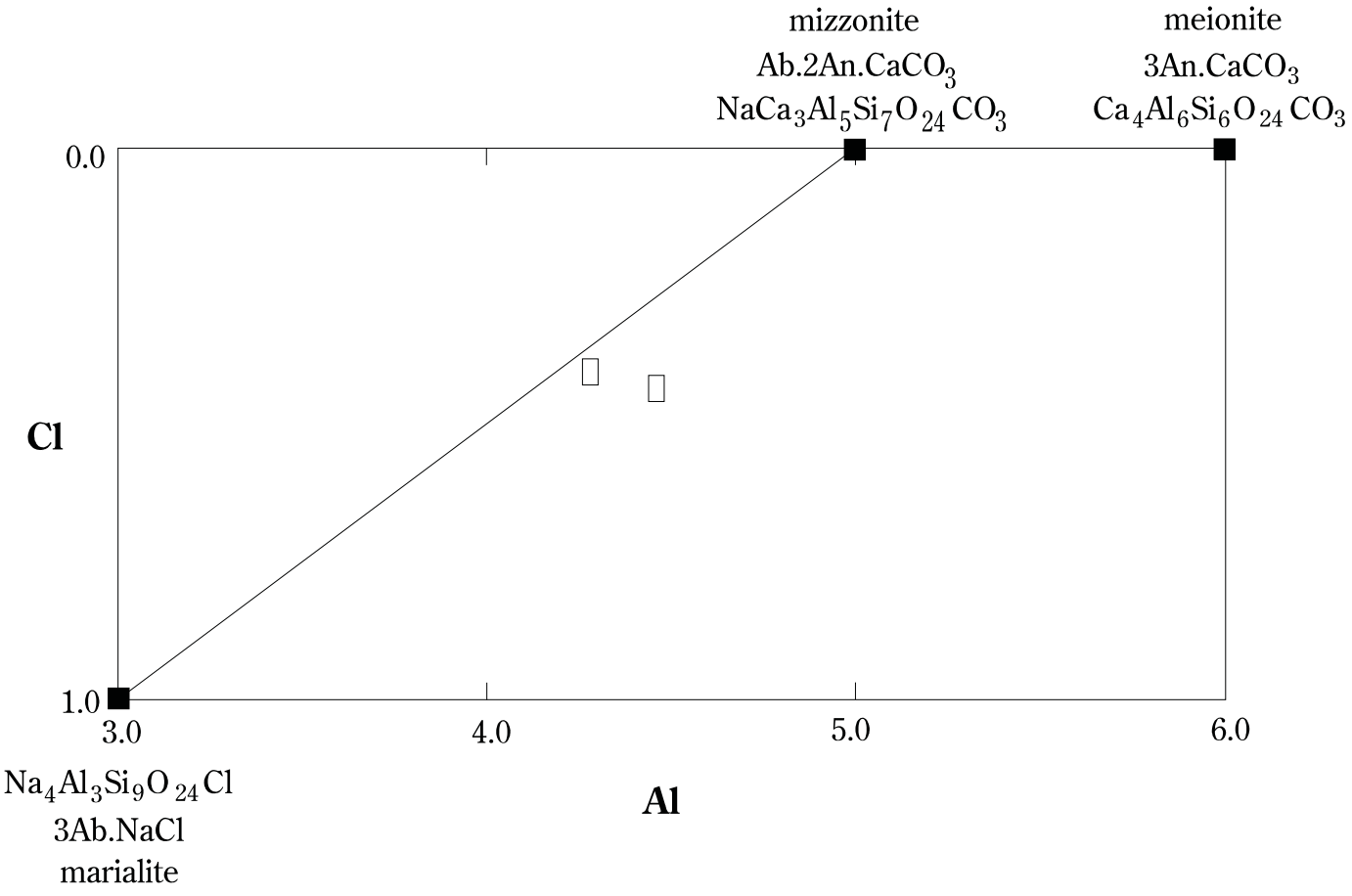

FIGURE 5.7: Plot of scapolite compositions from Mount Dore, on the diagram recommended by Orville (1975).

TABLE 5.5: Complete compositional data for epidote at Mount Dore. Structural formulae calculated on the basis of 12 oxygens per formula unit. FeO and Mn_2O_3 calculated from charge balance considerations. Samples with the prefix 59- are from the data set of Ophel (1980). Sample localities and brief descriptions are given in Tables D and D2 (Appendices).

	27130 /5/1	**27130 /5/2**	**27130 /5/3**	**27130 /5/4**	**27130 /5/5**	**27130 /5/6**	**27130 /5/7**	**27130 /5/8**	**27130 /5/9**	**27130 /5/10**	**27133 /4/1**	**27133 /4/2**	**27133 /4/3**	**27133 /4/4**	**27133 /4/5**	**27133 /4/6**	**27133 /4/7**	**27133 /4/8**	**27133 /4/9**	**27133 /4/10**	**27133 /4/11**	**27133 /4/12**
SiO_2	37.45	37.7	37.91	37.27	36.46	37.54	37.42	36.99	36.85	37.18	37.41	37.55	38.04	35.82	37.32	37.47	37.32	36.94	37.6	37.54	36.42	37.69
TiO_2	0	-	-	0.08	0.23	0.16	-	0.09	-	-	-	-	-	-	-	-	-	-	0.11	-	0	-
Al_2O_3	21.34	20.22	22.59	21.1	19.96	22.44	19.94	22.8	20.27	21.11	21.12	21.15	21.87	18.95	21.95	21.11	21.71	21.09	21.28	22.17	21.35	22.41
Fe_2O_3	15.75	15.58	14.32	15.37	15.67	9.99	16.88	12.78	12.31	15.1	16.08	15.89	14.22	5.79	14.12	14.91	14.51	15.75	14.49	14.49	14.45	13.46
Mn_2O_3	-	0.01	0.23	-	0.33	0.01	0.01	0.79	0.01	-	0.27	0.21	0.01	0.01	0.17	-	0.11	-	-	0.41	0.34	-
FeO	-	0.83	-	0.21	-	2.29	0.38	0	2.68	0.63	-	-	0.73	7.11	-	0.25	-	-	0.53	0	-	0.51
MnO	-	0.16	-	-	-	0.3	0.22	-	0.3	0.22	0.01	-	0.1	0.09	-	-	-	-	-	-	0	0.09
CaO	23.1	22.87	22.8	23.12	22.23	21.41	22.59	23.16	20.95	22.22	23.25	23.02	23.14	17.14	23.08	23.23	23.3	23.27	23.17	23.18	23.19	23.07
Na_2O	0.22	-	0.25	-	0.24	0.1	0.09	0.15	-	0.09	-	0.19	-	0.13	0.09	-	-	0.11	-	0.09	0.12	-
H_2O	1.78	1.85	1.88	1.86	1.78	1.82	1.85	1.75	1.79	1.85	1.87	1.82	1.88	1.64	1.84	1.85	1.85	1.74	1.86	1.85	1.67	1.87
TOTAL	**99.64**	**99.22**	**99.98**	**99**	**96.91**	**96.06**	**99.39**	**98.51**	**95.16**	**98.4**	**100.02**	**99.83**	**99.99**	**86.69**	**98.56**	**98.83**	**98.8**	**98.9**	**99.04**	**99.73**	**97.54**	**99.09**
#Si IV	3.007	3.059	3.021	3.021	3.023	3.098	3.039	2.981	3.105	3.031	3.007	3.015	3.043	3.288	3.020	3.038	3.020	2.991	3.040	3.006	2.979	3.032
#Al IV	-	-	-	-	-	-	-	0.019	-	-	-	-	-	-	-	-	-	0.009	-	-	0.021	0.000
Z site	**3.007**	**3.059**	**3.021**	**3.021**	**3.023**	**3.098**	**3.039**	**3.000**	**3.105**	**3.031**	**3.007**	**3.015**	**3.043**	**3.288**	**3.020**	**3.038**	**3.020**	**3.000**	**3.004**	**3.006**	**3.000**	**3.032**
#Al VI	2.020	1.934	2.121	2.015	1.950	2.183	1.908	2.147	2.013	2.029	2.001	2.002	2.062	2.050	2.094	2.017	2.070	2.004	2.028	2.092	2.038	2.125
#Fe +3	0.952	0.951	0.859	0.937	0.978	0.620	1.032	0.775	0.780	0.926	0.973	0.960	0.856	0.400	0.860	0.910	0.880	0.960	0.882	0.873	0.889	0.815
#Mn +3	-	0.001	0.013	-	0.020	0.001	0.001	0.047	0.001	-	0.017	0.012	-	0.001	0.009	-	0.006	-	-	0.024	0.020	-
#Ti	-	-	-	0.005	0.014	0.010	-	0.005	-	-	-	-	-	-	-	-	-	-	0.007	-	-	-
#Fe +2	-	0.056	-	0.013	-	0.158	0.026	-	0.189	0.037	-	-	0.049	0.545	-	0.016	-	-	0.035	-	-	0.034
#Mn +2	-	0.010	-	-	-	0.020	0.014	-	0.016	0.007	-	-	0.006	0.004	-	-	-	-	-	-	-	0.005
Y site	**2.971**	**2.952**	**2.993**	**2.971**	**2.963**	**2.992**	**2.981**	**2.975**	**2.999**	**2.999**	**2.990**	**2.974**	**2.973**	**3.000**	**2.963**	**2.943**	**2.960**	**2.964**	**2.951**	**2.990**	**2.948**	**2.979**
#Mn +3	-	-	0.001	-	0.001	-	-	0.001	-	-	-	0.001	-	-	0.001	-	0.001	-	-	0.001	0.001	-
#Mn +2	-	0.001	-	-	-	0.001	0.001	-	0.005	0.008	0.001	-	0.001	0.003	-	-	-	-	-	-	-	0.001
#Fe +2	-	-	-	0.001	-	-	-	-	-	0.006	-	-	-	0.001	-	0.001	-	-	0.001	-	-	-
#Ca	1.987	1.988	1.946	2.008	1.975	1.893	1.965	2.000	1.891	1.941	2.002	1.980	1.983	1.685	2.001	2.018	2.020	2.019	2.007	1.989	2.032	1.988
#Na	0.034	-	0.039	-	0.039	0.016	0.014	0.023	-	0.014	-	0.030	-	0.023	0.014	-	-	0.017	-	0.014	0.019	-
X site	**2.022**	**1.989**	**1.986**	**2.009**	**2.014**	**1.910**	**1.981**	**2.025**	**1.896**	**1.969**	**2.003**	**2.011**	**1.984**	**1.713**	**2.017**	**2.019**	**2.021**	**2.036**	**2.008**	**2.004**	**2.052**	**1.989**
#O	12.000	12.000	12.000	12.000	12.000	12.000	12.000	12.000	12.000	12.000	12.000	12.000	12.000	12.000	12.000	12.000	12.000	12.000	12.000	12.000	12.000	12.004
#OH	0.951	1.004	0.997	1.004	0.985	1.004	1.004	0.940	1.003	1.004	1.004	0.976	1.004	1.003	0.991	1.003	1.000	0.938	1.004	0.989	0.909	1.004
Total*	**20.951**	**21.004**	**20.997**	**21.004**	**20.985**	**21.004**	**21.004**	**20.94**	**21.003**	**21.004**	**21.004**	**20.976**	**21.004**	**21.003**	**20.991**	**21.003**	**21**	**20.938**	**21.004**	**20.989**	**20.909**	**21.004**

TABLE 5.5: Epidote (continued)

	59295 /16	**59295 /17**	**59295 /18**	**59295 /19**	**59295 /20**	**59295 /21**	**59314 /101**	**59314 /102**
SiO*2*	35.09	37.10	37.27	37.38	36.20	36.58	36.34	36.07
TiO*2*	-	0.01	-	0.04	0.01	-	-	-
Al2O*3*	22.76	22.38	23.39	22.98	21.49	22.10	21.31	19.88
Fe*2*O*3*	13.88	14.49	12.76	14.26	13.76	14.95	14.11	14.87
Mn2O*3*	0.24	0.08	0.02	0.11	0.10	0.10	0.08	-
FeO	-	-	-	-	-	-	-	-
MnO	-	-	-	-	-	-	-	-
CaO	23.87	23.84	25.06	23.97	23.45	23.69	22.90	22.89
Na2O	-	0.02	0.01	0.01	0.07	-	-	-
H2O	1.43	1.72	1.56	1.75	1.62	1.68	1.77	1.73
TOTAL	**97.27**	**99.64**	**100.07**	**100.50**	**96.70**	**99.10**	**96.51**	**95.44**
#Si IV	2.861	2.967	2.943	2.960	2.979	2.946	3.007	3.031
#Al IV	0.139	0.033	0.057	0.040	0.021	0.054	-	-
Z site	**3.000**	**3.000**	**3.000**	**3.000**	**3.000**	**3.000**	**3.007**	**3.031**
#Al VI	2.048	2.077	2.119	2.106	2.063	2.044	2.078	1.969
#Fe +3	0.848	0.872	0.758	0.850	0.852	0.906	0.879	0.940
#Mn +3	0.014	0.004	-	0.006	0.005	0.005	0.004	-
#Ti	-	0.001	-	0.002	0.001	-	-	-
#Fe +2	-	-	-	-	-	-	-	-
#Mn +2	-	-	-	-	-	-	-	-
Y site	**2.914**	**2.953**	**2.878**	**2.963**	**2.921**	**2.955**	**2.961**	**2.909**
#Mn +3	0.001	0.001	0.001	0.001	0.001	0.001	0.001	-
#Mn +2	-	-	-	-	-	-	-	-
#Fe +2	-	-	-	-	-	-	-	-
#Ca	2.085	2.043	2.122	2.034	2.067	2.044	2.030	2.061
#Na	-	0.003	0.002	0.002	0.011	-	-	-
X site	**2.085**	**2.047**	**2.122**	**2.037**	**2.079**	**2.045**	**2.031**	**2.061**
#O	12.000	12.000	12.000	12.000	12.000	12.000	12.000	12.000
#OH	0.776	0.919	0.820	0.926	0.890	0.902	0.977	0.970
Total*	**20.786**	**20.919**	**20.820**	**20.926**	**20.890**	**20.920**	**20.977**	**20.970**

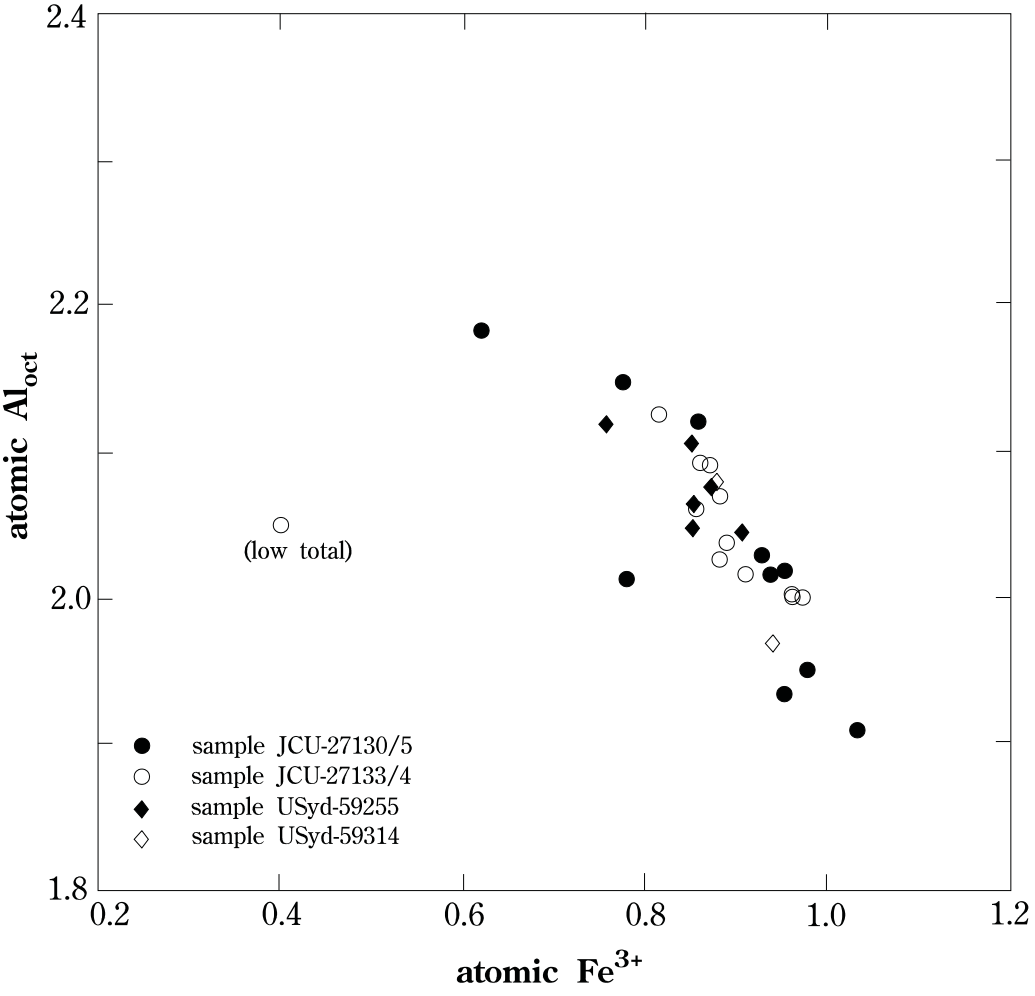

FIGURE 5.8: Total compositional data for epidotes from Mount Dore, plotted as Al_{tet} versus Fe^{3+}. All samples are from Staveley Formation meta-calcilutites. Note the anomalous analysis well to the left to the left of the others. This had a low total oxide content (see analysis 27133/4/4 in Table 5.5).

5.3.5 Garnet

One sample (JCU-27133) was found containing garnet. This sample is also from altered Staveley Formation. Eleven microprobe analyses were collected across the irregular aggregate of ragged grains, and structural formulae calculated assuming 16 cations (Table 5.6). End-member components were estimated using the technique of Rickwood (1968), and indicate that the garnet consists largely (greater than 92 mol%) of the andradite and grossular end-members (62-71 mol% and 22-31 mol%, respectively). The remainder is largely spessartine and almandine (2.32-4.08 mol% and 2.27-3.31 mol%, respectively; Figure 5.9). No compositional zoning is evident.

5.3.6 Microcline

Potassium feldspar alteration was sampled from each of the major lithologies at Mount Dore. 56 analyses from 18 grains in 15 specimens were obtained in this study, and 14 additional analyses from 4 samples taken from Ophel (1980). Structural formulae were calculated on the basis of 8 oxygens, and the results indicate there is remarkably little variation in feldspar chemistry (Table 5.7). Some substitution for K by Na, Ba and Ca occurs, but most samples closely approach the ideal potassium end-member composition. Minor Fe is also present. This may be substituting for Al^{3+} in the crystal lattice, but the abundant red-orange dusting characterising the feldspars suggests it may instead be present as fine haematite. Red-rock alteration is widespread in the regionally metamorphosed calcareous sediments of the Corella Formation (Edwards and Baker, 1953). It is in these instances interpreted to result from the release of iron in the ferric state during metasomatism attending metamorphism, and its precipitation as haematite in other minerals. A similar origin, albeit on a more local scale, is possible for the feldspathized rocks at Mount Dore.

TABLE 5.6: Garnet compositional data obtained in this study. Structural formulae calculated on the basis of 16 cations. End-members proportions have been calculated using the technique of Rickwood (1968). Sample locality and brief description is given in Table D1 (Appendices).

	27133 /1/1	27133 /1/2	27133 /1/3	27133 /1/4	27133 /1/5	27133 /1/6	27133 /1/7	27133 /1/8	27133 /1/9	27133 /1/10	27133 /1/11
SiO_2	36.24	36.25	36.67	36.51	36.51	36.42	36.73	36.23	36.39	36.23	36.55
TiO_2	0.58	0.82	0.66	0.65	0.84	0.66	0.55	0.69	0.92	0.82	-
Al_2O_3	6.98	7.19	8.08	6.81	7.29	7.67	7.76	6.22	6.16	6.89	7.56
Cr_2O_3	-	-	-	-	-	0.13	0.12	0.10	-	-	-
Fe_2O_3	21.45	20.90	19.79	21.50	20.90	19.99	19.88	21.93	21.82	21.32	20.54
FeO	1.46	1.90	1.35	1.43	1.43	1.59	1.25	1.27	1.49	1.49	1.21
MnO	1.50	1.48	1.61	1.60	1.55	1.30	1.77	1.51	1.42	1.64	1.00
MgO	0.18	0.06	0.20	0.19	0.15	0.09	-	0.21	-	0.07	0.00
CaO	31.61	31.46	31.88	31.63	31.87	31.82	31.98	31.49	31.74	31.61	32.15
Total	**100.00**	**100.07**	**100.24**	**100.32**	**100.53**	**99.67**	**100.04**	**99.65**	**99.94**	**100.07**	**99.01**
#Si IV	5.937	5.936	5.955	5.965	5.941	5.961	5.987	5.973	5.989	5.938	6.000
#Al IV	0.063	0.064	0.045	0.035	0.059	0.039	0.013	0.027	0.011	0.062	-
T site	**6.000**	**6.000**	**6.000**	**6.000**	**6.000**	**6.000**	**6.000**	**6.000**	**6.000**	**6.000**	**6.000**
#Al VI	1.284	1.323	1.501	1.277	1.339	1.440	1.478	1.181	1.184	1.269	1.463
#Ti VI	0.071	0.101	0.081	0.080	0.103	0.081	0.067	0.086	0.114	0.101	-
#Cr	-	-	-	-	-	0.017	0.015	0.013	-	-	-
#Fe +3	2.644	2.576	2.418	2.644	2.559	2.462	2.439	2.720	2.702	2.630	2.537
O site	**4.000**	**4.000**	**4.000**	**4.000**	**4.000**	**4.000**	**4.000**	**4.000**	**4.000**	**4.000**	**4.000**
#Fe +2	0.200	0.261	0.183	0.195	0.194	0.218	0.170	0.175	0.205	0.204	0.166
#Mn +2	0.208	0.205	0.221	0.221	0.214	0.180	0.244	0.211	0.198	0.228	0.139
#Mg	0.044	0.015	0.048	0.046	0.036	0.022	-	0.052	-	0.017	-
#Ca	5.548	5.519	5.547	5.537	5.556	5.580	5.585	5.562	5.597	5.551	5.655
A site	**6.000**	**6.000**	**6.000**	**6.000**	**6.000**	**6.000**	**6.000**	**6.000**	**6.000**	**6.000**	**5.959**
#O	24.004	24.018	24.018	24.023	24.022	24.021	24.027	24.029	24.051	24.020	23.959
almandine	2.301	3.311	2.322	2.692	2.267	2.999	2.633	2.482	3.244	2.399	3.439
andradite	68.614	67.643	62.945	68.484	67.199	63.997	62.791	70.461	70.540	68.988	63.434
grossular	24.839	25.341	30.202	24.337	26.326	29.188	30.107	22.335	22.911	24.491	30.810
pyrope	0.746	0.247	0.813	0.776	0.612	0.368	-	0.864	-	0.288	-
spessartine	3.506	3.458	3.719	3.712	3.596	3.023	4.082	3.530	3.305	3.834	2.317
uvarovite	-	-	-	-	-	0.423	0.387	0.327	-	-	-
% cation allocation	**98.946**	**98.929**	**99.247**	**99.420**	**99.011**	**99.344**	**99.789**	**99.546**	**99.814**	**98.968**	**100.256**

FIGURE 5.9: Total compositional data for garnet from Mount Dore, plotted on a (spessartine+almandine)-andradite-grossular ternary diagram. Note the predominance of the calcic components. The sample (JCU-27133) comes from hydrothermally altered Staveley Formation meta-calcilutites.

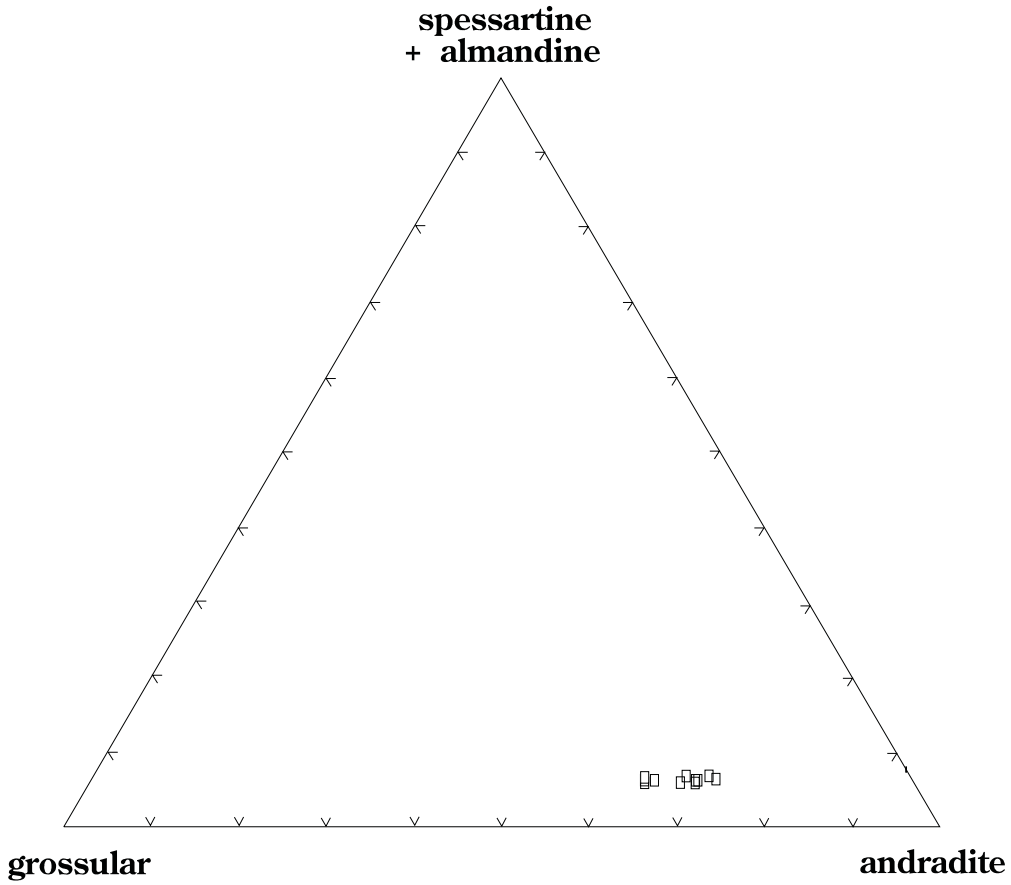

TABLE 5.7: Summary compositional data for microcline. Numbers in parentheses indicate number of analyses from each grain. Structural formulae calculated on the basis of eight oxygens per formula unit. Samples with the prefix 59- are from the data set of Ophel (1980). Sample localities and brief descriptions are given in Tables D1 and D2, and complete compositional data in Table D5 (all in Appendices).

	27064/3 (2)	**27064/5 (3)**	**27077/4 (3)**	**27102/2 (3)**	**27124/2 (3)**	**27124/4 (4)**	**27133/2 (3)**	**27146/3 (3)**	**27158/4 (3)**	**27175/3 (3)**	**27181/3 (4)**
SiO_2	64.335	64.303	63.203	64.667	63.507	63.632	64.563	65.257	62.873	64.537	61.74
Al_2O_3	18.495	18.473	18.07	17.927	17.813	17.835	18.373	18.447	17.78	18.413	17.635
FeO	0.16	0.033	0.513		0.047	0.345	0.073	0.333	0.047	0.083	3.66
CaO	0.225	0.157	0.173	0.13	0.087	0.255	0.187	0.173	0.087	018	0.138
BaO	0.725	0.35	0.777	0.183	0.303	0.35	0.57	0.177	0.803	0.357	0.273
Na_2O	0.46	0.407	0.33	0.633	0.31	0.085	0.46	0.273	0.493	0.313	0.157
K_2O	16.435	16.25	16.143	16.057	16.453	16.108	15.293	15.2	16.033	15.8	14.91
TOTAL	**100835**	**99.973**	**99.209**	**99.597**	**9852**	**98.61**	**99.519**	**9986**	**98.116**	**99.683**	**98.513**
#Si+4	2.976	2.985	2.976	3.006	2.996	2.997	2.998	3.007	2.988	2.995	2.946
#Al+3	1.008	1.011	1.003	0.982	0.991	0.99	1.005	1.002	0.996	1.007	0.992
#Fe+2	0.006	0.001	0.02	-	0.002	0.014	0.003	0.013	0.002	0.003	0.146
#Ca+2	0.011	0.008	0.009	0.006	0.004	0.013	0.009	0.009	0.004	0.009	0.007
#Ba+2	0.013	0.006	0.014	0.003	0.006	0.006	0.01	0.003	0.015	0.006	0.005
#Na+1	0.041	0.037	0.03	0.057	0.028	0.008	0.041	0.024	0.045	0.028	0.015
#K+1	0.97	0.962	0.97	0.952	0.99	0.968	0.906	0.894	0.972	0.935	0.908
# **cations**	**5.026**	**5.009**	**5.022**	**5.007**	**5.018**	**4.996**	**4.973**	**4.951**	**5.023**	**4.984**	**5.019**
charge	16.000	16.000	16.000	16.000	16.000	16.000	16.000	16.000	16.000	16.000	16.000

	27211/3 (3)	**27231/3 (3)**	**27242/2 (4)**	**27243/1 (3)**	**27277/2 (3)**	**27284/2 (3)**	**27284/4 (3)**
SiO_2	62.733	65.33	64.12	64.12	64.18	64.247	63.97
Al_2O_3	17.573	18.173	18.138	18.143	18.3	18.243	18.25
FeO	0.14	0.033	0.047	-	0.07	-	0.04
CaO	011	0.163	0.155	0.14	0.207	0.167	0.22
BaO	0.053	-	0.298	0.183	0.257	0.347	0.297
Na_2O	0.897	0.58	0.213	0.6	0.23	0.423	0.583
K_2O	13.703	13.92	15.938	16.063	16.2	15.693	15.727
TOTAL	**95.209**	**98.199**	**98.909**	**99.249**	**99.444**	**99.12**	**99.087**
#Si+4	3.016	3.031	3.0	2.993	2.991	2.997	2.99
#Al+3	0.996	0.994	1.0	0.998	1.005	1.003	1.005
#Fe+2	0.006	0.001	0.002	-	0.003	-	0.002
#Ca+2	0.006	0.008	0.008	0.007	0.01	0.008	0.011
#Ba+2	0.001	-	0.005	0.003	0.005	0.006	0.005
#Na+1	0.084	0.052	0.019	0.054	0.021	0.038	0.053
#K+1	0.84	0.824	0.951	0.957	0.963	0.934	0.938
# **cations**	**4.948**	**4.91**	**4.985**	**5.013**	**4.998**	**4.987**	**5.003**
		16.000	16.000	16.000	16.000	16.000	16.000

No examples of anomalously barian potassium feldspars were recorded in this study, but such have apparently been observed in both the southern (Scott, 1988; CSIRO-101330; maximum 12.4 mol% celsian; See Table D3 (Appendices) for sample locality) and northern (Ophel, 1980; USyd-59284; no BaO contents presented) parts of the Mount Dore prospect. Scott (1988) reports that barian feldspars are orthoclase, whereas "normal" potassium feldspar is microcline. These occurrences are very localised, however, and probably reflect host, rather than fluid compositions.

5.3.7 White mica

White mica was tentatively identified as muscovite during preliminary petrography. Thirty-eight analyses were collected from fourteen samples, encompassing the major lithologies at Mount Dore. A further twelve analyses were taken from Scott (1988). Structural formulae were calculated on the basis of 24(O+OH+Cl) per formula unit (Table 5.8). The analyses indicate that very few samples approach the stoichiometric requirements of muscovite - $K_2Al_4[Al_2Si_6O_{20}](OH)_4$. There are generally more than six Si atoms, and significantly fewer than two K atoms per formula unit. There is also significant Fe and Mg. The "mica" is therefore technically a combination illite-phengite. A plot of A-site occupancy against Si content (Figure 5.10a) shows no obvious relationship, although data for granite and carbonaceous slate are constrained to a small area and a narrow band, respectively. Charge balance must therefore be largely maintained by increasing the phengite component, via a coupled substitution:

$$Si^{4+} + (Fe^{2+},Mg^{2+}) \;===\; Al^{3+}_{tet} + Al^{3+}_{oct}$$

Figure 5.10b illustrates this nicely.

TABLE 5.8: Summary compositional data for white mica. Numbers in parentheses indicate number of analyses from each grain. Structural formulae have been calculated assuming 24(O+OH+F+Cl) per formula unit. Samples with the prefix 101- are from the data set of Scott (1988). Sample localities and brief descriptions are given in Tables D1 and D3, and complete compositional data for this study in Table D6 (all in Appendices).

	27064/4 (3)	**27077/2 (2)**	**27097/3 (3)**	**27130/3 (1)**	**27146/2 (3)**	**27156/2 (3)**	**27158/3 (3)**	**27175/1 (3)**	**27181/4 (3)**	**27181/5 (1)**	**27227/1 (3)**	**27235/1 (4)**	**27238/3 (3)**	**27281/2 (3)**
SiO_2	47.553	55.21	54.673	52.19	46.033	52.333	48.003	49.877	49.81	50.37	47.997	51.035	48.893	50.37
TiO_2	0.447	-	0.023	-	0.263	0.023	0.567	0.423	0.23	0.19	0.193	0.1	0.187	0.067
Al_2O_3	37.75	30	23.72	27.94	37.543	31.783	35.323	35.503	29.767	30.65	29.703	28.7	29.647	29.067
Cr_2O_3	0.07	0.055	0.023	-	-	-	0.057	0.037	-	-	-	-	0.03	-
FeO	1.097	1.145	2.86	1.51	2.37	0.883	2.187	1.367	5.46	4.51	4.99	3.75	4.65	0.873
MnO	0.023	0.055	0.067	0.09	0.053	-	-	-	-	0.09	0.03	-	-	0.043
MgO	0.5	2.625	4.893	4.76	0.103	3.423	1.18	0.877	2.067	1.85	2.997	3.36	2.927	5.477
CaO	0.107	0.175	0.18	0.16	0.113	0.127	0.123	0.05	0.13	0.13	0.07	0.083	0.117	0.073
Na_2O	0.257	0.07	-	-	0.17	0.067	0.133	0.233	-	-	0.117	0.052	-	-
K_2O	9.21	5.635	9.267	7.5	9.247	7.863	8.403	9.573	8.09	8.29	8.653	8.532	8.51	9.873
H_2O	4.572	4.706	4.545	4.616	4.537	4.632	4.558	4.564	4.503	4.53	4.472	4.525	4.486	4.54
Cl	-	0.02	-	-	-	-	0.04	0.017	0.02	-	0.04	0.04	0.063	0.027
O=Cl	-	-0.005	-	-	-	-	-0.009	-0.004	-0.005	-	-0.009	-0.009	-0.014	-0.006
TOTAL	**101.586**	**99.692**	**100.251**	**98.766**	**100.432**	**101.134**	**100.564**	**102.517**	**100.073**	**100.61**	**99.253**	**100.168**	**99.496**	**100.404**
#Si IV	6.135	7.050	7.194	6.869	6.057	6.696	6.264	6.378	6.620	6.626	6.471	6.736	6.546	6.614
#Al IV	1.865	0.950	0.806	1.131	1.943	1.304	1.736	1.622	1.380	1.374	1.529	1.264	1.454	1.386
#Ti IV	-	-	-	-	-	-	-	-	-	-	-	-	-	-
T site	**8.000**	**8.000**	**8.000**	**8.000**	**8.000**	**8.000**	**8.000**	**8.000**	**8.000**	**8.000**	**8.000**	**8.000**	**8.000**	**8.000**
#Al VI	3.875	3.565	2.873	3.202	3.879	3.489	3.697	3.729	3.282	3.378	3.191	3.200	3.224	3.113
#Ti VI	0.043	-	0.002	-	0.026	0.002	0.056	0.041	0.023	0.019	0.020	0.010	0.019	0.007
#Cr	0.007	0.006	0.002	-	-	-	0.006	0.004	-	-	-	-	0.003	-
#Fe +2	0.118	0.122	0.315	0.166	0.261	0.094	0.239	0.146	0.607	0.496	0.563	0.414	0.521	0.096
#Mn +2	0.003	0.006	0.007	0.010	0.006	-	-	-	-	0.010	0.003	-	-	0.005
#Mg	0.096	0.500	0.960	0.934	0.020	0.653	0.230	0.167	0.410	0.363	0.602	0.661	0.584	1.072
O site	**4.143**	**4.198**	**4.160**	**4.312**	**4.192**	**4.238**	**4.227**	**4.087**	**4.322**	**4.265**	**4.379**	**4.285**	**4.351**	**4.292**
#Ca	0.015	0.024	0.025	0.023	0.016	0.017	0.017	0.007	0.019	0.018	0.010	0.012	0.017	0.010
#Na	0.064	0.017	-	-	0.043	0.017	0.034	0.058	-	-	0.031	0.013	-	-
#K	1.516	0.918	1.556	1.259	1.552	1.283	1.399	1.562	1.372	1.391	1.488	1.437	1.454	1.654
A site	**1.595**	**0.959**	**1.581**	**1.282**	**1.612**	**1.317**	**1.450**	**1.626**	**1.390**	**1.410**	**1.529**	**1.462**	**1.470**	**1.664**
#O	20.000	20.000	20.000	20.000	20.000	20.000	20.000	20.000	20.000	20.000	20.000	20.000	20.000	20.000
#OH	4.000	3.996	4.000	4.000	4.000	4.000	3.991	3.996	3.995	4.000	3.991	3.991	3.986	3.994
#Cl	-	0.004	-	-	-	-	0.009	0.004	0.005	-	0.009	0.009	0.014	0.006
Charge	**0.000**	**0.000**	**0.000**	**0.000**	**0.000**	**0.000**	**0.000**	**0.000**	**0.000**	**0.000**	**0.000**	**0.000**	**0.000**	**0.000**
Si/(Si+Altet)	0.767	0.881	0.899	0.859	0.757	0.837	0.783	0.797	0.827	0.828	0.809	0.842	0.818	0.827
K/(Ca+Na+K)	0.950	0.957	0.984	0.982	0.963	0.974	0.965	0.961	0.987	0.987	0.973	0.983	0.989	0.994
Mg/(Mg+Fe)	0.449	0.804	0.753	0.849	0.071	0.874	0.490	0.534	0.403	0.423	0.517	0.615	0.529	0.918

TABLE 5.8: White mica (continued). Averaged compositional data of Scott (1988). Where identical sample numbers are listed, the first sample is phengite, and the second illite. The former is interpreted by Scott on textural grounds to have formed earlier than the latter.

	101276 (7)	**101292 (6)**	**101292 (2)**	**101330 (3)**	**101339 (6)**	**101339 (2)**	**101383 (5)**	**101383 (2)**	**101405 (2)**	**101405 (2)**	**101438 (7)**	**101507 (3)**
SiO_2	49.4	45.5	49.4	52.1	51.2	52.2	48.8	49.9	44.6	50.7	48.9	51.4
TiO_2	0.12	0.85	0.03	0.12	0.05	0.04	0.42	0.65	0.77	0.4	0.82	0.01
Al_2O_3	30.5	31.5	36.9	29.6	29.3	24.9	31.5	29.2	32.3	27.6	31.2	19.5
FeO	2.47	1.25	1.07	1.33	2.29	4.01	2.06	2.63	0.94	2.95	1.04	10.7
MnO	0.03	0.02	0.03	0.02	0.02	0.03	0.02	0.05	0.01	0.01	0.01	0.04
MgO	1.67	1.47	0.91	4.7	4.37	4.44	1.8	1.57	1.39	1.06	1.83	5.31
BaO	0.06	0.89	0.05	0.06	0.02	0.11	0.14	1.53	2.66	0.05	0.25	0.05
CaO	0.03	0.02	0.02	0.04	0.07	0.35	0.01	0.01	0.01	0.01	0.01	0.1
Na_2O	0.05	0.18	0.15	0.04	0.06	0.08	0.13	0.07	0.25	0.11	0.08	0.13
K_2O	6.96	9.83	10.3	7.9	9.47	6.1	7.92	7.01	10.1	10.5	5.19	8.34
H_2O	4.62	4.5	4.56	4.61	4.54	4.59	4.585	4.55	4.43	4.51	4.69	4.36
TOTAL	**95.91**	**96.01**	**103.42**	**100.52**	**101.39**	**96.85**	**97.385**	**97.17**	**97.46**	**97.9**	**94.02**	**99.94**
#Si IV	6.708	6.334	6.278	6.743	6.669	7.051	6.563	6.771	6.208	6.899	6.67	7.078
#Al IV	1.292	1.666	1.722	1.257	1.331	0.949	1.437	1.229	1.792	1.101	1.33	0.922
T site	**8.000**	**8.000**	**8.000**	**8.000**	**8.000**	**8.000**	**8.000**	**8.000**	**8.000**	**8.000**	**8.000**	**8.000**
#Al VI	3.589	3.502	3.805	3.258	3.167	3.015	3.556	3.441	3.506	3.325	3.685	2.243
#Ti VI	0.012	0.089	0.003	0.012	0.005	0.004	0.042	0.066	0.081	0.041	0.084	0.001
#Fe +2	0.28	0.146	0.114	0.144	0.249	0.453	0.232	0.298	0.109	0.336	0.119	1.232
#Mn +2	0.003	0.002	0.003	0.002	0.002	0.003	0.002	0.006	0.001	0.001	0.001	0.005
#Mg	0.338	0.305	0.172	0.907	0.849	0.894	0.361	0.318	0.288	0.215	0.372	1.09
O site	**4.223**	**4.044**	**4.097**	**4.322**	**4.272**	**4.37**	**4.193**	**4.129**	**3.986**	**3.917**	**4.261**	**4.571**
#Ba	0.003	0.049	0.002	0.003	0.001	0.006	0.007	0.081	0.145	0.003	0.013	0.003
#Ca	0.004	0.003	0.003	0.006	0.01	0.051	0.001	0.001	0.001	0.001	0.001	0.015
#Na	0.013	0.049	0.037	0.01	0.015	0.021	0.034	0.018	0.067	0.029	0.021	0.035
#K	1.206	1.746	1.67	1.304	1.574	1.051	1.359	1.213	1.793	1.823	0.903	1.465
A site	**1.226**	**1.846**	**1.712**	**1.323**	**1.6**	**1.129**	**1.402**	**1.315**	**2.007**	**1.856**	**0.939**	**1.517**
#O	20.000	20.000	20.000	20.000	20.000	20.000	20.000	20.000	20.000	20.000	20.000	20.000
#OH	4.000	4.000	4.000	4.000	4.000	4.000	4.000	4.000	4.000	4.000	4.000	4.000
Charge	**0.000**	**0.000**	**0.000**	**0.000**	**0.000**	**-**	**0.000**	**0.000**	**0.000**	**0.000**	**0.000**	**0.000**
$Si/(Si+Al_{tet})$	0.838	0.792	0.785	0.843	0.834	0.881	0.82	0.846	0.776	0.862	0.834	0.885
K/(Ba+Ca+Na+K)	0.983	0.946	0.975	0.986	0.984	0.931	0.97	0.923	0.893	0.982	0.962	0.966
Mg/(Mg+Fe)	0.547	0.677	0.603	0.863	0.773	0.664	0.609	0.516	0.725	0.39	0.758	0.469

FIGURE 5.10: Total compositional data for white mica from Mount Dore:
(a) plot of A-site occupancy versus Si-content, showing the significant departure from ideal muscovite composition;
(b) plot of Si+Mg+Fe versus Al_{tet}+Al_{oct}, demonstrating phengite substitution;
(c) plot of Mg/(Mg+Fe) versus Al-content illustrating chemical differences in micas from different lithologies. Data includes the "averages" of Scott (1988).

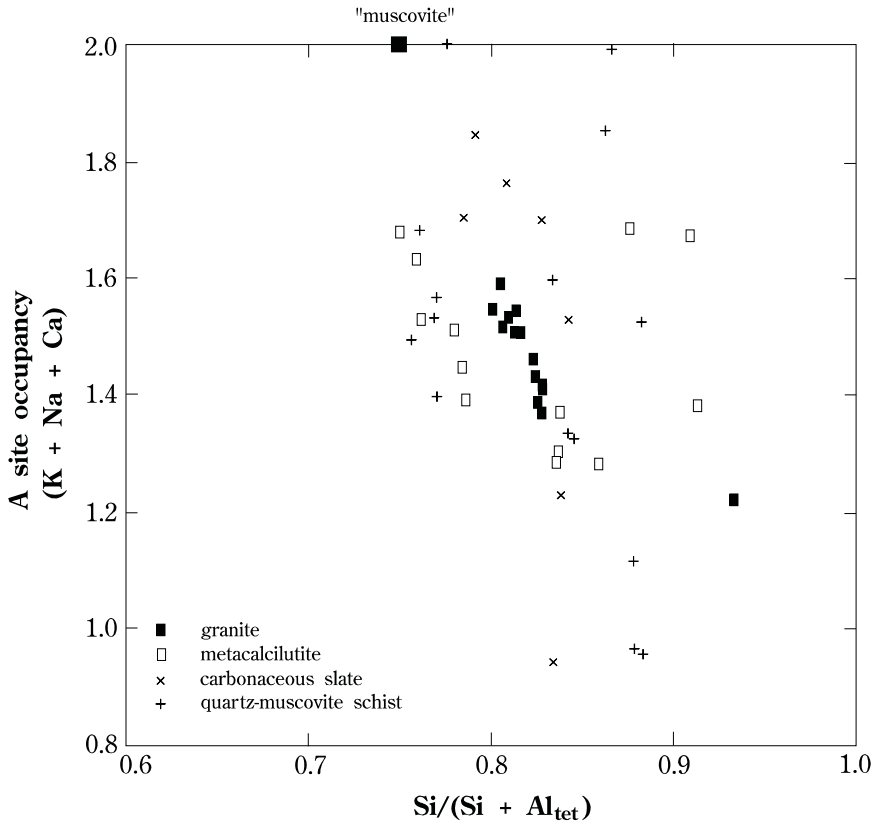

(a)

FIGURE 5.10 (continued)

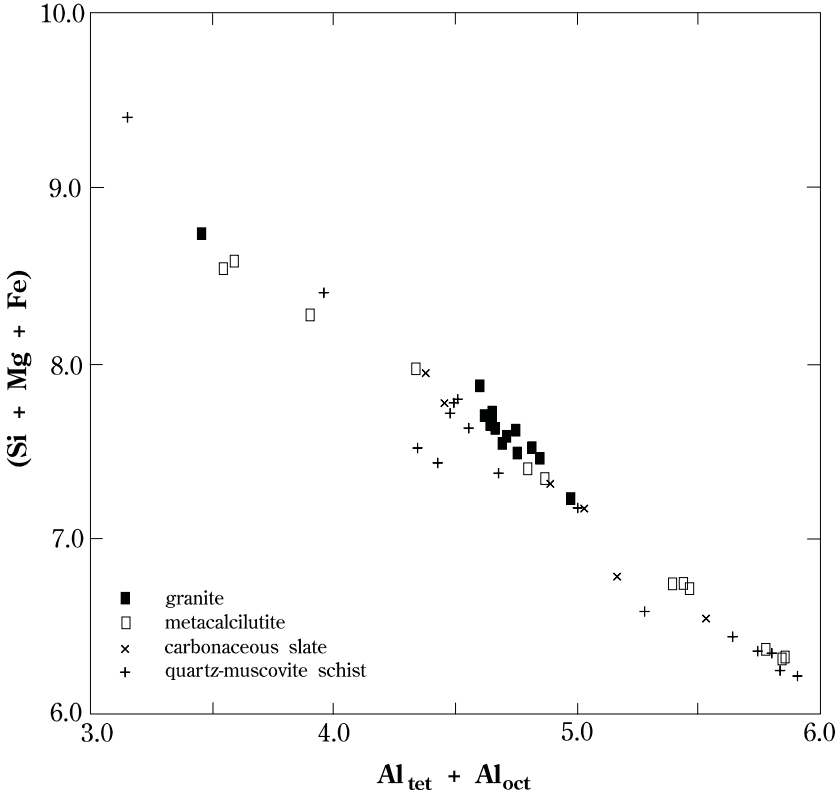

(b)

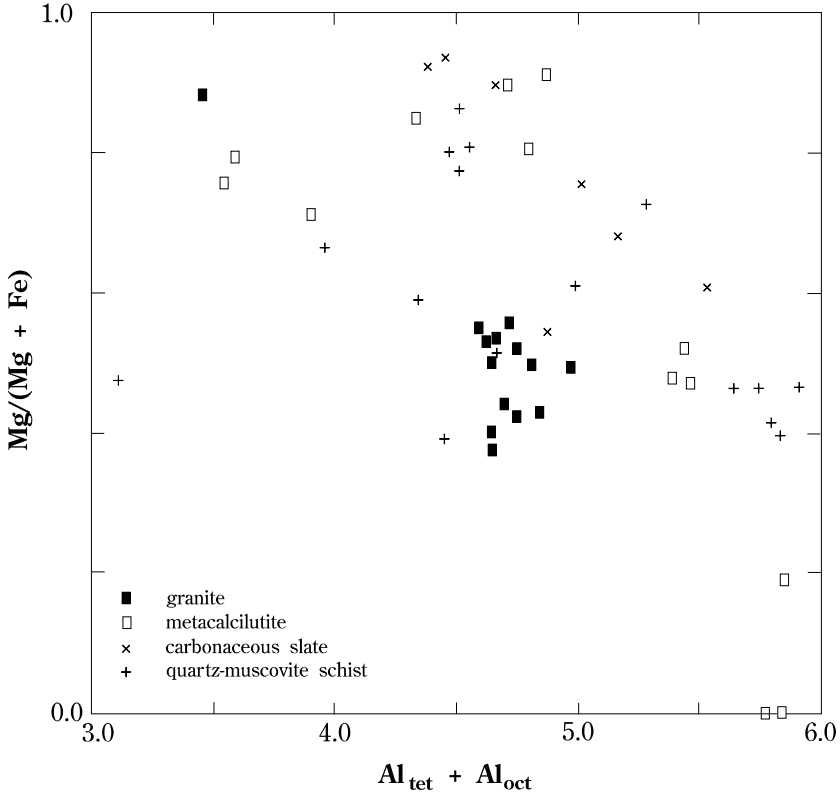

(c)

A plot of Mg/(Mg+Fe) versus Al-content (Figure 5.10c) also illustrates some interesting features. Data for carbonaceous slates show a general increase in Mg over Fe with decreasing total Al. The trend for calcareous Staveley Formation lithologies is similar, though more poorly defined. White mica composition in the granites is essentially constant, and in quartz-muscovite schists no regular trend is evident. Compositional variations are therefore unlikely to relate to an evolving fluid chemistry, and the textural features of the mica indicate it is definitely the product of hydrothermal alteration, occurring at a uniform position in the paragenesis. The variability in white mica chemistry therefore probably reflects variability in host rock composition. Elevated amounts of Ba detected by Scott (1988) probably also reflect local variations in Ba-content in the host lithology. The granite is expected to have a more uniform composition relative to the other, metasedimentary lithologies, which are more chemically diverse.

5.3.8 Tourmaline

One hundred and nine analyses were made of 22 tourmaline grains from 16 samples representing all the major lithologies, and an additional 6 analyses from 2 samples were taken from Ophel (1980). Structural formulae have been calculated on the basis of 31(O+OH+Cl) (Table 5.9). Tourmaline analyses are inherently not as accurate as those for other silicates, because contents of light elements (*e.g.* Li, B and H) cannot be measured with the electron microprobe. Tourmaline is assumed to be adequately described in terms of schorl and dravite components. All Fe is therefore assumed to be FeO, and Li_2O is assumed to be negligible. B_2O_3 abundance has been back-calculated assuming three boron atoms per formula unit. The amount of H_2O could not be assessed, nor could it be assumed that there were four hydroxyl anions (less the Cl content) per formula unit, since F can also substitute in this site, and its abundance is also unknown.

On an Na_2O-MgO-FeO ternary diagram tourmaline compositions lie on or close to the schorl-dravite join (Figure 5.11a). All compositions lie away from the

TABLE 5.9: Summary compositional data for tourmaline. Numbers in parentheses indicate number of analyses from each grain. Structural formulae have been calculated on the basis of 31(O+OH+Cl). All Fe is assumed to be FeO, Li_2O is assumed to be negligible. B_2O_3 abundance has been back-calculated assuming three boron atoms per formula unit. The amount of H_2O could not be assessed. Samples with the prefix 59- are from the data set of Ophel (1980). Sample localities and brief descriptions are given in Tables D1 and D2, and complete compositional data in Table D7 (all in Appendices).

	27064 /1	**27064 /2**	**27064 /5**	**27077 /3**	**27102 /1**	**27102 /2**	**27121 /1**	**27145 /2**	**27146 /5**	**27160 /2**	**27162 /1**	**27175 /2**	**27181 /1**	**27211 /1**	**27220 /1**	**27232 /1**	**27238 /2**	**27238 /4**	**27242 /3**	**27243 /2**	**59278**	**59288**
	(5)	(5)	(3)	(6)	(6)	(6)	(2)	(4)	(4)	(2)	(8)	(6)	(5)	(5)	(5)	(11)	(11)	(9)	(7)	(5)	(3)	(3)
SiO_2	36.63	36.3	36.74	35.94	36.4	36.52	36.37	36.02	36.33	36.48	36.52	36.23	35.94	35.02	36.93	35.21	35.69	35.79	35.94	36.83	38.38	36.53
TiO_2	1.35	0.55	0.89	1.08	0.93	0.94	0.76	0.46	0.45	0.31	0.7	0.88	1.02	0.86	0.73	1.02	1.06	0.98	1.04	0.49	0.87	1.26
B_2O_3	10.61	10.64	10.69	10.41	10.55	10.55	10.53	10.4	10.43	10.58	10.58	10.49	10.36	9.93	10.76	10.17	10.28	10.34	10.33	10.66	11.64	10.52
Al_2O_3	28.87	32.57	30.4	27.87	29.34	29.15	29.1	26.79	27.38	31.47	29.9	29.04	26.96	26.35	31.8	26.71	26.35	27.36	26.59	30.83	36.01	28.31
Cr_2O_3	0.04	-	0.06	0.06	0.08	0.04	0.03	0.03	0.05	0.09	0.05	-	0.04	0.01	0.19	-	0.02	0.01	0.06	-	-	-
FeO	7.88	7.74	6.84	9.88	7.35	7.61	8.57	9.46	10.39	8.46	7.99	8.51	9.7	8.22	3.94	13.43	10.38	9.8	9.91	6.07	4.15	5.44
MnO	-	-	0.03	-	0.02	0.04	-	0.07	-	-	0.03	0.03	0.02	0.02	0.02	0.06	0.03	-	-	0.03	0.01	0.02
MgO	8.9	6.55	8.72	8.15	8.82	8.71	8.48	9.65	8.75	6.72	8.15	8.24	8.77	7.77	9.31	6.24	8.57	8.35	8.7	8.83	10.46	9.98
CaO	0.93	0.57	0.81	1.08	0.79	0.87	0.6	2.47	1.25	0.39	0.72	0.75	1.58	1.11	0.61	1.35	1.81	1.45	1.7	0.61	0.93	1.41
Na_2O	2.3	2.2	2.44	2.29	2.44	2.42	2.59	1.49	2.22	2.48	2.43	2.46	2.04	2.15	2.37	2.12	1.91	2.1	1.98	2.51	2.23	2.25
K_2O	0.04	-	0.04	0.05	0.07	0.03	0.06	0.05	0.02	0.03	0.02	0.04	0.03	0.3	0.05	0.05	0.04	0.03	0.04	0.03	0.02	0.03
Cl	-	0.01	-	0.07	0.01	-	-	-	-	-	-	0.03	-	0.02	0.01	0.01	-	0.01	-	0.02	-	0.06
O=Cl	-	0.00	-	-0.02	0.00	-	-	-	-	-	-	-0.01	-	-0.01	-0.01	0.00	-	0.00	-	-0.01	-	-0.02
TOTAL	**97.55**	**97.13**	**97.66**	**96.88**	**96.8**	**96.88**	**97.09**	**96.89**	**97.27**	**97.01**	**97.09**	**96.69**	**96.46**	**91.75**	**96.71**	**96.37**	**96.14**	**96.22**	**96.29**	**96.9**	**104.7**	**95.79**
#Si+4	6.003	5.930	5.975	6.003	5.996	6.016	6.005	6.019	6.054	5.994	6.004	6.006	6.030	6.134	5.969	6.020	6.035	6.018	6.049	6.005	5.734	6.040
#Ti+4	0.166	0.068	0.109	0.136	0.115	0.116	0.094	0.058	0.056	0.038	0.087	0.110	0.129	0.113	0.089	0.131	0.135	0.124	0.132	0.060	0.098	0.157
#B+3	3.001	3.000	3.001	3.001	3.000	3.000	3.001	3.000	3.000	3.001	3.002	3.002	3.000	3.002	3.002	3.001	3.001	3.001	3.001	3.000	3.002	3.002
#Al+3	5.576	6.270	5.827	5.486	5.696	5.660	5.663	5.276	5.377	6.094	5.793	5.674	5.331	5.439	6.057	5.382	5.251	5.422	5.275	5.924	6.341	5.517
#Cr+3	0.005	-	0.008	0.008	0.010	0.005	0.004	0.004	0.007	0.012	0.006	-	0.005	0.001	0.024	-	0.003	0.001	0.008	-	-	-
#Fe+2	1.080	1.057	0.930	1.380	1.013	1.048	1.183	1.322	1.448	1.162	1.098	1.180	1.361	1.204	0.533	1.920	1.468	1.378	1.395	0.828	0.519	0.752
#Mn+2	-	-	0.004	-	0.003	0.006	-	0.010	-	-	0.004	0.004	0.003	0.003	0.003	0.009	0.004	-	-	0.004	0.001	0.003
#Mg+2	2.174	1.595	2.114	2.029	2.166	2.139	2.087	2.404	2.174	1.646	1.997	2.037	2.194	2.029	2.243	1.590	2.160	2.093	2.183	2.146	2.330	2.460
#Ca+2	0.163	0.100	0.141	0.193	0.139	0.154	0.106	0.442	0.223	0.069	0.127	0.133	0.284	0.208	0.106	0.247	0.328	0.261	0.307	0.107	0.149	0.250
#Na+1	0.731	0.697	0.769	0.742	0.779	0.773	0.829	0.483	0.717	0.790	0.775	0.791	0.664	0.730	0.743	0.703	0.626	0.685	0.646	0.793	0.646	0.721
#K+1	0.008	-	0.008	0.011	0.015	0.006	0.013	0.011	0.004	0.006	0.004	0.008	0.006	0.067	0.010	0.011	0.009	0.006	0.009	0.006	0.004	0.006
#Cl	-	0.003	-	0.020	0.003	-	-	-	-	-	-	0.008	-	0.006	0.003	0.003	-	0.003	-	0.006	-	0.017
# cations	**18.909**	**18.716**	**18.887**	**18.990**	**18.932**	**18.924**	**18.987**	**19.029**	**19.059**	**18.813**	**18.898**	**18.945**	**19.008**	**18.930**	**18.778**	**19.014**	**19.020**	**18.991**	**19.004**	**18.873**	**18.822**	**18.908**
charge	58.000	57.997	58.000	57.980	57.997	58.000	58.000	58.000	58.000	58.000	58.000	57.992	58.000	57.994	57.997	57.997	58.000	57.997	58.000	57.994	58.000	57.983
Mg/(Fe+Mg)	0.668	0.601	0.694	0.595	0.681	0.671	0.638	0.645	0.600	0.586	0.645	0.633	0.617	0.628	0.808	0.453	0.595	0.603	0.610	0.722	0.818	0.766
100Ti/(Ti+Al)	2.891	1.073	1.836	2.419	1.979	2.008	1.633	1.087	1.031	0.620	1.480	1.902	2.363	2.035	1.448	2.376	2.506	2.236	2.441	1.003	1.522	2.767
Ca/(Ca+Na)	0.182	0.125	0.155	0.206	0.151	0.166	0.113	0.478	0.237	0.080	0.141	0.144	0.300	0.222	0.125	0.260	0.344	0.276	0.322	0.119	0.187	0.257

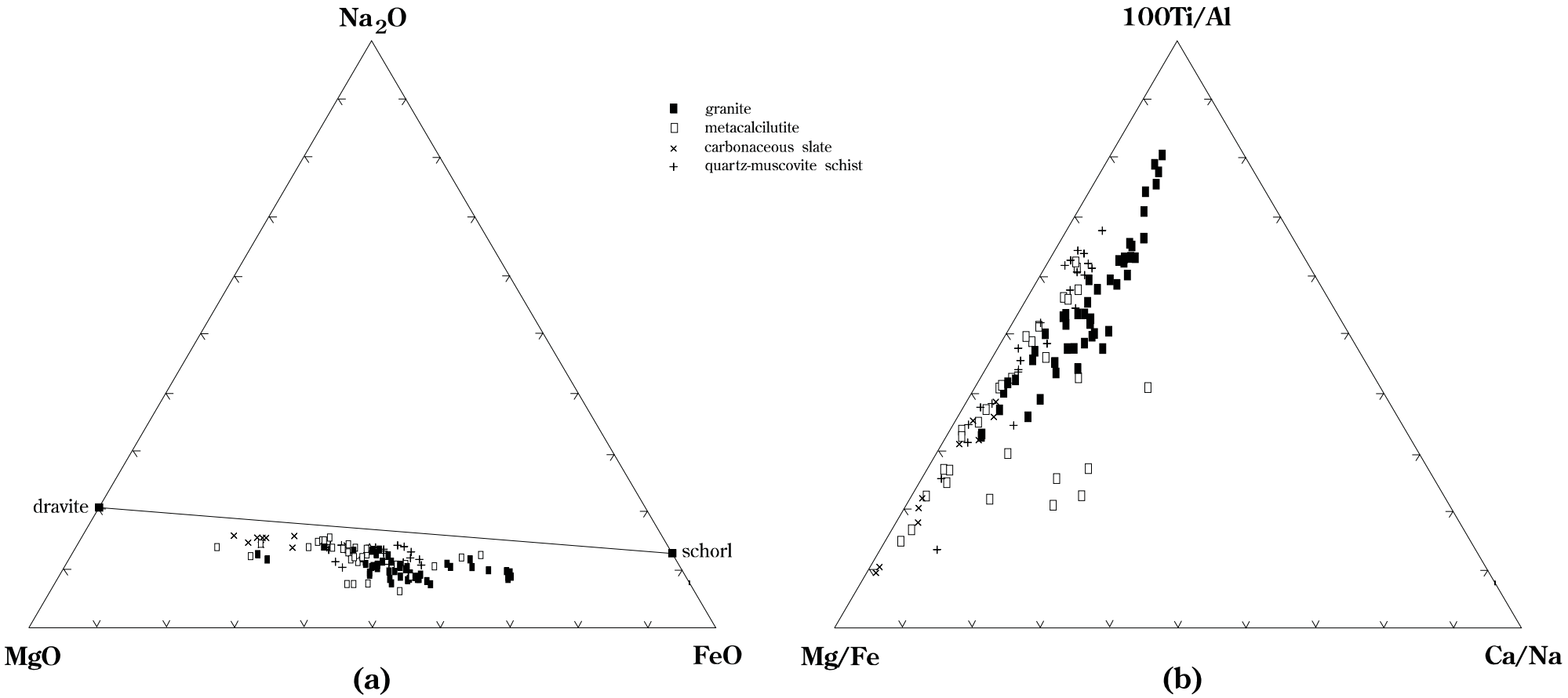

FIGURE 5.11: Geochemical plots of total compositional data for tourmalines from Mount Dore: (a) "standard" Na_2O-MgO-FeO ternary diagram, showing no clear separation of tourmalines developed in different lithologies; (b) a clearer separation is obtained when data are plotted on a 100Ti/AlÊ-ÊCa/NaÊ-ÊMg/Fe (as atomic ratios) ternary diagram. (Figure continued overleaf).

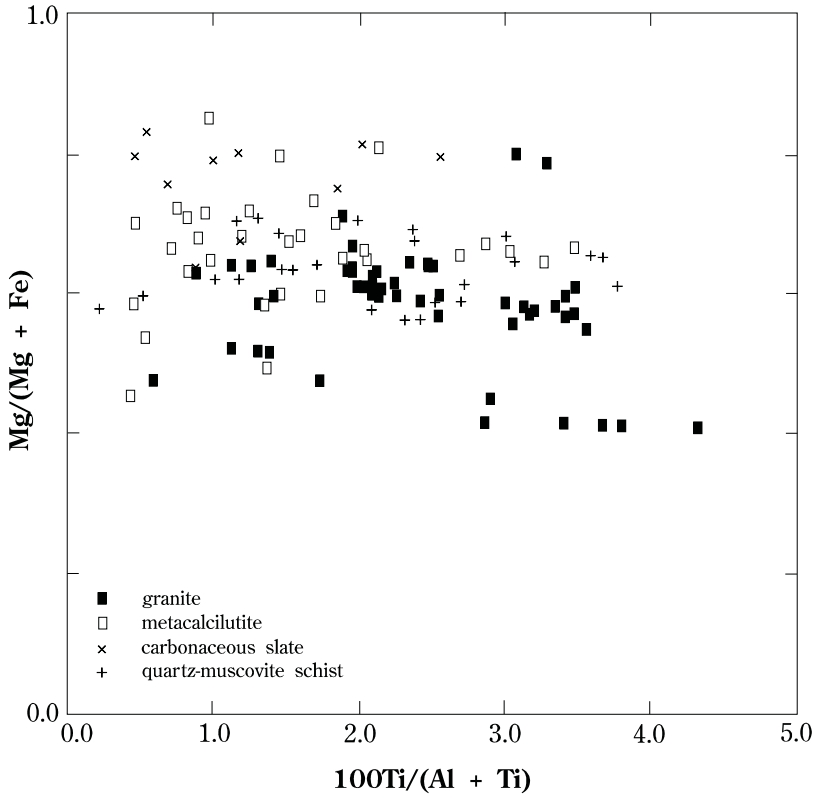

(c)

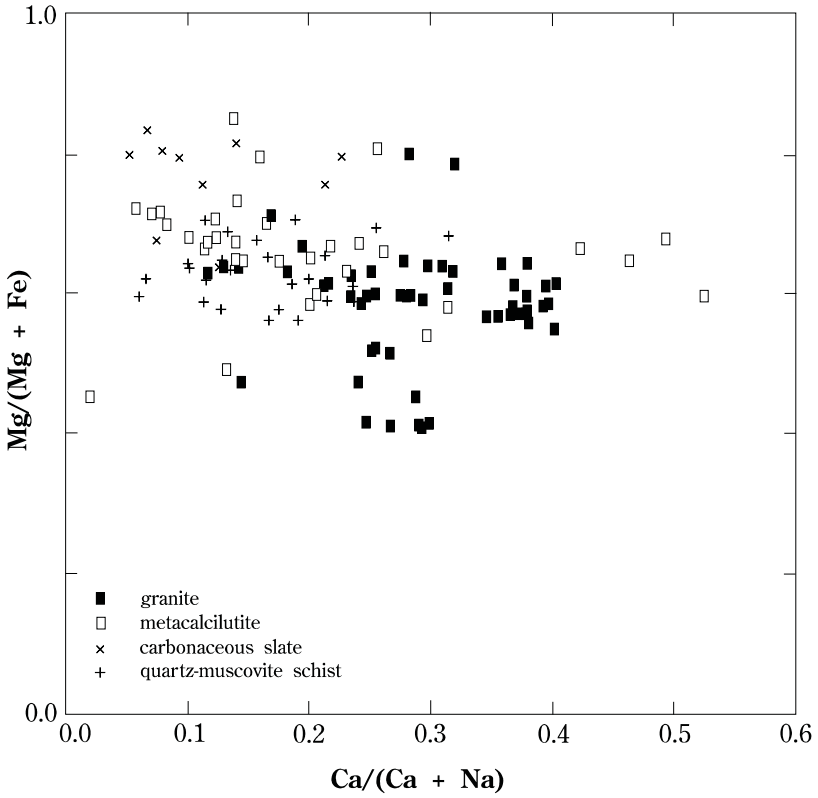

(d)

FIGURE 5.11: (continued): (c) Mg/(Mg+Fe) vs Ca/(Ca+Na) (atomic ratios); (d) 100Ti/(Al+Ti) vs Ca/(Ca+Na) (atomic ratios); (e) (following page) Mg/(Mg+Fe) vs 100Ti/(Al+Ti) (atomic ratios). Variations in compositions of tourmaline from different lithiologies are attributed to differences in host composition.

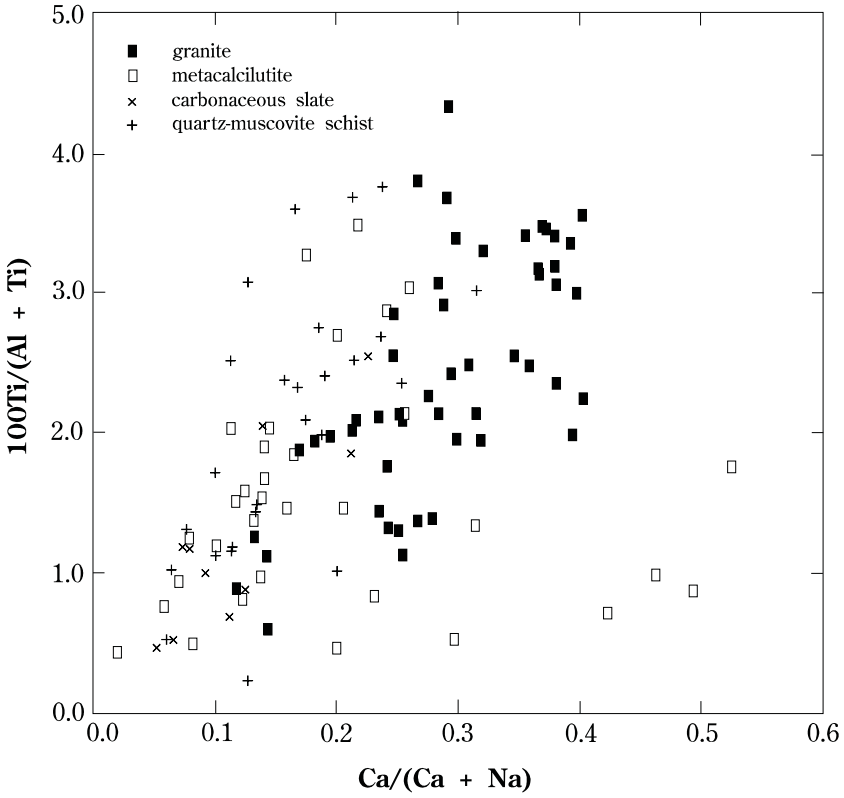

(e)

FIGURE 5.11 (continued)

granitic-pegmatitic tourmaline field of Neiva (1974), and are difficult to differentiate on the basis of this standard plot. This is not surprising, given the fact that they are all demonstrably related to a single episode of alteration. In his study of the tourmalines associated with the nearby Starra mineralization, Davidson (1988) encountered similar problems discriminating tourmalines from different interpreted environments of formation when using the Na_2O-MgO-FeO ternary plot. He attempted to resolve these by plotting a ternary diagram which reflected the relative occupancies of the X, Y and Z sites by various cations.

Following this example a plot of 100Ti/Al - Ca/Na - Mg/Fe shows a clearer separation of tourmalines from different lithologies (Figure 5.11b). Most analyses lie towards the left-hand edge of the diagram, indicating the predominance of Na^+ in the X-site, but some samples from the calcareous rocks of the Staveley Formation have elevated Ca^{2+}, and the tourmaline from the granite is slightly richer in Ca^{2+} than that in the carbonaceous slates and quartz-muscovite schists of the Toole Creek Volcanics. These trends are better illustrated in Figure 5.11 (c and d). Figure 5.11b also shows that tourmalines in the carbonaceous slate and quartz-muscovite schists have compositions falling into distinct groups which are, however, each essentially continuations of the other. From Figure 5.11e it is clear that the separation of these groups arises largely because of differences in Mg/(Mg+Fe) ratios; the carbonaceous slates are relatively richer in Mg. Within each of these lithological groupings, however, this ratio is roughly constant. All tourmalines are interpreted to have formed at a broadly similar time, from the same hydrothermal system. The variations in mineral chemistry therefore probably reflect, at least in part, the variations in chemistry in the different lithologies in which they are found.

Colour banding, presumed to reflect compositional zoning, was noted in many specimens. Microprobe traverses across portions of four tourmaline grains revealed variations in relative abundances of Mg, Ti and Ca (Figure 5.12). Ti and Ca contents generally rise and fall sympathetically with each other, and behave antipathetically with Mg. Three of the grains analysed (JCU-27211/1, JCU-27238/2 and JCU-27238/4) suggest that, as tourmaline grew, Mg-contents initially rose outwards from grain cores,

FIGURE 5.12: Chemical zoning in tourmalines from Mount Dore, as revealed by electron microprobe analyses of variations in Mg, Ti and Ca contents. The significance of these fluctuations is not known. Note that all specimens analysed come from Mount Dore Granite. All grains are less than 1 mm in diameter.

FIGURE 5.12

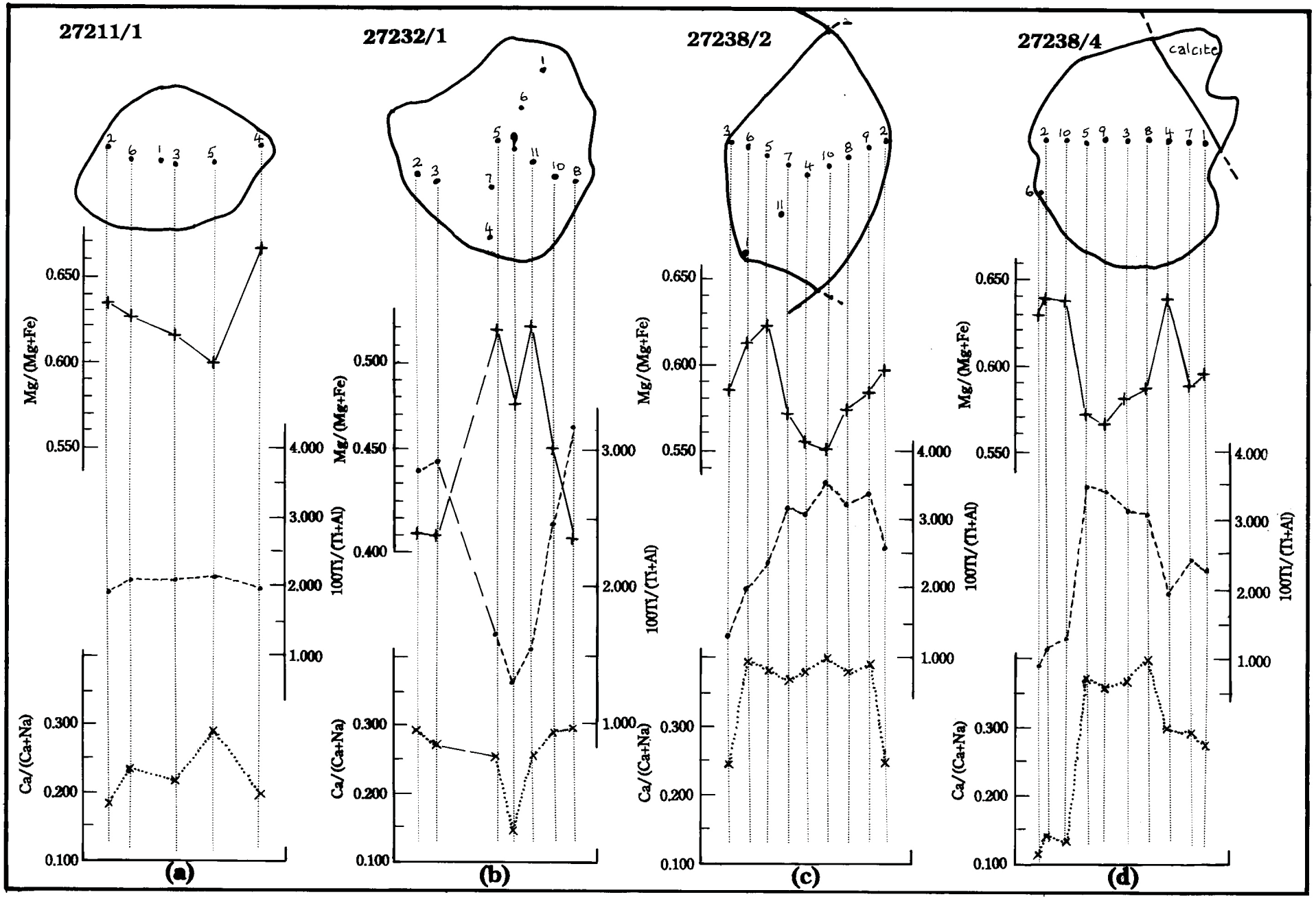
27211/1
27232/1
27238/2
27238/4
calcite
Mg/(Mg+Fe)
100Ti/(Ti+Al)
Ca/(Ca+Na)
(a)
(b)
(c)
(d)

before falling again towards the margins. No traverse was made across the entire width of any well-formed tourmaline crystal, however, and all grains studied come from altered granite. It is therefore hazardous to gauge overall trends in composition from cores to rims for both granitic tourmaline, and for that from other lithologies.

5.3.9 Apatite

Apatite can be a useful indicator of F and Cl abundances in the hydrothermal fluid from which it precipitated (*e.g.* Korzhinskiy, 1981; Sisson, 1987; Yardley, 1985). At Mount Dore apatite formed prior to dolomite and sulphides, and can therefore potentially provide valuable information on the chemistry of the fluid immediately preceding mineralization. Apatite has therefore been extensively analysed. A total of 93 analyses were made of nine grains or aggregates from seven samples representing the major lithologies. Structural formulae were calculated assuming eight cations per unit cell (Table 5.10).

Fifty of the apatite samples (17 out of 24 from the granite; 31 out of 60 from the carbonaceous slates; and 1 out of 5 from calcareous metasediments) yielded apparently greater than stoichiometric amounts of Cl and F per unit cell. The proportion of hydroxylapatite cannot be estimated in these specimens, since this component is assumed to make up the remainder of any unit cell after fluor- and chlorapatite components have been calculated. Where the latter two components sum to greater than 1.0, the hydroxylapatite content was calculated as zero, although this is probably not correct. The reason for the anomalously high halogen contents is unknown, but it is likely that the hydroxylapatite component is also present in significant amounts.

Where all three components are recognised, fluorapatite is dominant, and when hydroxylapatite abundance can be estimated, is generally more abundant than chlorapatite by a factor of three or greater (Figure 5.13). Those analyses of apatite from the granite which allowed abundances of all components to be estimated proved it to be

TABLE 5.10: Summary compositional data for apatite. Numbers in parentheses indicate number of analyses from each grain. Structural formulae have been calculated on the basis of eight cations per unit cell. #OH = 1-(#Cl+#F), where #F+#Cl < 1. Sample localities and brief descriptions are given in Table D1, and complete compositional data in Table D8 (both in Appendices).

	27121/2 (6)[1]	**27145/3 (5)**	**27202/5 (12)**	**27238/1 (6)**	**27238/2 (18)**	**27277/3 (14)**[1]	**27278/2 (10)**	**27278/3 (8)**	**27284/1 (14)**
FeO	0.015	0.042	0.063	-	0.039	0.063	0.154	0.08	0.08
MgO	0.038	0.022	0.072	0.03	0.014	0.030	0.053	0.026	0.011
CaO	56.295	56.016	55.755	55.363	56.109	54.455	54.499	54.525	55.238
Na_2O	0.113	0.06	0.057	0.087	0.072	0.053	0.048	0.031	0.03
P_2O_5	43.020	42.866	42.634	42.125	42.305	41.904	41.796	41.74	42.371
Cl	0.185	0.756	0.335	0.062	0.052	0.149	0.487	0.606	0.107
F	2.922	2.572	3.095	5.068	4.098	4.479	3.452	3.171	4.093
O=Cl,F	-1.272	-1.254	-1.379	-2.148	-1.737	-1.920	-1.564	-1.472	-1.748
TOTAL	**101.316**	**101.08**	**100.632**	**100.587**	**100.952**	**99.213**	**98.925**	**98.707**	**100.182**
#Fe+2	0.001	0.003	0.004	-	0.003	0.004	0.011	0.006	0.006
#Mg+2	0.005	0.003	0.009	0.004	0.002	0.004	0.007	0.003	0.001
#Ca+2	4.973	4.976	4.973	4.985	5.003	4.964	4.965	4.976	4.974
#Na+1	0.018	0.01	0.009	0.014	0.012	0.009	0.008	0.005	0.005
#P+5	3.003	3.009	3.005	2.997	2.981	3.019	3.009	3.01	3.015
# cations	**8.000**	**8.000**	**8.000**	**8.000**	**8.000**	**8.000**	**8.000**	**8.000**	**8.000**
#Cl	0.026	0.106	0.047	0.009	0.007	0.021	0.07	0.087	0.015
#F	0.762	0.674	0.815	1.347	1.079	1.205	0.928	0.854	1.088
#OH	0.212	0.219	0.138	-	-	-	0.001	0.058	-
X(Cl-ap)	0.026	0.106	0.047	0.007	0.007	0.017	0.07	0.087	0.014
X(F-ap)	0.762	0.674	0.815	0.993	0.993	0.983	0.928	0.854	0.986
X(OH-ap)	0.212	0.219	0.138	-	-	-	0.001	0.058	-

[1] These samples had two analyses each removed, because they had been repeated to test for F burnoff.

FIGURE 5.13: Ternary plot of compositional data for apatite from Mount Dore, in terms of chlor-, fluor- and hydroxy- end-member components. Only those 48 analyses where all three components could be estimated are plotted. The remaining 50 analyses had greater than stoichiometric requirements of fluor- and chlorapatite, and the hydroxyapatite contents could not be calculated.

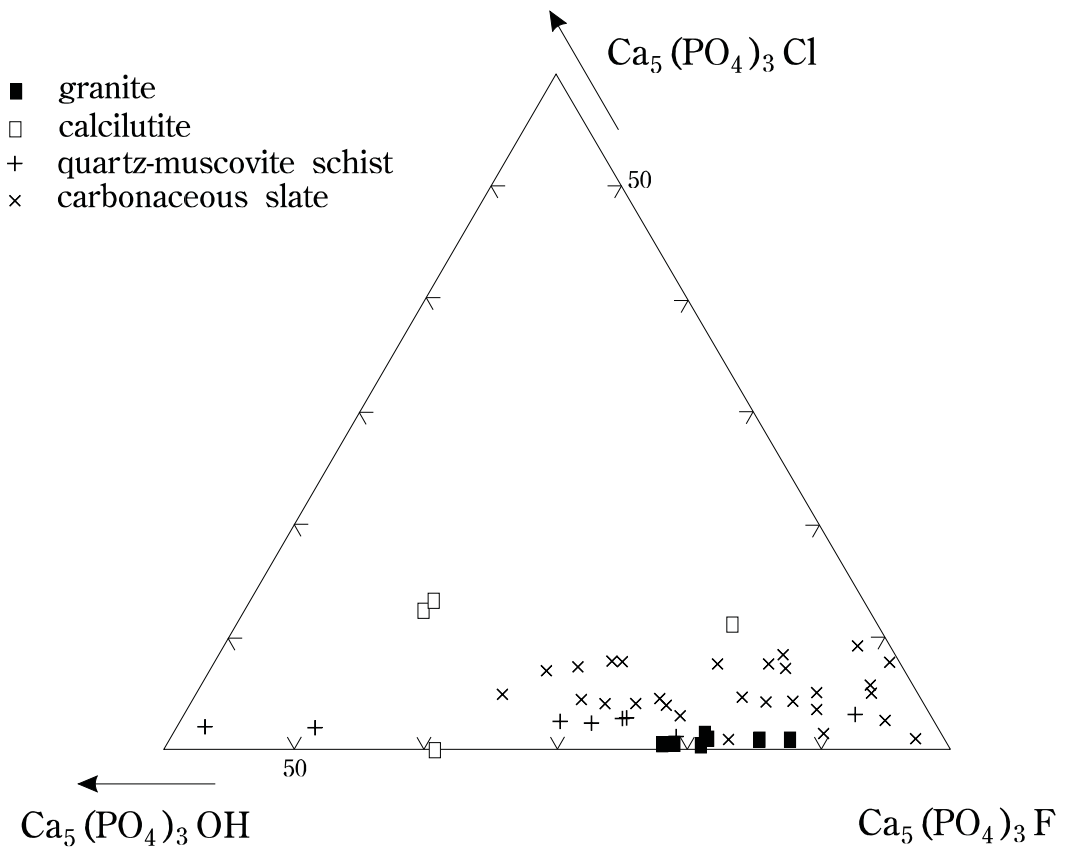

the richest of any in fluorapatite. Apatites from metasediments generally have lower fluorapatite abundances. Those from Staveley Formation lithologies have the lowest fluorapatite abundance, and are also significantly enriched in the chlorapatite component over that from other lithologies. Hydroxylapatite abundances are greater than for apatites from carbonaceous slate or granite, but are comparable or slightly less than for those from quartz-muscovite schist. Apatites from carbonaceous slates are slightly enriched in chlorapatite relative to those from granite or quartz-muscovite schist.

Several grains of apatite were tested for compositional zoning (Figure 5.14). Most are from granite, and several of these are "hyperstoichiometric" (F+Cl>1.0). These analyses do show a variation in the absolute abundances of F and Cl, and the flat, featureless plots (Figure 5.14b,c,g) suggest that the ratio of fluor- to chlorapatite component is relatively constant. Where all three components are present, variation appears to be mainly in the relative abundances of fluor- and hydroxylapatite components, with the former usually decreasing and the latter increasing towards grain margins. Zoning is less regular in apatites from carbonaceous slate, and the ratio of fluor- to chlorapatite is variable. Zoning in apatites from other lithologies remain untested.

Hyperstoichiometric analyses cannot be included in fluid geochemical calculations, because estimates of mole proportions of all components are required. Fortunately, many of the "hyper-stoichiometric" analyses are from apatites in the granite, which is essentially unmineralized. Enough "normal" analyses exist from host rocks where all three end-member components are present in non-zero proportions to perform some preliminary calculations (Appendix E).

FIGURE 5.14: Maps and compositional data for traverses across selected apatite grains, to examine variations in contents of end-member components. All grains are less than 1 mm in diameter (most considerably so).

FIGURE 5.14

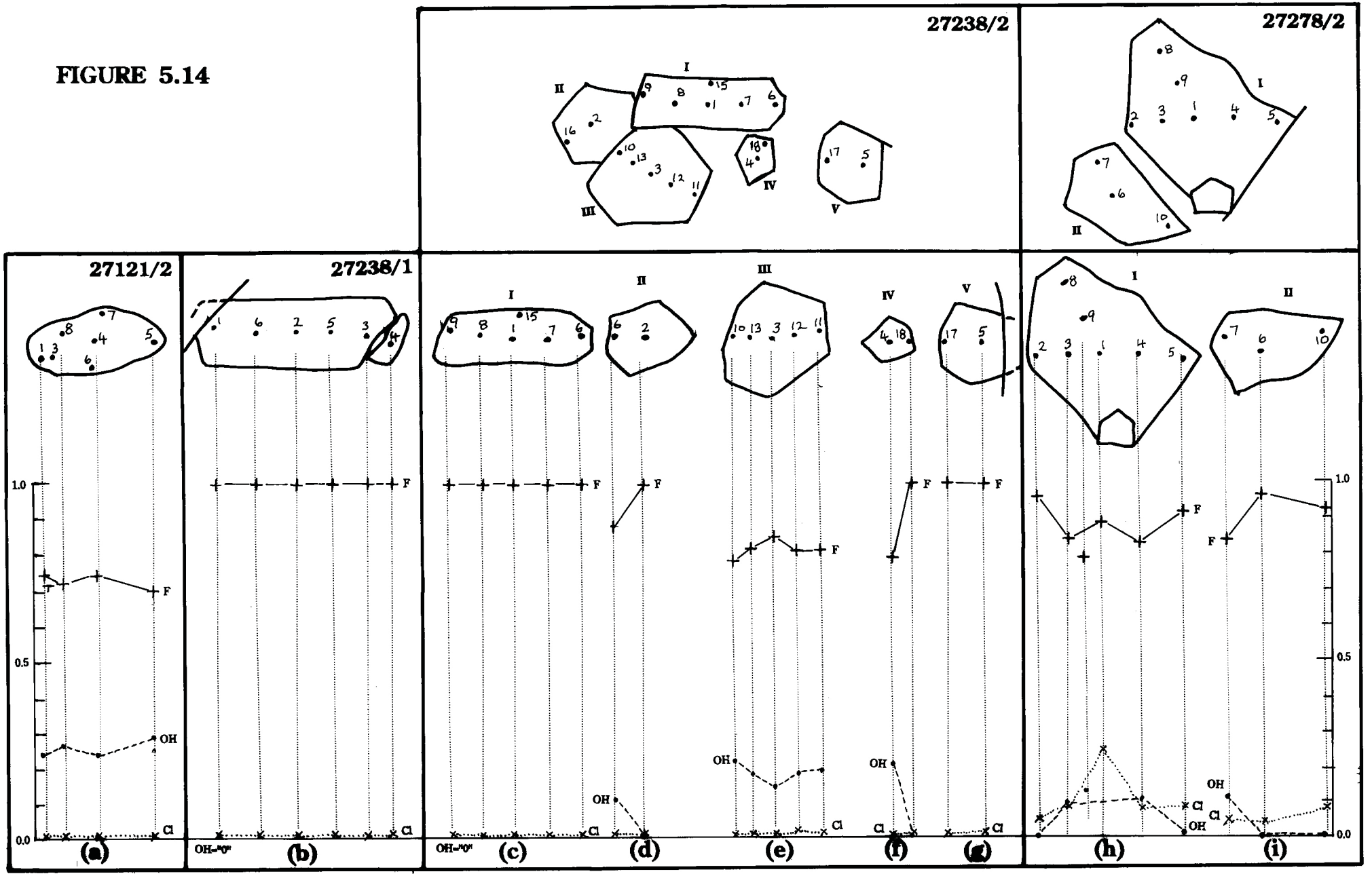
27238/2
27278/2
27121/2
27238/1
I
II
III
IV
V
1.0
0.5
0.0
F
OH
Cl
OH="0"
(a)
(b)
(c)
(d)
(e)
(f)
(g)
(h)
(i)

5.3.10 Biotite

A total of 49 analyses were made of 19 grains of biotite from 13 samples, and a further 9 analyses from two samples were extracted from the data of Ophel (1980). Stoichiometry has been calculated assuming 24(O+OH+Cl+F)(Table 5.11). There was some difficulty involved with sample selection, because much of the biotite has been partly to completely replaced by chlorite. In some instances, partly to completely chloritized biotites have obviously been analysed, and many of the columns in Table 5.11 represent not so much a summary of the overall biotite composition, but a measure of the degree to which it has been chloritized (see below).

Biotite compositions are conventionally described in terms of four ideal end members, between which there is complete solid solution; *viz:*

phlogopite	$K_2Mg_6(Si_6Al_2)O_{20}(OH)_2$
annite	$K_2Fe^{2+}_6(Si_6Al_2)O_{20}(OH)_2$
eastonite	$K_2(Mg_5Al)(Si_5Al_3)O_{20}(OH)_2$
siderophyllite	$K_2(Fe_5Al)(Si_5Al_3)O_{20}(OH)_2$

This system is divided into "phlogopites", where Mg/(Mg+Fe) > 0.667, and "biotites", where Mg/(Mg+Fe) < 0.667. Biotites from Mount Dore plot predominantly in the "phlogopite" field (Figure 5.15a), although seven analyses fall outside the four-component field altogether, through having considerably more than one octahedrally coordinated Al^{3+} cation per formula unit. These are probably partly to completely chloritized specimens, and all are from samples of altered Staveley Formation meta-sediments. Biotites in the granite lie roughly along the biotite-phlogopite join, and are generally more iron-rich than other types (Figure 5.15a). The diagram is, however, somewhat misleading, because it assumes all samples have a full complement of two cations in the A-site. This is clearly not the case, as Figure 5.15b illustrates. Analyses on this diagram fall into two groups. Relatively fresh biotites are regarded to be those in the tightly clustered group of 34 analyses having greater than 1.75 cations in the A-site, and less than 0.5 octahedral Al^{3+} cations per formula unit (shown more clearly in

TABLE 5.11: Summary compositional data for biotite. Numbers in parentheses indicate number of analyses from each grain. Structural formulae have been calculated on the basis of 24(O+OH+F+Cl), after removing those analyses which were obviously of heavily chloritized biotite. Some mildly chloritized samples are probably still represented. Samples with the prefix 59- are from the data set of Ophel (1980). Sample localities and brief descriptions are given in Tables D1 and D2, and complete compositional data in Table D9 (all in Appendices).

TABLE 5.11: Biotite

	27097/1 (4)	**27099/3 (3)**	**27099/4 (4)**	**27130/3 (1)**	**27140/1 (3)**	**27140/2 (2)**	**27140/3 (2)**	**27141/1 (3)**	**27145/4 (3)**	**27160/1 (4)**	**27202/2 (2)**	**27202/4 (2)**	**27227/3 (3)**	**27231/1 (3)**	**27231/5 (3)**	**27281/2 (1)**	**27283/2 (2)**	**27284/2 (2)**	**27284/3 (3)**	**59288 (3)**	**59299 (6)**
SiO_2	37.368	43.623	39.243	46.78	39.193	40.09	39.015	39.127	38.627	38.162	40.59	39.74	38.583	38.877	38.647	41.36	39.47	35.59	39.893	38.73	38.702
TiO_2	1.232	0.117	0.6	-	1.043	0.655	1.145	0.703	1.333	0.635	0.42	0.1	3.333	1.793	2.08	0.88	1.065	0.495	0.723	0.62	1.017
Al_2O_3	16.795	19.647	15.407	25.36	14.313	13.405	13.955	13.983	13.077	19.25	12.97	12.685	13.823	13.63	13.62	12.2	13.16	14.95	13.31	13.137	13.955
Cr_2O_3	-	-	0.04	0.18	0.1	-	-	-	0.027	0.025	0.06	0.05	0.023	0.023	0.033	-	0.04	-	-	-	0.008
FeO	12.887	8.157	13.15	3.52	10.353	9.44	10.255	7.75	11.613	14.742	11.45	12.21	12.87	14.32	14.013	5.18	6.995	9.98	6.96	9.833	15.727
MnO	-	0.075	0.037	0.29	0.05	-	-	0.027	0.17	0.303	0.04	0.055	-	0.033	0.087	0.08	-	0.09	-	0.1	0.122
MgO	16.243	14.327	18.75	11.99	19.953	21.155	20.08	23.75	20.333	14.155	20.035	19.8	15.1	15.92	15.987	23.89	22.335	23.195	21.99	23.943	17.063
CaO	0.132	0.213	0.14	0.23	0.13	0.12	0.115	0.103	0.157	0.097	0.125	0.16	0.917	0.063	0.137	0.07	0.26	0.04	0.11	0.02	0.013
Na_2O	0.05	0.027	0.147	-	0.123	-	-	-	0.107	0.023	0.06	0.23	0.047	0.12	0.13	0.08	0.145	0.135	-	0.077	0.035
K_2O	7.19	6.337	8.987	5.27	9.927	9.79	10.265	9.4	8.307	3.91	9.83	9.335	10.037	10.6	10.713	10.73	8.115	4.705	10.21	6.153	8.933
H_2O	4.072	4.294	3.962	4.529	4.051	4.091	4.06	4.155	4.034	4.18	4.029	3.982	3.99	3.952	3.963	4.175	4.199	4.198	4.138	4.171	3.962
Cl	0.27	0.22	0.52	0.03	0.273	0.235	0.22	0.11	0.327	0.138	0.325	0.43	0.267	0.303	0.257	0.15	0.12	0.105	0.187	0.16	0.313
O=Cl	-0.061	-0.05	-0.117	-0.007	-0.062	-0.053	-0.05	-0.025	-0.074	-0.031	-0.073	-0.097	-0.06	-0.068	-0.058	-0.034	-0.027	-0.024	-0.042	-0.036	-0.071
TOTAL	**96.178**	**96.987**	**100.865**	**98.173**	**99.448**	**98.928**	**99.06**	**99.083**	**98.039**	**95.589**	**99.861**	**98.68**	**98.93**	**99.565**	**99.609**	**98.761**	**95.877**	**93.46**	**97.479**	**96.908**	**99.78**
#Si IV	5.629	6.204	5.692	6.303	5.733	5.854	5.737	5.661	5.736	5.686	5.924	5.898	5.761	5.808	5.773	5.962	5.844	5.417	5.865	5.694	5.751
#Al IV	2.371	1.796	2.308	1.697	2.267	2.146	2.263	2.339	2.264	2.314	2.076	2.102	2.239	2.192	2.227	2.038	2.156	2.583	2.135	2.276	2.249
#Ti IV	-	-	-	-	-	-	-	-	-	-	-	-	-	-	-	-	-	-	-	0.030	-
T site	**8.000**	**8.000**	**8.000**	**8.000**	**8.000**	**8.000**	**8.000**	**8.000**	**8.000**	**8.000**	**8.000**	**8.000**	**8.000**	**8.000**	**8.000**	**8.000**	**8.000**	**8.000**	**8.000**	**8.000**	**8.000**
#Al VI	0.611	1.497	0.326	2.330	0.200	0.161	0.156	0.046	0.025	1.067	0.154	0.117	0.193	0.208	0.171	0.035	0.140	0.099	0.172	-	0.195
#Ti VI	0.140	0.013	0.065	-	0.115	0.072	0.127	0.076	0.149	0.071	0.046	0.011	0.374	0.201	0.234	0.095	0.119	0.057	0.080	0.039	0.114
#Cr	-	-	0.005	0.019	0.012	-	-	-	0.003	0.003	0.007	0.006	0.003	0.003	0.004	-	0.005	-	-	-	0.001
#Fe +2	1.623	0.970	1.595	0.397	1.266	1.153	1.261	0.938	1.442	1.837	1.397	1.515	1.607	1.789	1.751	0.624	0.866	1.270	0.856	1.209	1.954
#Mn +2	-	0.009	0.005	0.033	0.006	-	-	0.003	0.021	0.038	0.005	0.007	-	0.004	0.011	0.010	-	0.012	-	0.012	0.015
#Mg	3.648	3.037	4.054	2.408	4.351	4.605	4.402	5.123	4.501	3.144	4.359	4.381	3.361	3.546	3.560	5.134	4.930	5.263	4.820	5.248	3.780
O site	6.021	5.526	6.050	5.188	5.949	5.990	5.946	6.186	6.142	6.160	5.968	6.037	5.538	5.751	5.731	5.898	6.059	6.702	5.927	6.508	6.059
#Ca	0.021	0.032	0.022	0.033	0.020	0.019	0.018	0.016	0.025	0.015	0.020	0.025	0.147	0.010	0.022	0.011	0.041	0.007	0.017	0.003	0.002
#Na	0.015	0.007	0.041	-	0.035	-	-	-	0.031	0.007	0.017	0.066	0.014	0.035	0.038	0.022	0.042	0.040	-	0.022	0.010
#K	1.382	1.150	1.663	0.906	1.852	1.824	1.926	1.735	1.574	0.743	1.830	1.767	1.912	2.020	2.042	1.973	1.533	0.914	1.915	1.154	1.693
A site	1.418	1.190	1.726	0.939	1.908	1.842	1.944	1.751	1.630	0.765	1.867	1.859	2.072	2.065	2.101	2.006	1.616	0.960	1.932	1.179	1.706
#O	20.000	20.000	20.000	20.000	20.000	20.000	20.000	20.000	20.000	20.000	20.000	20.000	20.000	20.000	20.000	20.000	20.000	20.000	20.000	20.000	20.000
#OH	3.931	3.947	3.872	3.993	3.932	3.942	3.945	3.973	3.918	3.965	3.920	3.892	3.932	3.923	3.935	3.963	3.970	3.973	3.953	3.960	3.921
#Cl	0.069	0.053	0.128	0.007	0.068	0.058	0.055	0.027	0.082	0.035	0.080	0.108	0.068	0.077	0.065	0.037	0.030	0.027	0.047	0.040	0.079
Charge	**0.000**	**0.000**	**0.000**	**0.000**	**0.000**	**0.000**	**0.000**	**0.000**	**0.000**	**0.000**	**0.000**	**0.000**	**0.000**	**0.000**	**0.000**	**0.000**	**0.000**	**0.000**	**0.000**	**0.000**	**0.000**
Mg/(Mg+Fe)	0.692	0.758	0.718	0.858	0.775	0.800	0.777	0.845	0.757	0.631	0.757	0.743	0.677	0.665	0.670	0.892	0.851	0.806	0.849	0.813	0.659
$Si/(Si+Al_{tet})$	0.704	0.775	0.711	0.788	0.717	0.732	0.717	0.708	0.717	0.711	0.740	0.737	0.720	0.726	0.722	0.745	0.730	0.677	0.733	0.714	0.719

FIGURE 5.15: Total compositional data for biotites from Mount Dore:
(a) Plot of Mg/(Fe+Mg) vs Al_{oct}, showing that most "biotites" actually lie in the phlogopite field, and that biotite from the granite has the most tightly constrained composition, and thus likely to be igneous. Seven analyses are not shown here, as they plot to the far right hand side of the diagram. These analyses are of extensively chloritized biotite, and are all from Staveley Formation hosts;
(b) plot of A-site occupancy vs Al_{oct}. The wide spread of data is due to extensive chloritization of the biotite. Again, granitic biotite compositions are closely clustered;]
(c) excerpt from (b) illustrating field of biotites interpreted to have undergone minimal alteration to chlorite.

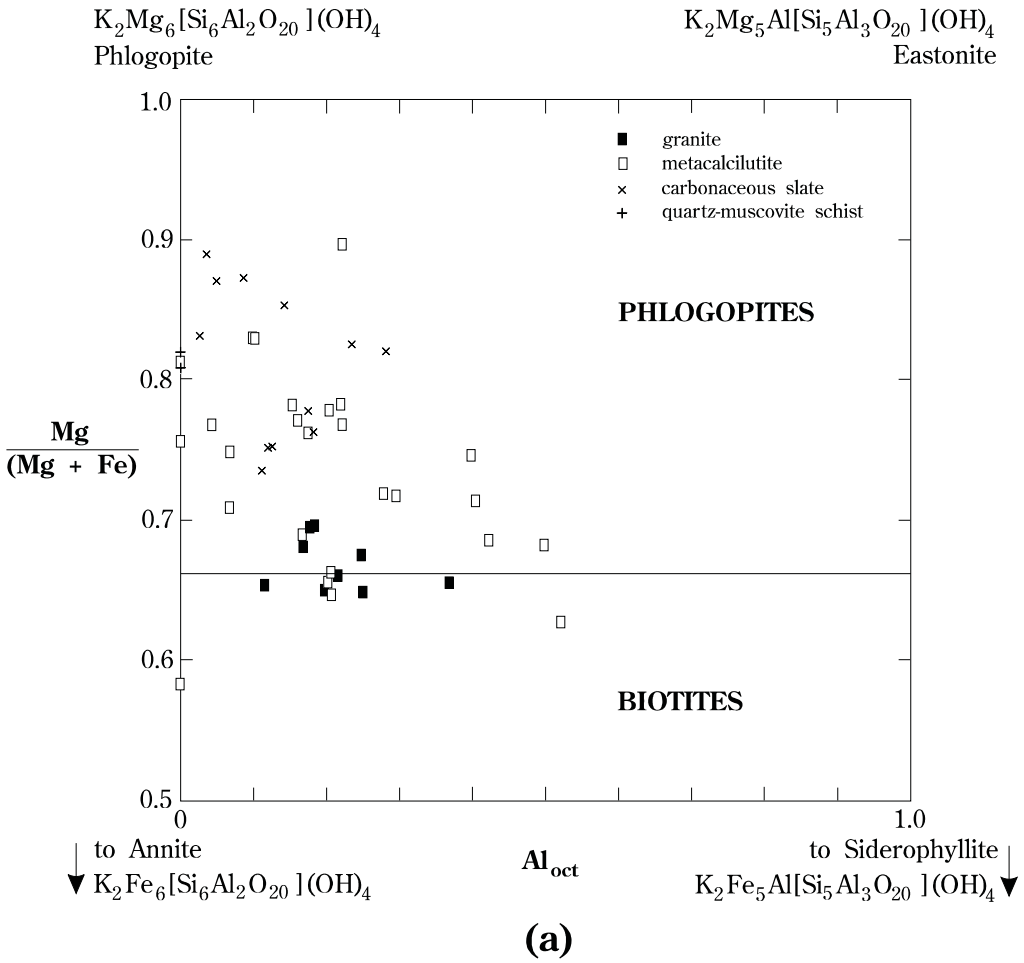

(a)

FIGURE 5.15 (continued)

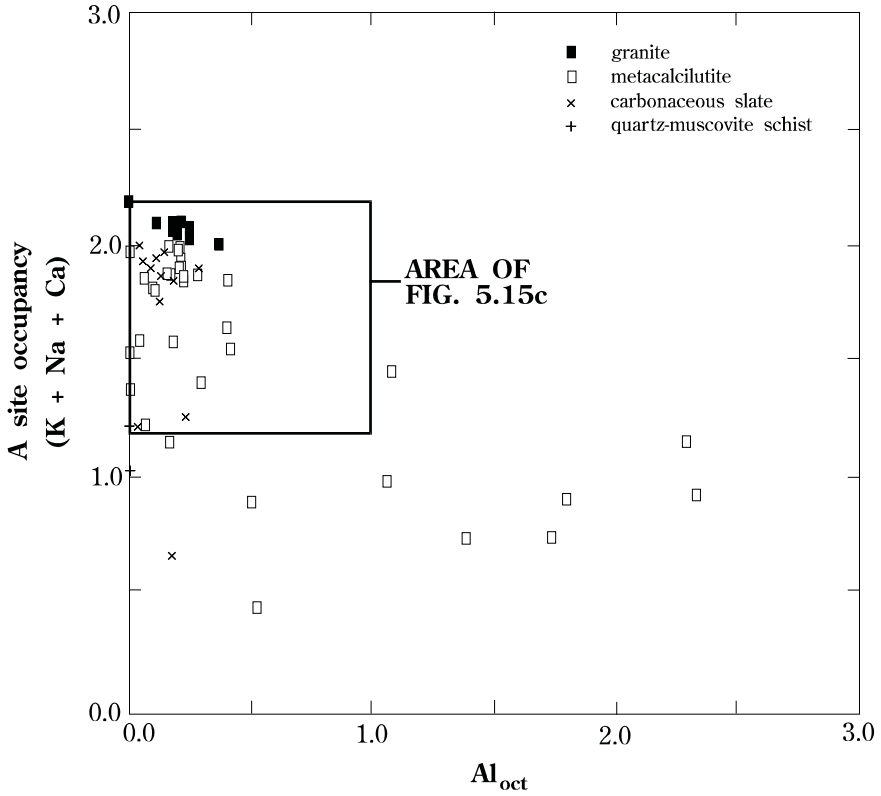

(b)

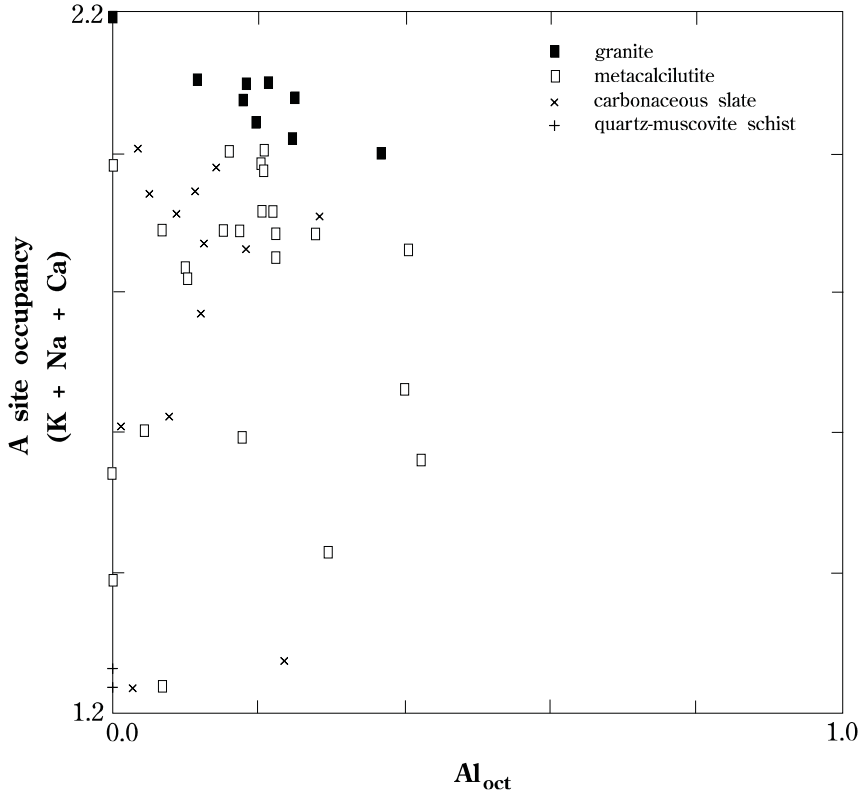

(c)

Figure 5.15c). The remaining twenty-four analyses, having A-site occupancies of less than 1.75, and octahedral Al^{3+} contents ranging from zero up to 2.3 per formula unit are biotites which have enjoyed varying degrees of chloritization.

Of the "true" biotites, that in the granite is interpreted on textural grounds to be late magmatic in origin, rather than alteration-related. It occurs only where the granite, although deformed, remains comparatively unaltered. Where alteration is more prevalent, granitic biotite is completely replaced by chlorite. Granitic biotite also generally has higher TiO_2 content than analysed biotites from other lithologies, which are regarded - also on textural criteria - to be exclusively of hydrothermal origin.

5.3.11 Carbonate

Seventy analyses were obtained from 16 grains in 15 samples, and a further three analyses from a single sample were taken from the data set of Ophel (1980; Table 5.12). Stoichiometry was calculated on the basis of six oxygen atoms per formula unit. Both dolomite and calcite were identified, although in any particular specimen only one of these phases is present. Fe and Mn occur in only minor amounts in both phases, and stoichiometries are generally close to ideal. The carbonate in granite at a distance from the mineralized zone is calcite. Closer to the contact with mineralized meta-sediments, where brecciation occurs, the carbonate is dolomite. Carbonate in the carbonaceous slates is predominantly dolomite. Both calcite and dolomite occur in altered Staveley Formation lithologies. Both appear to be in a similar position in the alteration paragenesis, but the reason for the development of one or the other is not clear.

TABLE 5.12: Summary composition data for carbonates. Numbers in parentheses indicate number of analyses from each grain. Structural formulae have been calculated on the basis of six oxygen atoms per formula unit, using the CARBONAT.EXE subroutine in **MINFILE** (Afifi and Essene, 1988). Sample with the prefix 59- is from the data set of Ophel (1980). Sample localities and brief descriptions are given in Tables D1 and D2, and complete compositional data in Table D10 (all in Appendices).

	27097/2 (6)	**27102/4 (6)**	**27124/5 (6)**	**27130/2 (4)**	**27133/4 (6)**	**27140/2 (3)**	**27146/1 (4)**	**27158/2 (3)**	**27211/2 (3)**	**27220/1 (4)**	**27238/2 (4)**	**27238/4 (7)**	**27242/1 (3)**	**27278/1 (4)**	**27281/1 (3)**	**27287/1 (4)**	**59288 (3)**
CaO	32.643	33.092	59.678	60.103	59.597	60.27	29.208	29.297	27.427	29.08	55.362	51.291	29.3	28.927	29.047	29.798	29.98
MgO	24.342	25.422	0.05	0.015	0.045	0.07	22.362	22.25	22.083	22.315	0.262	3.296	22.123	21.267	22.157	21.44	21.577
FeO	0.918	0.458	0.075	0.057	0.032	0.087	0.203	0.337	0.35	0.52	0.138	0.43	0.273	1.492	0.483	0.918	0.683
MnO	0.732	0.612	0.503	0.7	0.212	0.407	0.652	0.793	0.457	0.355	0.51	0.514	0.263	0.52	0.633	0.5	0.263
CO_2	53.214	54.389	47.247	47.653	46.97	47.68	47.869	47.985	46.135	47.727	44.134	44.433	47.482	47.161	47.678	47.668	47.67
TOTAL	**111.849**	**113.973**	**107.553**	**108.528**	**106.856**	**108.514**	**100.294**	**100.662**	**96.452**	**99.997**	**100.406**	**99.964**	**99.441**	**99.367**	**99.998**	**100.324**	**100.173**
#Ca	0.963	0.955	1.983	1.98	1.991	1.984	0.958	0.958	0.933	0.956	1.969	1.812	0.969	0.963	0.956	0.981	0.987
#Mg	0.999	1.021	0.002	0.001	0.002	0.003	1.02	1.013	1.045	1.021	0.013	0.162	1.018	0.985	1.015	0.982	0.988
#Fe	0.021	0.01	0.002	0.001	0.001	0.002	0.005	0.009	0.009	0.013	0.004	0.012	0.007	0.039	0.012	0.024	0.018
#Mn	0.017	0.014	0.013	0.018	0.006	0.011	0.017	0.021	0.012	0.009	0.014	0.014	0.007	0.014	0.016	0.013	0.007
#CO_3	2.000	2.000	2.000	2.000	2.000	2.000	2.000	2.000	2.000	2.000	2.000	2.000	2.000	2.000	2.000	2.000	2.000
PARENT[1]	1	1	1	1	1	1	1	1	2	3	2	2	2	3	3	3	3

[1] **PARENT** refers to the interpreted original lithology, sometimes still recognisable; in other instances it is inferred from surrounding identifiable lithologies; *e.g.* heavily altered breccia in lutites, *etc.* 1 = variably calcareous lutites of the Staveley Formation; 2 = Mount Dore Granite; 3 = carbonaceous slates of the Toole Creek Volcanics.

5.3.12 Chlorite

Compositional data for chlorites from Mount Dore come from: eighty-nine analyses of thirty grains from twenty samples from this study; thirty-five analyses of ten samples collected and studied by Ophel (1980); and a further fourteen chlorite averages from the work of Scott (1988), based on seventy-six determinations (for which full data are unfortunately unavailable). Stoichiometry, including H_2O content, was calculated assuming 18(O+OH+Cl) per formula unit. All iron is assumed to be ferrous (Table 5.13).

Natural chlorite compositions most commonly lie between those of the two end members antigorite $Mg_6Si_4O_{10}(OH)_8$ and amesite $(Mg_4Al_2)(Si_2Al_2)O_{10}(OH)_8$, and are obtained via a coupled exchange reaction: $Si^{4+}M^{2+} == Al^{3+}_{TET}Al^{3+}_{OCT}$. Fe^{2+} may substitute partly to completely for Mg^{2+} (Phillips and Griffin, 1981). Other significant substitutions which may occur are Fe^{3+} for Al^{3+}, in either the tetrahedral or octahedral site, or Fe^{3+} for divalent cations, in which case protons are lost from the structure, and oxidised chlorites result (Walshe, 1986). Unfortunately, it is not possible to directly assess the amount of substitution of Al^{3+} by Fe^{3+} from microprobe analyses.

Chlorites from Mount Dore show a broad spectrum of compositions, from Mg-rich to Fe-rich (Figure 5.16). There is also an overall trend of decreasing Mg^{2+} with increasing Al^{3+}. This trend may be a temporal one. Optical examination of coarser replacement and vein infill chlorites suggests that early material was more magnesian (paler green pleochroism), and later material was more ferrous (darker green pleochroism). This was, however, specifically tested in only two specimens. In a traverse across a vein (JCU-27130), early formed, partly replacive (after dolomite) chlorite is relatively Mg-rich, and the material towards the centre of the vein is more Fe-rich. In sample JCU-27287/2, chlorite and carbonate are replacing an unidentifiable prismatic phase (actinolite? scapolite?) in a calcareous Staveley Formation lithology. The chlorite towards the centre is more magnesian than that towards the edge.

TABLE 5.13: Summary compositional data for chlorite. Numbers in parentheses indicate number of analyses from each grain. Structural formulae have been calculated on the basis of 18(O+OH+Cl) per formula unit, using the CHLORITE.EXE subroutine in **MINFILE** (Afifi and Essene, 1988). All iron is assumed to be ferrous. Samples with the prefix 59- are from the data set of Ophel (1980), and those with the prefix 101- are from Scott (1988). Sample localities and brief descriptions are given in Tables D1, D2 and D3, and complete compositional data in Table D11 (all in Appendices).

	27077/2 (2)	**27102/3 (3)**	**27124/4 (3)**	**27124/5 (2)**	**27130/2 (6)**	**27130/3 (3)**	**27140/1 (1)**	**27146/4 (3)**	**27158/1 (3)**	**27181/5 (3)**	**27202/1 (3)**	**27202/2 (1)**	**27202/4 (2)**	**27227/2 (3)**	**27231/4 (3)**	**27238/1 (3)**	**27238/3 (2)**	**27243/2 (3)**
SiO_2	24.665	29.467	25.55	25.895	29.625	33.66	30.81	28.187	25.73	27.013	38.647	38.53	32.245	26.12	26.4	27.28	29.415	26.937
TiO_2	-	-	-	-	-	0.027	0.06	-	0.053	0.023	0.023	-	0.404	0.117	0.047	-	0.035	0.087
Al_2O_3	20.465	14.083	19.443	19.56	15.687	15.237	17.58	16.083	22.52	18.697	15.73	16.3	13.155	20.673	20.327	18.283	17.775	20.603
FeO	21.845	16.547	29.347	28.785	19.517	11.413	10.15	27.42	21.077	35.797	6.23	11.06	18.34	22.99	22.447	22.657	22.095	20.12
MnO	0.245	0.417	1.67	1.825	1.395	0.87	0.19	0.407	0.207	0.597	-	-	-	0.947	0.4	0.063	0.07	0.563
MgO	12.99	22.383	11.343	11.635	19.425	25.02	27.93	14.497	17.517	5.943	26.263	24.01	17.76	15.383	16.813	14.643	17.48	17.733
CaO	0.025	0.043	0.03	0.12	0.207	0.153	0.4	0.127	0.037	0.047	0.38	0.53	0.115	0.087	0.017	0.42	0.18	0.017
Na_2O	0.055	0.043	0.06	0.05	2.232	0.15	0.21	0.043	-	0.133	0.337	0.27	0.475	0.133	0.143	0.12	0.125	0.213
K_2O	0.25	0.033	0.073	-	0.017	0.247	0.05	0.017	-	0.78	0.26	0.15	3.375	-	-	0.02	0.575	-
H_2O	11.609	11.934	11.152	11.211	11.654	12.316	12.351	11.364	11.72	10.891	12.77	12.51	11.577	11.572	11.63	11.627	11.682	11.758
Cl	0.025	0.04	0.057	-	0.037	0.013	-	-	0.057	0.017	0.05	0.05	0.37	0.02	0.023	0.017	0.02	0.043
O=Cl	-0.006	-0.009	-0.013	-	-0.008	-0.003	-	-	-0.013	-0.004	-0.011	-0.01	-0.083	-0.005	-0.005	-0.004	-0.005	-0.01
TOTAL	**92.168**	**94.981**	**98.712**	**99.081**	**99.788**	**99.103**	**99.731**	**98.145**	**98.905**	**99.934**	**100.679**	**103.4**	**97.732**	**98.037**	**98.242**	**95.126**	**99.448**	**98.065**
#Si IV	2.794	3.137	2.784	2.799	3.053	3.311	3.001	3.038	2.662	2.976	3.597	3.552	3.378	2.767	2.776	2.977	3.037	2.806
#Al IV	1.206	0.863	1.216	1.201	0.947	0.689	0.999	0.962	1.338	1.024	0.403	0.448	0.622	1.233	1.224	1.023	0.963	1.194
T site	**4.000**	**4.000**	**4.000**	**4.000**	**4.000**	**4.000**	**4.000**	**4.000**	**4.000**	**4.000**	**4.000**	**4.000**	**4.000**	**4.000**	**4.000**	**4.000**	**4.000**	**4.000**
#Al VI	1.526	0.904	1.281	1.291	0.959	1.077	1.019	1.081	1.408	1.403	1.323	1.324	1.002	1.349	1.295	1.328	1.200	1.336
#Ti	-	-	-	-	-	0.002	0.004	-	0.004	0.002	0.002	-	0.032	0.009	0.004	-	0.003	0.007
#Fe +2	2.069	1.473	2.674	2.602	1.682	0.939	0.827	2.472	1.824	3.298	0.485	0.853	1.607	2.037	1.974	2.068	1.908	1.753
#Mn +2	0.024	0.038	0.154	0.167	0.122	0.072	0.016	0.037	0.018	0.056	-	-	-	0.085	0.036	0.006	0.006	0.050
#Mg	2.194	3.552	1.843	1.875	2.984	3.668	4.055	2.330	2.702	0.976	3.644	3.300	2.774	2.430	2.636	2.382	2.691	2.754
#Ca	0.003	0.005	0.004	0.014	0.023	0.016	0.042	0.015	0.004	0.006	0.038	0.052	0.013	0.010	0.002	0.049	0.020	0.002
#Na	0.012	0.009	0.013	0.010	0.446	0.029	0.040	0.009	-	0.028	0.061	0.048	0.096	0.027	0.029	0.025	0.025	0.043
#K	0.036	0.004	0.010	-	0.002	0.031	0.006	0.002	-	0.110	0.031	0.018	0.451	-	-	0.003	0.076	-
O site	**5.864**	**5.986**	**5.979**	**5.960**	**6.218**	**5.834**	**6.009**	**5.946**	**5.961**	**5.878**	**5.584**	**5.595**	**5.975**	**5.946**	**5.975**	**5.861**	**5.929**	**5.944**
#O	10.000	10.000	10.000	10.000	10.000	10.000	10.000	10.000	10.000	10.000	10.000	10.000	9.845	10.000	10.000	10.000	10.000	10.000
#OH	7.995	7.993	7.989	8.000	7.994	7.998	8.000	8.000	7.990	7.997	7.992	7.992	8.089	7.996	7.996	7.997	7.997	7.992
#Cl	0.005	0.007	0.011	-	0.006	0.002	-	-	0.010	0.003	0.008	0.008	0.066	0.004	0.004	0.003	0.003	0.008
Charge	**0.000**	**0.000**	**0.000**	**0.000**	**0.000**	**0.000**	**0.000**	**0.000**	**0.000**	**0.000**	**0.000**	**0.000**	**0.000**	**0.000**	**0.000**	**0.000**	**0.000**	**0.000**
Mg/(Mg+Fe)	0.515	0.707	0.408	0.419	0.640	0.796	0.831	0.485	0.597	0.228	0.883	0.795	0.633	0.544	0.572	0.535	0.585	0.611

TABLE 5.13: Chlorite (continued)

	27243/4 (3)	**27277/1 (4)**	**27278/1 (5)**	**27278/2 (3)**	**27281/1 (3)**	**27281/2 (3)**	**27283/1 (4)**	**27283/3 (2)**	**27284/2 (1)**	**27284/3 (2)**	**27284/5 (3)**	**27287/2 (6)**	**59278 (9)**	**59284 (5)**	**59287 (3)**	**59288 (2)**	**59299 (3)**	**59306 (1)**
SiO_2	26.3	27.605	31.572	30.743	27.85	28.447	29.347	31.58	29.95	28	27.64	31.805	25.608	31.69	28.74	33.125	34.41	29.13
TiO_2	0.07	-	0.198	0.268	0.03	-	0.093	-	-	0.035	0.033	-	0.068	0.032	0.017	0.75	0.01	0.11
$Al2O_3$	20.39	14.785	14.64	14.127	21.667	20.977	18.233	18.265	17.53	20.45	16.377	13.668	25.387	17.24	19.147	14.93	16.387	18.06
FeO	19.767	24.07	18.75	15.945	10.59	10.723	9.932	18.205	17.05	13.34	31.523	17.278	38.561	18.624	16.03	12.735	17.4	18.99
MnO	0.517	0.28	0.294	0.075	0.183	0.167	0.108	0.04	0.08	0.165	0.327	0.207	0.138	0.532	0.257	0.17	0.357	0.8
MgO	18.403	15.767	20.784	20.343	25.123	25.65	26.225	20.945	20.65	24.07	11.17	22.6	5.421	22.688	23.64	24.66	22.977	19.86
CaO	0.013	0.085	0.132	0.083	0.077	0.057	0.023	0.195	0.14	0.025	0.09	0.348	0.11	0.076	0.07	0.115	0.103	0.01
Na_2O	0.183	0.087	0.024	0.043	0.037	0.133	0.12	0.12	-	0.155	0.25	0.057	0.05	0.008	-	0.14	-	0.04
K_2O	0.03	0.183	1.012	2.152	0.013	0.013	0.317	0.05	0.44	-	0.037	0.012	0.044	0.026	0.03	1.66	0.393	0.53
H_2O	11.757	11.467	11.808	11.798	12.342	12.327	12.35	11.999	11.97	12.175	11.128	11.968	10.943	11.935	12.026	12.085	12.055	11.82
Cl	0.027	0.05	0.098	0.282	-	0.023	0.02	-	0.04	-	0.027	0.018	0.004	0.006	-	0.215	-	-
O=Cl	-0.006	-0.011	-0.022	-0.064	-	-0.005	-0.005	-	-0.009	-	-0.006	-0.004	-0.001	-0.001	-	-0.049	-	-
TOTAL	**97.451**	**94.368**	**99.289**	**95.795**	**97.912**	**98.511**	**96.763**	**101.399**	**97.841**	**98.415**	**98.596**	**97.957**	**106.333**	**102.856**	**99.957**	**100.536**	**104.092**	**99.35**
#Si IV	2.761	3.079	3.225	3.258	2.772	2.814	2.958	3.107	3.073	2.809	3.025	3.261	2.620	3.084	2.868	3.251	3.271	2.979
#Al IV	1.239	0.921	0.775	0.742	1.228	1.186	1.042	0.893	0.927	1.191	0.975	0.739	1.380	0.916	1.132	0.749	0.729	1.021
T site	**4.000**	**4.000**	**4.000**	**4.000**	**4.000**	**4.000**	**4.000**	**4.000**	**4.000**	**4.000**	**4.000**	**4.000**	**4.000**	**4.000**	**4.000**	**4.000**	**4.000**	**4.000**
#Al VI	1.283	1.023	0.988	1.023	1.314	1.260	1.124	1.225	1.193	1.227	1.137	0.913	1.681	1.061	1.119	0.978	1.107	1.155
#Ti	0.006	-	0.015	0.021	0.002	-	0.007	-	-	0.003	0.003	-	0.005	0.002	0.001	0.055	0.001	0.008
#Fe +2	1.735	2.245	1.602	1.413	0.882	0.887	0.837	1.498	1.463	1.119	2.885	1.482	3.299	1.516	1.338	1.045	1.383	1.624
#Mn +2	0.046	0.026	0.025	0.007	0.015	0.014	0.009	0.003	0.007	0.014	0.030	0.018	0.012	0.044	0.022	0.014	0.029	0.069
#Mg	2.880	2.622	3.165	3.214	3.728	3.783	3.940	3.072	3.159	3.600	1.822	3.455	0.827	3.291	3.516	3.608	3.256	3.028
#Ca	0.001	0.010	0.014	0.009	0.008	0.006	0.002	0.021	0.015	0.003	0.011	0.038	0.012	0.008	0.007	0.012	0.010	0.001
#Na	0.037	0.019	0.005	0.009	0.007	0.026	0.023	0.023	-	0.030	0.053	0.011	0.010	0.002	-	0.027	-	0.008
#K	0.004	0.026	0.132	0.291	0.002	0.002	0.041	0.006	0.058	-	0.005	0.002	0.006	0.003	0.004	0.208	0.048	0.069
O site	**5.993**	**5.971**	**5.947**	**5.988**	**5.959**	**5.977**	**5.984**	**5.848**	**5.895**	**5.995**	**5.946**	**5.919**	**5.852**	**5.927**	**6.007**	**5.947**	**5.834**	**5.963**
#O	10.000	10.000	10.000	10.000	10.000	10.000	10.000	10.000	10.000	10.000	10.000	10.000	10.000	10.000	10.000	10.000	10.000	10.000
#OH	7.995	7.991	7.983	7.949	8.000	7.996	7.997	8.000	7.993	8.000	7.995	7.997	7.999	7.999	8.000	7.964	8.000	8.000
#Cl	0.005	0.009	0.017	0.051	-	0.004	0.003	-	0.007	-	0.005	0.003	0.001	0.001	-	0.036	-	-
Charge	**0.000**	**0.000**	**0.000**	**0.000**	**0.000**	**0.000**	**0.000**	**0.000**	**0.000**	**0.000**	**0.000**	**0.000**	**0.000**	**0.000**	**0.000**	**0.000**	**0.000**	**0.000**
Mg/(Mg+Fe)	0.624	0.539	0.664	0.695	0.809	0.810	0.825	0.672	0.683	0.763	0.387	0.700	0.200	0.685	0.724	0.775	0.702	0.702

TABLE 5.13: Chlorite (continued)

	59308 (2)	**59313 (3)**	**59314 (1)**	**59315 (6)**	**101276 (3)**	**101292 (5)**	**101295 (8)**	**101330 (6)**	**101339 (8)**	**101340 (9)**	**101377/1 (7)**	**101377/2 (4)**	**101463/1 (4)**	**101463/2 (5)**	**101507/1 (3)**	**101507/2 (4)**	**101509 (8)**	**101840 (2)**
SiO_2	33.175	26.123	25.33	29.342	34.5	29.3	33.9	29	32.1	32.8	24.8	32.2	25.7	32.7	33.4	26.4	34.5	25
TiO_2	0.015	0.06	-	0.04	0.12	0.69	0.52	0.04	0.03	0.28	0.03	0.18	0.02	0.01	0.01	0.05	0.02	0.04
Al_2O_3	10.3	22.85	19.53	15.375	30.6	18.9	28.3	19.9	19.3	17.3	14.5	14.9	19.4	15.8	21.2	19.9	15.6	17.7
FeO	12.365	32.093	26.39	27.605	3.5	18	6.85	17	13.6	15.8	22.7	7.61	20.9	6.11	13.7	34.5	17.7	15
MnO	0.755	1.78	0.17	0.563	0.02	0.29	0.02	0.14	0.31	0.31	0.48	0.1	0.46	0.02	0.04	0.29	0.22	0.16
MgO	24.185	11.203	14.63	15.587	7.47	18.3	6.5	21.9	21.3	16.7	11.8	23.4	14.7	16	19.9	6.71	18.3	13.9
CaO	1.14	0.05	0.22	0.127	0.19	0.05	0.55	0.06	0.16	0.11	0.04	0.25	0.07	0.22	0.07	0.02	0.54	0.12
Na_2O	0.48	0.02	0.02	0.012	1.62	0.02	1.6	0.03	0.03	0.03	0.01	0.02	0.03	0.08	0.05	0.03	0.09	0.06
K_2O	0.08	-	-	0.18	0.03	0.5	0.06	0.05	0.15	0.2	0.16	0.04	0.05	0.96	0.01	0.22	0.35	0.04
H_2O	12.158	11.142	11.389	11.367	13.25	11.93	12.97	12.01	12.273	12.18	11.44	12.62	11.69	12.81	12.37	11.02	12.06	12.03
Cl	0.015	-	-	-	-	-	-	-	-	-	-	-	-	-	-	-	-	-
O=Cl	-0.003	-	-	-	-	-	-	-	-	-	-	-	-	-	-	-	-	-
TOTAL	**94.665**	**105.321**	**97.679**	**100.198**	**91.3**	**97.98**	**91.27**	**100.13**	**99.25**	**95.71**	**85.96**	**91.32**	**93.02**	**84.71**	**100.75**	**99.14**	**99.38**	**84.05**
#Si IV	3.483	2.653	2.739	3.089	3.471	3.016	3.484	2.893	3.164	3.395	3.089	3.398	2.864	3.714	3.212	2.902	3.456	3.044
#Al IV	0.517	1.347	1.261	0.911	0.529	0.984	0.516	1.107	0.836	0.605	0.911	0.602	1.136	0.286	0.788	1.098	0.544	0.956
T site	**4.000**	**4.000**	**4.000**	**4.000**	**4.000**	**4.000**	**4.000**	**4.000**	**4.000**	**4.000**	**4.000**	**4.000**	**4.000**	**4.000**	**4.000**	**4.000**	**4.000**	**4.000**
#Al VI	0.757	1.388	1.228	0.997	3.100	1.308	2.912	1.232	1.405	1.506	1.217	1.252	1.411	1.830	1.615	1.481	1.297	1.585
#Ti	0.001	0.005	-	0.003	0.009	0.053	0.040	0.003	0.002	0.022	0.003	0.014	0.002	0.001	0.001	0.004	0.002	0.004
#Fe +2	1.086	2.726	2.387	2.430	0.294	1.549	0.589	1.418	1.121	1.368	2.364	0.672	1.948	0.580	1.102	3.172	1.483	1.528
#Mn +2	0.067	0.153	0.016	0.050	0.002	0.025	0.002	0.012	0.026	0.027	0.051	0.009	0.043	0.002	0.003	0.027	0.019	0.017
#Mg	3.785	1.696	2.358	2.446	1.120	2.808	0.996	3.257	3.129	2.577	2.191	3.681	2.442	2.709	2.853	1.100	2.733	2.523
#Ca	0.128	0.005	0.025	0.014	0.020	0.006	0.061	0.006	0.017	0.012	0.005	0.028	0.008	0.027	0.007	0.002	0.058	0.016
#Na	0.098	0.004	0.004	0.002	0.316	0.004	0.319	0.006	0.006	0.006	0.002	0.004	0.006	0.018	0.009	0.006	0.017	0.014
#K	0.011	-	-	0.024	0.004	0.066	0.008	0.006	0.019	0.026	0.025	0.005	0.007	0.139	0.001	0.031	0.045	0.006
O site	**5.933**	**5.977**	**6.018**	**5.967**	**4.866**	**5.819**	**4.925**	**5.941**	**5.725**	**5.544**	**5.858**	**5.666**	**5.868**	**5.306**	**5.591**	**5.823**	**5.653**	**5.692**
#O	10.000	10.000	10.000	10.000	10.000	10.000	10.000	10.000	10.000	10.000	10.000	10.000	10.000	10.000	10.000	10.000	10.000	10.000
#OH	7.997	8.000	8.000	8.000	8.000	8.000	8.000	8.000	8.000	8.000	8.000	8.000	8.000	8.000	8.000	8.000	8.000	8.000
#Cl	0.003	-	-	-	-	-	-	-	-	-	-	-	-	-	-	-	-	-
Charge	**0.000**	**0.000**	**0.000**	**0.000**	**0.000**	**0.000**	**0.000**	**0.000**	**0.000**	**0.000**	**0.000**	**0.000**	**0.000**	**0.000**	**0.000**	**0.000**	**0.000**	**0.000**
Mg/(Mg+Fe)	0.777	0.384	0.497	0.502	0.792	0.644	0.628	0.697	0.736	0.653	0.481	0.846	0.556	0.824	0.721	0.257	0.648	0.623

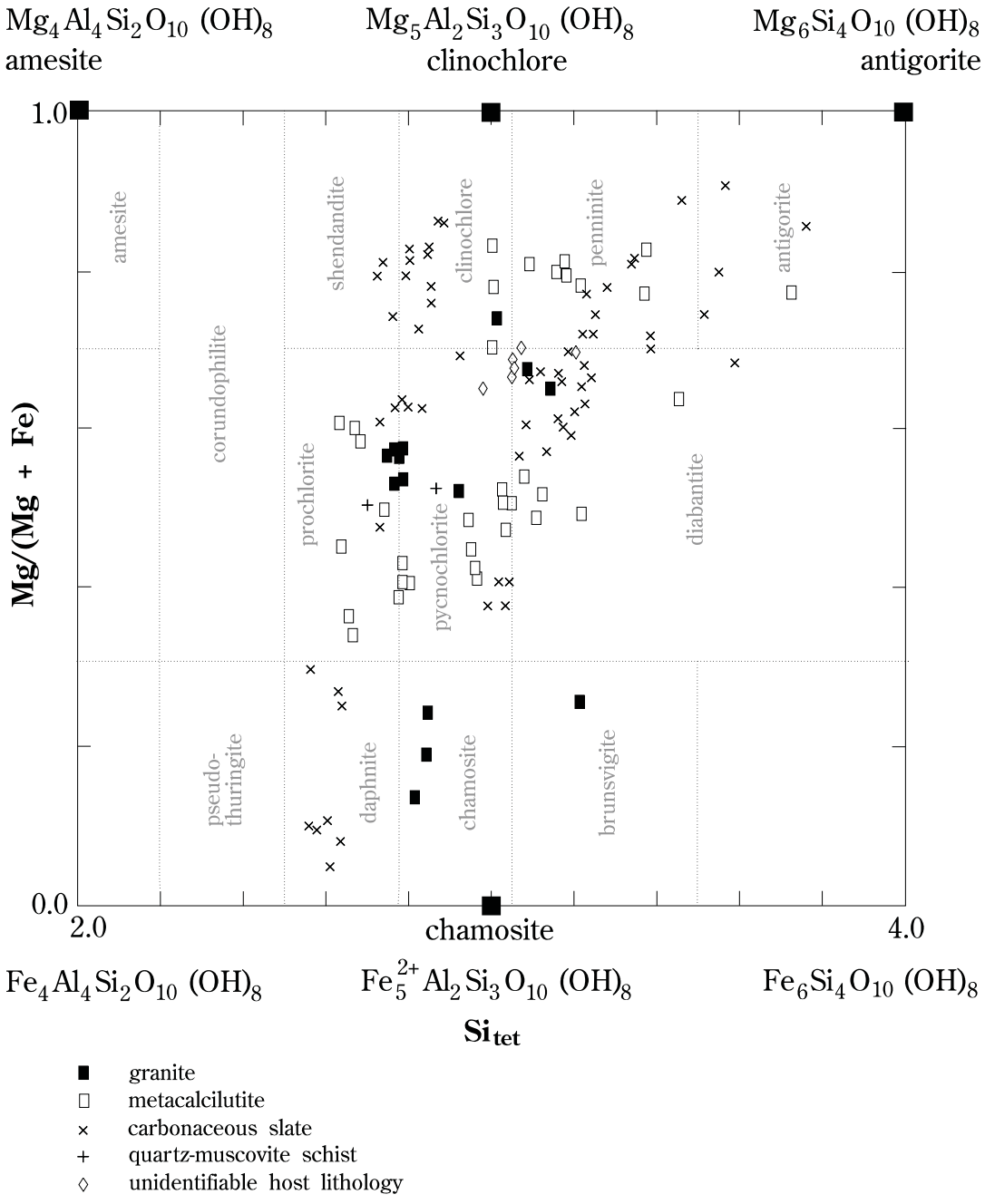

FIGURE 5.16: Total compositional data for chlorites from Mount Dore, represented as a plot of Mg/(Mg+Fe) versus Si_{tet}. There is a considerable spread of compositions regardless of the host rock in which chlorite is developed. Areas of chlorite species and nomenclature are those of Phillips (1964).

5.3.13 Sulphides

Scott (1988) analysed several sulphide species for trace metal contents (Table 5.14). He identified four types of pyrite on the basis of textures and Co+Ni contents, although no such distinction could be determined in the present study. Early (his Type I) pyrite, which he interpreted to be syngenetic, has a high Ni and low Co and Cu. All other types (II to IV) have variable Ni contents and elevated Cu or Co, commonly where associated with chalcopyrite. Chalcopyrite generally has Ag contents up to 200 ppm, and elevated Co values where associated with high-Co pyrite (*e.g.* CSIRO-101295). Chalcopyrite associated with sphalerite has a high Zn content (*e.g.* CSIRO-101330). The FeS content of sphalerite is generally low, apparently varying with the presence of carrollite (a Cu-Co,Ni-sulphide). In the presence of this phase, sphalerite contains about 3 mol% FeS (*e.g.* CSIRO-101463), but in the more usual case where carrollite is absent, sphalerite has only 0.5 mol% FeS with up to 0.15% Co (*e.g.* CSIRO-101295).

Neither galena nor chalcocite were analysed, but other secondary copper sulphides have inherited trace metal characteristics from associated primary phases (Scott, 1988). Bornite and covellite associated with sphalerite have elevated Ag and Co contents (*e.g.* CSIRO-101295). Digenite is free of other chalcophile elements when it occurs rimming chalcopyrite (*e.g.* CSIRO-101507) or pyrite (*e.g.* CSIRO-101840), but when intergrown with sphalerite or carrollite it is significantly contaminated by Co and Zn (*e.g.* CSIRO-101330, 101463). Djurleite contains up to 0.5% Ag (average 0.32%), and is often associated with Al-rich and Ag-poor chrysocolla (*e.g.* CSIRO-101340).

TABLE 5.14: Trace metal contents of base metal sulphides, according to Scott (1988). All values are in parts per million by weight. Data for each mineral are generally averages of six to eight determinations. Sample localities and brief descriptions are given in Table D3 (Appendices).

CSIRO CATALOGUE NUMBER	ANALYSED MINERALS	Ag	As	Co	Cu	Ni	Zn
101295	bornite	400	<200	1900	NA	250	15600[2]
	chalcopyrite	<200	400	800	NA	200	10400[2]
	covellite	400	<200	1900	NA	<200	<200
	pyrite (III)	NA	1500	10200	600	<500	<500
	sphalerite	NA	NA	1500	NA	NA	NA
101330	chalcopyrite	<200	<200	<200	NA	<200	580
	digenite	<200	<200	2200	NA	<200	7300[2]
	pyrite (I)	NA	1200	<500	<500	37400	500
	pyrite (II)	NA	<500	<500	1900	2000	800
101340	djurleite	820	330	<200	NA	<200	<200
	djurleite	3200	200	<200	NA	<200	<200
101377	pyrite (III)	NA	700	11600	<500	<500	<500
	pyrite (IVa)	NA	4500	<500	<500	<500	<500
	pyrite (IVb)	NA	12200	<500	<55	<500	<500
101383	chalcopyrite	300[1]	500	<200	NA	<200	200
	pyrite (III)	NA	<500	19000	1100	<500	<500
	pyrite (IVa)	NA	<500	<500	2500	<500	<500
	pyrite (IVb)	NA	600	<500	<500	<500	<500
101405	pyrite (III)	NA	<500	10700	<500	<500	<500
	pyrite (IVb)	NA	1100	<500	<500	<500	<500
101463	pyrite (IVa)	NA	2800	<500	1600	<500	<500
	pyrite (IVb)	NA	3200	<500	<500	<500	<500
	sphalerite	NA	NA	NA	NA	NA	NA
101507	chalcopyrite	<200	220	<200	NA	<200	<200
	digenite	500	280	270	NA	<200	<200
	pyrite (II)	NA	1700	1800	13600	4200	<500
	pyrite (II)	NA	500	500	8900	1800	<500
101840	digenite	500	<200	<200	NA	<200	<200
	pyrite (II)	NA	<500	<500	20600	11000	<500
	pyrite (II)	NA	2500	3200	10600	1200	<500
101841	chalcopyrite	<200	300	<200	NA	<200	400
	pyrite (II)	NA	600	<500	<500	900	<500
	pyrite (III)	NA	<500	5200	<500	500	<500

[1] one value up to 800 ppm recorded
[2] sphalerite contamination

5.4 IMPLICATIONS OF MINERAL PARAGENESES FOR FLUID GEOCHEMISTRY

5.4.1 Potassic alteration and fluid redox state

Alteration and mineralization parageneses provide some constraints on the initial and subsequently evolving chemistry of the fluid (dissolved species, pH, f_{O_2}, f_{S_2}, *etc.*). Although there is some variation in alteration parageneses with differing rock types, there is an overall consistency. The earliest alteration common to all rock types involved potassic metasomatism. A K^+-bearing fluid produced mainly microcline, but also lesser biotite and muscovite. In the simplest case, microcline is replacing quartz-muscovite schists, probably via a reaction such as:

$$\underset{\text{muscovite}}{KAl_3Si_3O_{10}(OH)_2} + 6SiO_2 + 2K^+ \;===\; \underset{\text{microcline}}{3KAlSi_3O_8} + 2H^+$$

Both major phases are consumed, and the fluid pH decreases. Extra SiO_2 may also have been introduced. In the Mount Dore Granite and Staveley Formation, plagioclase is instead replaced by microcline, possibly by a reaction like:

$$\underset{\text{albite}}{NaAlSi_3O_8} + \underset{\text{anorthite}}{CaAlSi_2O_8} + 4SiO_2 + 3K^+ \;===\; \underset{\text{microcline}}{3KAlSi_3O_8} + Na^+ + Ca^{2+}$$

The fluid pH does not change in this case, but sodium and calcium are added to it. In granite towards the periphery of the alteration zone, plagioclase is altered to muscovite instead of microcline, via hydrolysis; *e.g.*:

$$\underset{\text{Albite}}{NaAlSi_3O_8} + \underset{\text{anorthite}}{CaAlSi_2O_8} + K^+ + 2H^+ \;===\; \underset{\text{muscovite}}{KAl_3Si_3O_{10}(OH)_2} + 2SiO_2 + Na^+ + Ca^{2+}$$

The hydrogen required for this reaction may have been partly derived from reactions occurring in adjacent metasediments. SiO_2 is released, and if saturation

occurs, quartz may precipitate; this may explain the spatial association of quartz veining and muscovite alteration.

Biotite is present in addition to microcline in the southern part of the prospect, in Staveley Formation lithologies. Petrography indicates that it formed contemporaneously with microcline, which is the dominant K-rich phase to the north, in altered carbonaceous slates and quartz-muscovite schists. Experimental studies have shown that biotite and K-feldspar in hydrothermal regimes may be related by reactions of the type:

$$2KAlSi_3O_8 + Fe_2O_3 + 2H_2O === 2KFe_3AlSi_3O_{10}(OH)_2 + 0.5\ O_2$$

(Eugster and Wones, 1962; Rutherford, 1969, 1973; Beane, 1974). These reactions are dependent on temperature, pressure, and more particularly the redox state of the fluid. Phase relations between these phases in the presence of quartz indicate that biotite will be favoured over K-feldspar at higher temperatures, or lower oxygen fugacities (Figure 5.17). Increasing pressure or substitution of Mg and Al into the annite structure will increase its stability field (Rutherford, 1973; Beane, 1974). If a single fluid is responsible for potassic alteration throughout the prospect, temperatures and pressures for any depth were unlikely to differ much, and a difference in fluid redox seems more probable. Supporting evidence is the prevalence of haematite in association with microcline in the north, and of magnetite with biotite in the south.

That microcline and haematite formed in graphite-rich Toole Creek lithologies indicate that the fluid was relatively oxidizing, certainly above the haematite-magnetite buffer. Carbon was released from these rocks during potassic and later alteration, and must have acted to reduce the fluid, probably by producing CO_2 (suggested by the abundance of carbonates; see below). Microcline veining in quartz-biotite schists of the Staveley Formation also indicates an oxidizing fluid. Development of hydrothermal biotite in more highly brecciated rocks indicates, however, that the redox state of fluids reacting with these rocks is variable, and the fluid may in part be reduced fluid from the north. Later partial alteration of magnetite to haematite may occur if the fluid again became oxidizing, or simply cooled.

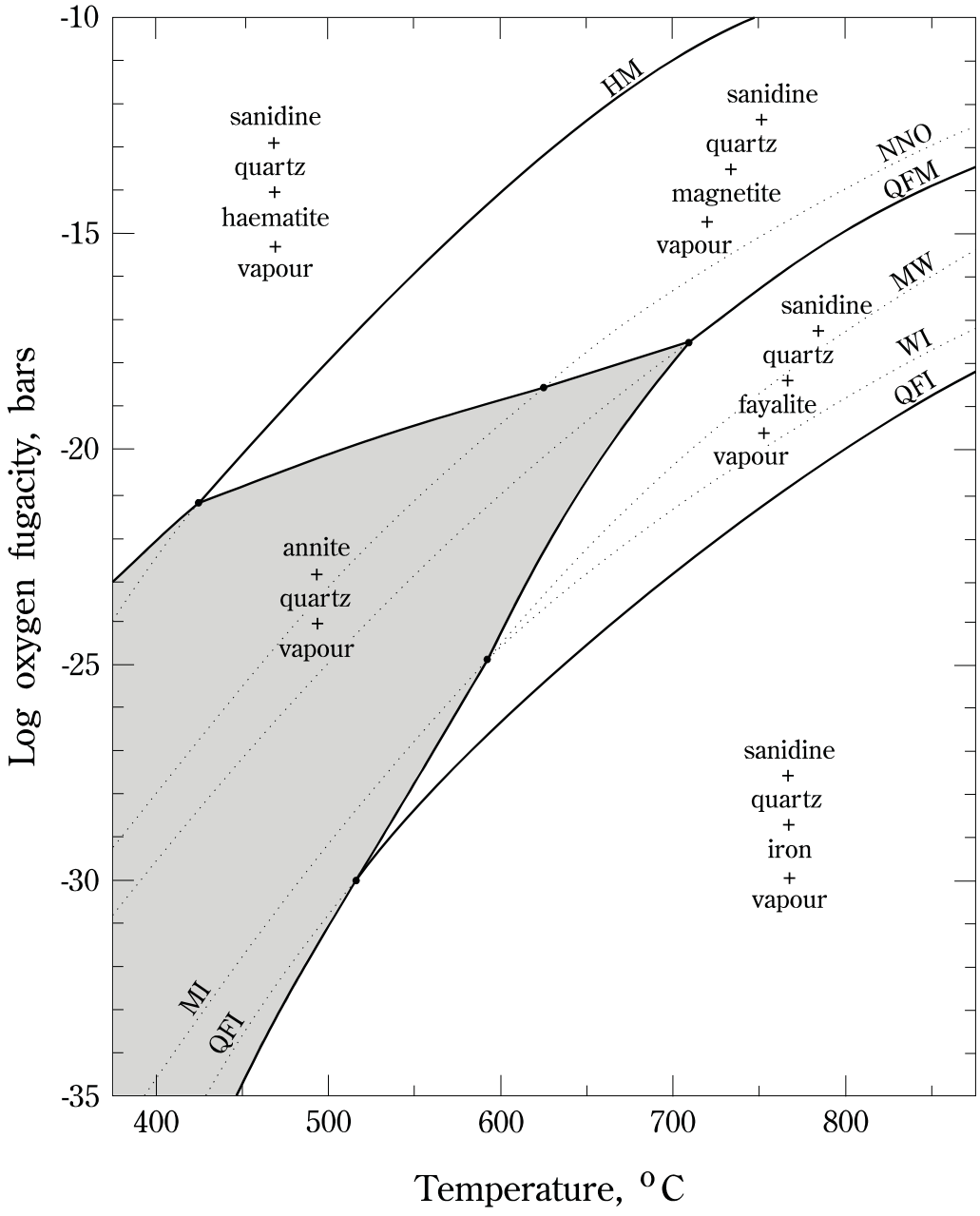

FIGURE 5.17: Phase relations of annite + 3 quartz (+ vapour) bulk composition as a function of oxygen fugacity and temperature at constant total pressure of 207 MPa (the possible pressure at which hydrothermal activity was occurring at Mount Dore). Oxygen buffer curves are as follows: QFI - quartz-fayalite-iron; WI - wüstite-iron; MI - magnetite-iron; MW - magnetite-wüstite; QFM - quartz-fayalite-magnetite; NNO - nickel-nickel oxide; HM - haematite-magnetite (after Figure 6 of Eugster and Wones, 1962).

5.4.2 Calc-silicates and retrograde reactions

Diopside-scapolite assemblages can form by isochemical regional metamorphism of halite-bearing calcareous shales (*e.g.* White, 1959; Ramsay and Davidson, 1969). Such assemblages occur at Mount Dore in Staveley Formation rocks, which are known to have been halite-bearing (Blake *et al.*, 1983; Chapter 2). They are, however, only locally developed, and textures clearly indicate growth after regional metamorphism. Contact metamorphism would produce the same mineral assemblages. The temperature at which diopside will form is a function of the total pressure and the mole fraction of CO_2 in the fluid, decreasing with both these parameters for X_{CO_2} less than 0.7. Extensive brecciation and the presence of some vuggy material suggest relatively low pressures, perhaps as little as 100 MPa or less, at which diopside can form at temperatures as low as 450^{o}C. The maximum temperature at which it can form at this pressure is about 540^{o}C. At higher total pressures the temperature of formation will increase (Figure 5.18).

Some actinolite may also be contact metamorphic in origin, but much of it, and all of the epidote apparently formed after diopside and scapolite, possibly via retrograde reactions involving the cooling H_2O-CO_2 fluid, or a hydrothermal fluid introduced into the rock; *viz.*:

$$5\ CaMgSi_2O_6 + Ca_4Al_6Si_6O_{24}.CO_3 + 2H_2O + 2CO_2 ===$$

diopside meionite

$$Ca_2Mg_5Si_8O_{22}(OH)_2 + 2\ Ca_2Al_3Si_3O_{12}(OH) + 3\ CaCO_3 + 2\ SiO_2$$

Tremolite zoisite calcite quartz

(modified after White, 1959). Garnet may have formed via related reactions. Calcite and quartz may initially go into solution, to be precipitated later with changing conditions.

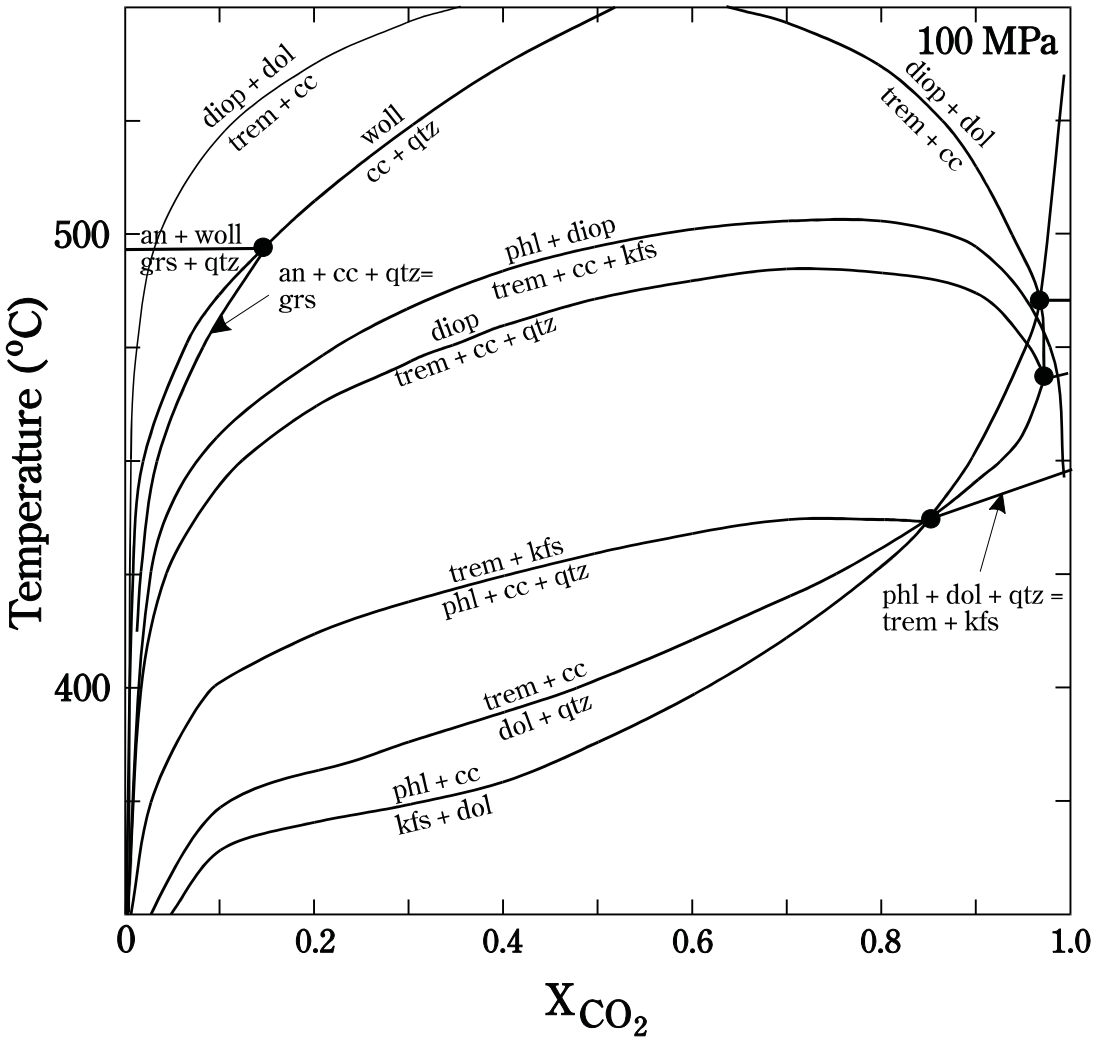

FIGURE 5.18: X_{CO_2} versus temperature diagram at 100 Mpa for selected reactions in the KCMAS(H_2O-CO_2) system, to indicate the stability field of diopside, and hence the minimum temperature at which it is likely to form as a hydrothermal alteration phase (after Figure 15 of Tracy and Frost, 1991). *Mineral abbreviations:* **an** - anorthite; **cc** - calcite; **diop** - diopside; **dol** - dolomite; **grs** - grossular; **kfs** - K-feldspar; **phl** - phlogopite; **qtz** - quartz; **trem**Ê- tremolite; **woll** - wollastonite.

5.4.3 Boron and silica metasomatism

Tourmaline, though not as common as potassic phases, is still conspicuous in the early part of the paragenesis. Experiments by Frondel and Collette (1957) indicated that tourmaline will form by interaction of acid to mildly alkaline, Na^+- and borate-bearing solutions with a great variety of common aluminosilicate minerals, at temperatures of 400°C or greater. It will not be favoured, however, if the reactant minerals have high Ca or (Ca+Mg+Fe)/(Al+Si) or produce a strongly alkaline solution when dissolved. This may explain why tourmaline at Mount Dore is more prevalent in the argillaceous metasediments of the Toole Creek Volcanics, and comparatively uncommon in calcareous Staveley Formation lithologies.

Boron in a fluid may also control other alteration types. For instance, it increases the solubility of SiO_2 in comparison with pure water, or with an H_2O-HCl fluid (Pichavant, 1981, 1983; Manning and Pichavant, 1984). Formation of tourmaline by fluid-rock reactions will remove boron from solution, and will therefore reduce the SiO_2 solubility, potentially causing supersaturation and precipitation of quartz. The pronounced spatial and temporal association between tourmaline and quartz alteration at Mount Dore strongly suggests this mechanism may have been at least partly responsible for quartz alteration.

5.4.4 Carbonate alteration

Carbonate solubility is strongly dependent on the pH and the CO_2 fugacity of the fluid, via reactions such as:

$$CaCO_3 + CO_2 + H_2O \text{ === } Ca^{2+} + 2HCO_3^-$$

$$CaCO_3 + H^+ \text{ === } Ca^{2+} + HCO_3^-$$

Solubility is increased by increasing f_{CO_2} or decreasing pH in the fluid (Ellis, 1959).

Increasing NaCl also increases solubility (Ellis, 1963; Malinin and Kanukov, 1971). Early alteration would have acted to increase carbonate solubility, by release of protons, sodium and CO_2 to the fluid. Simply cooling such a fluid would not precipitate carbonates, because they show retrograde solubility (Holland and Malinin, 1979). They must therefore be precipitated by physically removing, or otherwise decreasing the activities of CO_2, NaCl or H^+ in the fluid. Such mechanisms include boiling, where CO_2 is partitioned into the vapour phase and subsequently lost, fluid-rock reaction, which can use H^+, thereby increasing the amount of CO_3^{2-} in solution, or by simple dilution (fluid mixing), which will reduce the activities of all components.

Whether dolomite or calcite precipitates depends on the ratio of the activities of calcium and magnesium at the temperature of precipitation (Rosenberg and Holland, 1964). High magnesium contents are not required to form dolomite (Figure 5.19). At Mount Dore there is a notable association of calcite with Mg-rich alteration phases such as biotite and calc-silicates, whereas dolomite occurs in association with Mg-poor microcline-quartz alteration and metasediments of the Toole Creek Volcanics. Fluid producing the Mg-rich alteration is likely to have been depleted in Mg, thereby raising the $a_{Ca^{2+}}/a_{Mg^{2+}}$ ratio, and encouraging the formation of calcite. Fluid producing the Mg-poor assemblage would have a lower $a_{Ca^{2+}}/a_{Mg^{2+}}$ ratio, and dolomite would be favoured.

5.4.5 Sulphur fugacity and sulphide formation

Fine haematite dusting in the microcline alteration, and by the precipitation of coarser haematite and magnetite in quartz veins demonstrate that iron was in solution in the earliest fluid. Boctor *et al.* (1980) determined that the dominant Fe species in solution in equilibrium with either magnetite or haematite close to the haematite-magnetite buffer at temperatures of 400 to 600^{o}C and pressures between 100 and 200 Mpa (likely conditions during early alteration at Mount Dore) is $FeCl_2^o$. Pyrite did not form until during or after silicification. Reduced sulphur is required for its precipitation, and the late formation therefore suggests that sulphur was absent from

FIGURE 5.19: Mole fractions of $m_{Ca^{2+}}/(m_{Ca^{2+}}+m_{Mg^{2+}})$ in solutions in equilibrium with calcite + dolomite and dolomite + magnesite at temperatures between 275° and 420°C. Squares indicate runs in which dolomite was replaced by calcite; circles, dolomite replaced by magnesite; and triangles, calcite or magnesite replaced by dolomite (after Rosenberg and Holland, 1964).

the fluid, or was in an unusable oxidized state (SO_4^{2-}). This is consistent with previously noted evidence for an oxidized fluid (Figure 5.17). Small amounts of reduced sulphur may have been produced during reduction of the fluid attending release of graphite during alteration, or may alternatively have been released from syngenetic sulphides. This reduced sulphur was apparently quickly scavenged by dissolved Fe into pyrite, or rarer associated arsenosulphides (cobaltite, arsenopyrite).

Other base metal sulphides are dominated by chalcopyrite, sphalerite and galena. Silver sulphides have not been observed, and Ag was apparently precipitated in other sulphide phases. All have a pronounced association with either carbonate, or pyrite or both. Partial replacement of both phases is usual. Precipitation of base metal sulphides by reduction with carbon seems unlikely, because most graphite had been removed during earlier alteration. Replacement of earlier pyrite suggests moreover that the fluid remained low in reduced sulphur even after pyrite precipitation, and that base metals had to scavenge such sulphur from the pyrite and from each other in order to form. Carbonate replacement may have occurred via reactions like:

$$CaCO_3 + Zn^{2+} + HS^- === ZnS + Ca^{2+} + HCO_3^-$$

(Holland and Malinin, 1979), where bisulphide was released from pyrite.

5.4.6 Accessory phases

These are important for indicating the presence of minor components in the fluid, and in some cases for estimating activities. Apatite formed before carbonate, and indicates the presence of PO_4^{3-}, HF and HCl in the solution at this time. Precipitation of minor fluorite after carbonate indicates some fluorine remained in the fluid even after apatite formation. Factors controlling apatite solubility are poorly known, but fluorite is only sparingly soluble in hydrothermal fluids, although solubility increases with increasing pressure and chloride salt concentrations (Holland and Malinin, 1979).

Decreasing temperature is likely to be the important deposition mechanism for fluorite, though dilution of the fluid may also achieve this.

Fugacities of HF and HCl may be derived from apatite-fluid equilibria, because apatite re-equilibrates only sluggishly or not at all as conditions change from those of formation (Tacker and Stormer, 1989), and the thermochemistry of the relevant equilibria are moderately well constrained (Korzhinskiy, 1981). Preliminary HF and HCl fugacity calculations using apatite from Mount Dore are presented in Appendix E.

5.4.7 Fluid "dregs"

The formation of muscovite/illite away from the core of the alteration zone, or later in the paragenesis, indicates a either a more acid or a cooler fluid than that which produced orthoclase and biotite. Chlorite is a widespread hydrothermal phase, forming last and partly replacing most earlier alteration phases. It changed composition from initially Mg-rich to progressively Fe-rich, a trend consistent with decreasing temperature. At a very late stage in the history of the deposit, it was raised to shallow levels, and meteoric waters became dominant, causing supergene enrichment, largely of copper as chalcocite and more oxidized species.

5.5 CONCLUSIONS

Alteration at the Mount Dore prospect affects all lithologies, and clearly occurred later than granite intrusion and attendant contact metamorphism, largely as replacement in heavily fractured and brecciated zones. The early fluid was hot and enriched in K^+, B_2O_3 and SiO_2, and initially produced haematite-dusted microcline and more locally biotite and magnetite. Tourmaline and quartz were precipitated shortly thereafter, possibly partly in response to falling temperature, but in the case of quartz possibly also in response to decreasing solubility due to loss of boron from the fluid. In calcareous Staveley Formation rocks there was additional complex interaction with

SiO_2-rich fluids producing a variety of calc-silicate minerals at temperatures probably greater than 500°C.

The fluid in the northern part of the prospect was relatively oxidized (above the haematite-magnetite buffer), but that in the south had a more variable, and lower f_{O_2}, stabilizing both microcline and biotite, and magnetite. These more reduced fluids may have been partly derived from the north by reaction of fluids there with carbon-rich metasediments. This suggests possible fluid movement from north to south (and upwards?).

Later carbonate alteration indicates the presence of CO_2 in the fluid. Precipitation is likely due to increasing pH or decreasing fluid f_{CO_2} attending boiling, or through dilution. Occurrence as dolomite or calcite is a function of the ratio of Ca^{2+} and Mg^{2+} activities in the fluid. This ratio was apparently determined during formation of early potassic phases. Precipitation of microcline maintained a low $a_{Ca^{2+}}/a_{Mg^{2+}}$ and caused dolomite to precipitate, whereas this ratio was larger when Mg^{2+} was used in biotite, and calcite formed instead.

The dominant sulphides are pyrite and chalcopyrite, but lesser sphalerite and galena are present in the deep northern part of the prospect. Pyrite formed during or just after silicification, when reduced sulphur species became available through sulphate reduction by graphite released from the metasediments. Chalcopyrite and other primary sulphides precipitated after carbonate, but before chlorite, in the order Zn-, Pb, then Cu-sulphide. They also show a strong spatial association with pyrite, and in many instances are clearly replacing it. This suggests the late fluid was also poor in reduced sulphur, and base-metals in solution precipitated by scavenging sulphur from earlier pyrite.